Jül-4282

Jülich Center for Hadron Physics (JCHP)
Institut für Kernphysik (IKP)
COSY

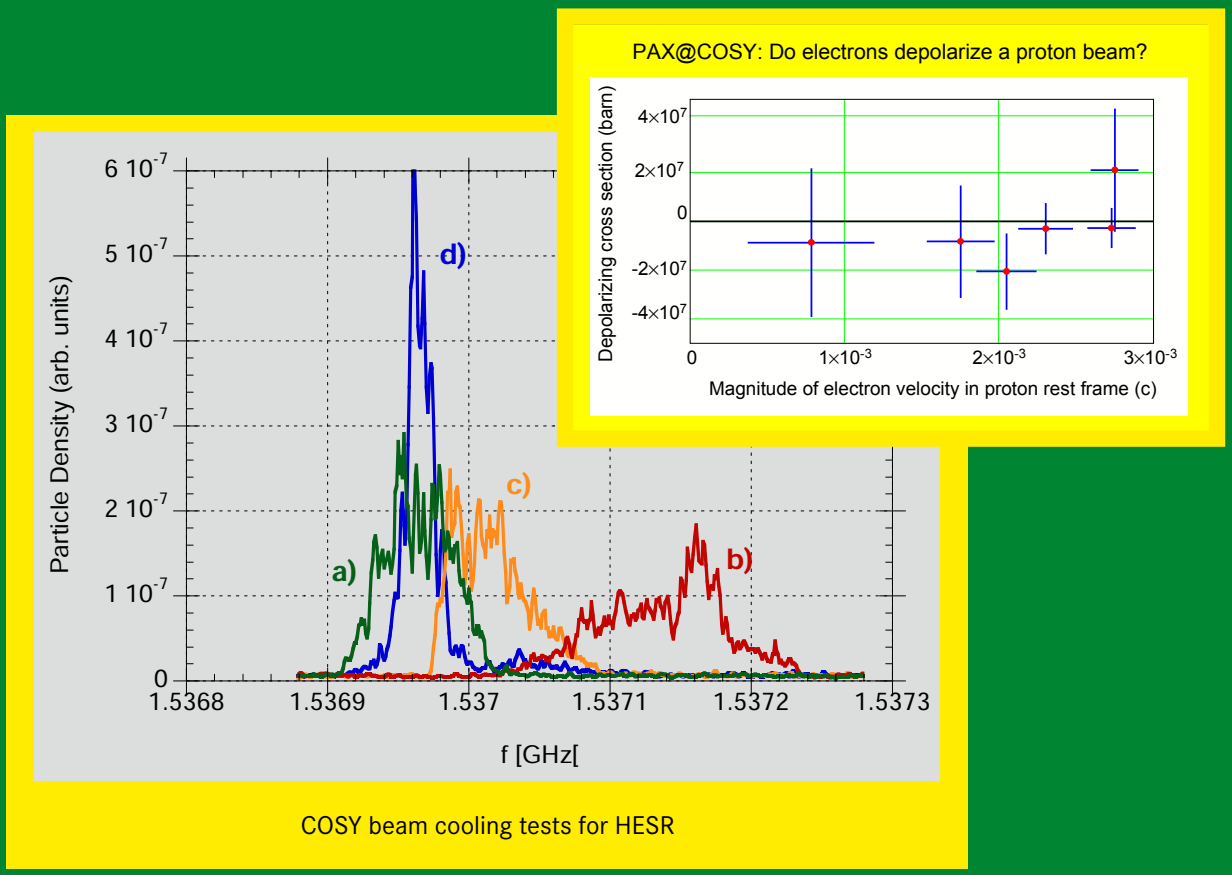

COSY beam cooling tests for HESR

ANNUAL REPORT 2008

Mitglied der Helmholtz-Gemeinschaft

JÜLICH
FORSCHUNGSZENTRUM

Annual Report 2008

Institut für Kernphysik / COSY

Cover picture:

Lower figure: COSY has been used to develop methods to compensate the mean energy loss and energy spread of the stored antiproton beam at HESR during internal target experiments. The Schottky spectra of the COSY proton beam has been measured using the WASA frozen-pellet target, a prototype barrier bucket HF cavity for the HESR and COSY's stochastic cooling system: a) starting distribution, b) final distribution after 160 s only pellet-target, c) final distribution with longitudinal stochastic cooling and d) final distribution with cooling and barrier bucket (cf. Sect. 2.2).
Upper figure: The measurement of the depolarizing $\vec{p}e$ cross section settled a long-standing controversy about the role of electrons to the polarization buildup of a stored beam by spin-flipping. Electrons in the COSY e-cooler have been used to study their depolarizing effect on a 49.3 MeV proton beam. The depolarizing cross section is plotted as a function of the electron velocity in the proton rest frame, indicating an upper limit of a few 10^7 b (cf. Sect. 1.2.8).

Preface

On July 1, the board of directors of the Forschungszentrum Jülich (FZJ) founded the **Jülich Center for Hadron Physics (JCHP).** The main goal of the JCHP is to coordinate the hadron physics activities at the FZJ for the FAIR project. This includes activities at the Institute for Advanced Simulations (IAS), the Institut für Kernphysik (IKP), the Zentralinstitut für Elektronik (ZEL) and the Zentralabteilung Technologie (ZAT). Within the Helmholtz Association (HGF) research field *Structure of Matter*, the FZJ operates the COSY facility and has achieved an excellent international reputation due to the close cooperation between accelerator physicists, experimentalists and theoreticians. In cooperation with ZEL and ZAT, the IKP is in charge of the construction and operation of the High Energy Storage Ring HESR and makes a strong contribution to the PANDA detector and its physics. PAX is exploiting methods to effectively polarize (anti-)protons for a possible future upgrade at FAIR.

The FZJ operates the JUGENE/JSC supercomputer and hosts the John von Neumann institute which develops lattice gauge simulation calculations of quantum chromodynamics (QCD) and hadron structure. The JCHP coordinates these activities by establishing a direct connection between the lattice QCD simulation groups and hadron physicists. Moreover, the infrastructure provided by the IAS for mass storage, presently used for COSY data, may handle FAIR data and perform Monte Carlo simulations of HESR experiments.

External users are essential for the success of an accelerator complex, therefore, the JCHP facilitates the contact of external users with the FZJ and supports external activities in the field of hadron physics. Presently an initiative of the universities within North-Rhine Westfalia and the FZJ, called NRW-FAIR, is forming to coordinate their FAIR-related activities.

Starting December 1, 2008, the IKP-3 theorists also work in IAS-4, the strong interaction physics branch of the Institute for Advanced Simulations (IAS). The Virtual Institute *Spin and Strong QCD* has presented its first results on June 1 in Ferrara.

The IKP has initiated a cooperation with the 100-TW laser facility at the Heinrich-Heine University Düsseldorf. The potential of new particle acceleration technologies with limited-mass targets will be explored, exploiting the know-how on frozen-pellet targets gained at the IKP.

The year 2008 has seen important experimental and theoretical progress:

- The WASA-at-COSY facility began operation in 2007, and in 2008 the first results have been submitted for publication. Data on the $\eta \to 3\pi^0$ decay was used to determine the quadratic slope parameter $\alpha = -0.027 \pm 0.008(\text{stat}) \pm 0.005(\text{syst})$, consistent with previous measurements, and clearly indicating the importance of pion-pion final state interactions. WASA has also taken exclusive high statistics data on the $pn \to pn\pi^0\pi^0$ process to study the ABC effect, and a strong resonance-like structure has been observed in the excitation function.
- ANKE has published results on isolation of the $\Lambda(1405)$ hyperon in the $\Sigma^0\pi^0$ channel, diproton formation in the γ- and π final states, kaon pair production and kaon final state interaction, and neutron-proton charge-exchange amplitudes at 585 MeV. In addition, it has presented a paper about the Schottky method for luminosity determination in internal experiments.

- TOF has performed first experiments using the new straw tube tracker. This is an important technological progress directly relevant for the central detector of PANDA. Moreover, it is the first step to determine the spin dependence of the Λp scattering length.
- PAX has performed and analysed depolarization experiments with the COSY electron cooler, thereby showing that the cross section is much smaller than needed for effectively polarizing the beam.
- The theory institute has studied three-nucleon forces in chiral effective field theory including the Δ_{33} resonance as an explicit degree of freedom with subsequent applications to isospin violating effects in few-nucleon systems. Nuclear lattice simulations with three-body forces have been performed to obtain the neutron-deuteron S-wave phase shifts. The $Y(4660)$ resonance recently observed at BES does not fit into the conventional quark model. An interpretation as a quasi-bound state consisting of the ψ' and the $f_0(980)$ mesons has been worked out and predictions for the $K\bar{K}$ decay have been made, which eventually will be tested at PANDA. Scaling laws in the Coulomb excitation of neutron halo nuclei have been proposed.
- IKP-4 has developed components for the HESR and new methods in parallel to the routine operation of COSY. This research and development benefits from the unique capabilities provided by COSY. First successful operations of the barrier-bucket cavity beam with pellet target and stochastic cooling have been performed. The HESR lattice has been completed with normal conducting magnets. The physical specifications for all components have been finished. New insights into the loss mechanisms while operating the electron cooling show potential for an intensity increase. A new technique to overcome spin-deploarizing resonances based on Kondratenko crossing has been tested.

In October 2008, Prof. U.-G. Meißner has been elected as Dean of the Faculty of Mathematics and Natural Sciences of the University of Bonn. We congratulate both M. Wolke and C. Hanhart for having received offers from Uppsala University. Prof. J. Ritman and PD C. Hanhart have been elected as members of the scientific-technical council (WTR) and its executive committee (HK) in 2008, C. Hanhart has become vice chair of the WTR. Congratulations are given to Prof. H. Machner for receiving the Merentibus Medal of the University of Cracow.

Finally I would like to express my sincere gratitude to all our colleagues and co-workers, since without their help and support, we would not have been able to achieve our milestones. We also acknowledge the continuous support by the board of management of the FZJ and HGF.

Jülich, January 2009 James Ritman

Contents

1 Physics at COSY

1.1 Overview

The cooler synchrotron and storage ring COSY delivers unpolarized and polarized beams of protons and deuterons with momenta up to 3.7 GeV/c for two internal experiments — ANKE and WASA — and one experiment — TOF — at an external target position. All three detection systems are operated by large international collaborations.

- **ANKE** (Apparatus for Studies of Nucleon and Kaon Ejectiles) is a large acceptance forward magnetic spectrometer at an internal target station in the COSY ring. The central dipole is movable to adjust the momenta of the detected particles independent of the beam momentum. Using deuterium cluster targets, reactions on the neutron are tagged by detecting the low-energy recoil proton in silicon strip detectors in vacuum next to the target. In addition, a polarized internal target with a storage cell can be used.
- **TOF** (Time Of Flight) is a non-magnetic spectrometer combining excellent tracking capabilities with large acceptance and full azimuthal symmetry allowing to measure complete Dalitz plots. TOF is optimized for final states with strangeness. With the new straw tube tracking system (STT), TOF will have a significantly improved mass resolution and reconstruction efficiency.
- **WASA** (Wide Angle Shower Apparatus), an internal 4π spectrometer for neutral and charged particles, is operated at the internal COSY beam. WASA comprises an electro-magnetic calorimeter, a very thin superconducting solenoid, inner and forward trigger and tracking detectors, and a frozen-pellet target.

In addition, the unique COSY capabilities are used by the SPIN@COSY-, dEDM- and PAX-collaborations to investigate spin-manipulations, to build a dedicated EDM-storage ring experiment, and to prepare experiments on polarization buildup in storage rings.

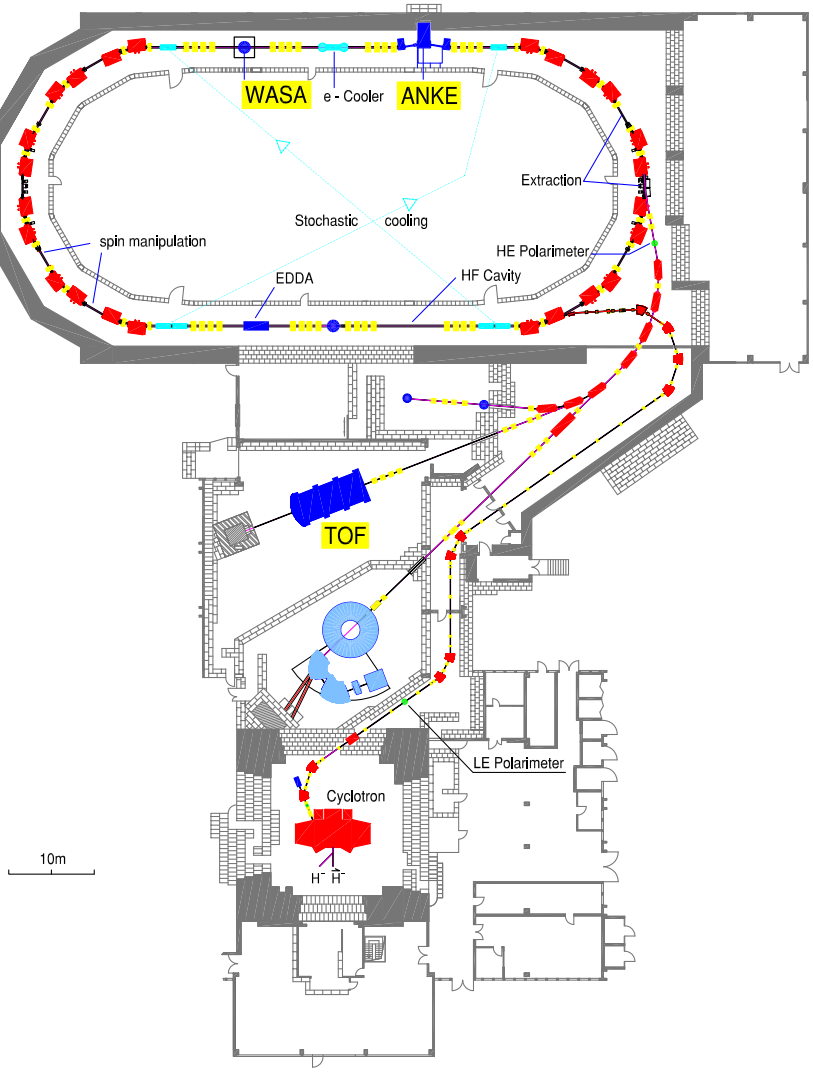

1.2 Major Physics Results at COSY

1.2.1 Dalitz Plot Distribution for $\eta \to 3\pi^0$

Final results have been obtained from the first production run of the **WASA-at-COSY** facility on the Dalitz plot distribution of the $\eta \to 3\pi^0$ decay.
Isospin violating $\eta \to 3\pi$ decays are driven by a term in the QCD Lagrangian which is proportional to the light quark mass difference, and thus allow to determine $m_d - m_u$, since electromagnetic corrections are expected to be small. While Current Algebra predicts a constant decay amplitude $\mathscr{A}$, experimentally a small deviation from a uniform density distribution in the Dalitz plot is observed, which is in part due to $\pi\pi$ final state interactions, providing a sensitive test for Chiral Perturbation Theory (ChPT). The deviation usually is parametrized in an expansion of the matrix element about the centre of the Dalitz plot. The first term in the expansion

$$|\mathscr{A}(z)|^2 = c(1+2\alpha z) \qquad (1)$$

depends on the kinematical variable z

$$z = \frac{2}{3}\sum_{i=1}^{3}\left(\frac{T_i - \langle T\rangle}{\langle T\rangle}\right)^2$$

that parameterizes the square of the distance from the centre of the Dalitz plot ρ in units of its maximum allowed value ρ_{max} and involves a constant c and the quadratic slope α as parameters. T_i and $\langle T\rangle$ denote the kinetic energy of the i^{th} pion and the pion mean kinetic energy, respectively.
A small but negative value for the slope α as reported in previous experiments implies a slight decrease of the Dalitz plot density at the border. Recent NNLO ChPT calculations involve a large uncertainty that does not allow to decide about the sign of the slope. Calculations of the slope parameter are in reasonable agreement with experiment as soon as rescattering effects are considered to infinite orders, either via unitarization of the decay amplitude using dispersion relations or via iteration of the Bethe-Salpeter equation.
In the first production run of the WASA detector at COSY, η mesons have been produced in the reaction $pp \to pp\eta$ at a kinetic energy of $T_p = 1400\,\text{MeV}$, corresponding to an excess energy of 56 MeV. The $2.4\,\text{pb}^{-1}$ of data collected correspond to 94 hours of data taking. On the trigger level, events have been recorded with two or more tracks in the forward detector, at least two hit groups in the electromagnetic calorimeter with an energy deposition larger than 50 MeV and with no hit by a charged particle in the central detector. In the analysis, $\eta \to 3\pi^0$ events have been identified via the missing mass with respect to two protons detected in the forward detector and hit clusters in the calorimeter corresponding to six photons from the subsequent $\pi^0 \to \gamma\gamma$ decays. Considering all fifteen possible combinations of the three photon pairs, the one with a minimum χ^2 value reconstructing the $3\pi^0$ final state has been selected. After a kinematical fit of the $\eta \to 3\pi^0$ decay system, the background contribution from non-resonant $3\pi^0$ production is less than 4 % in the final event sample.
Figure 1 shows the radial density distribution of the $\eta \to 3\pi^0$ Dalitz plot. The efficiency correction has been obtained by dividing the measured z distribution by a Monte Carlo simulation assuming $\alpha = 0$. A linear fit to the data points has been used to extract the slope parameter α with the result

$$\alpha = -0.027 \pm 0.008\,(stat) \pm 0.005\,(syst)$$

based on 120000 events. The systematic uncertainty is dominated by a spread in the vertex position due to an uncertain fraction of interactions with residual gas. Within one standard deviation the result agrees with the previous high statistics measurements by the KLOE and Crystal Ball collaborations, and is also consistent with the result obtained using the WASA detector at CELSIUS.

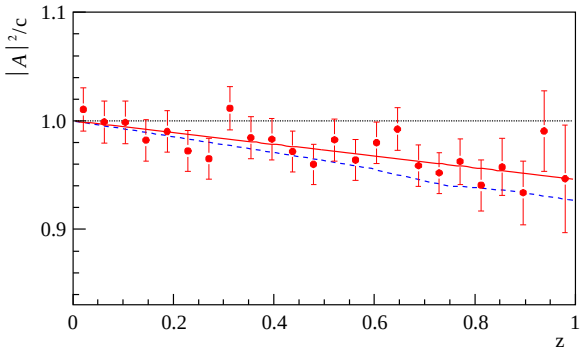

Fig. 1: Radial density distribution of the $\eta \to 3\pi^0$ Dalitz plot measured with WASA-at-COSY. The solid line is a linear fit according to Eq. (1) to extract the slope parameter α, the dotted line corresponds to $\alpha = 0$. The dashed line has been calculated including the cusp effect due to the $\pi^+\pi^-$ threshold.

Since the $\eta \to 3\pi^0$ decay covers the $\pi^0\pi^0 \to \pi^+\pi^-$ rescattering process, the amplitude is no longer a function only on the radial distance from the centre of the Dalitz plot, but has to explicitly depend on the Mandelstam variables. Similar effects are known in $K^+ \to \pi^0\pi^0\pi^+$ decays (NA48/2) and $K_L \to 3\pi^0$ (KTeV), providing a precise determination of a combination of the $I = 0$ and $I = 2$ $\pi\pi$ s-wave scattering lengths a_0 and a_2.
Using a parametrization of the $\eta \to \pi^+\pi^-\pi^0$ decay amplitude from the KLOE collaboration and $\pi\pi$ scattering lengths, the influence of the cusp effect can be predicted and is shown in Fig. 1 by the dashed line. The cusp leads to a broad minimum in the range $0.6 < z < 0.9$ of the Dalitz plot, but the present statistical precision of the experimental data is not sufficient to investigate the effect in more detail. The statistical accuracy needed can be obtained in future combining the high production cross section in proton-proton induced reactions and the capability of the WASA detector to operate at design luminosities of $10^{32}\,\text{cm}^{-2}\text{s}^{-1}$.

1.2.2 Two-Pion production in NN collisions — from the ABC-effect to the ABC-resonance?

Complementary to the studies of photo- and pion-induced two-pion production on the nucleon at electron accelerators and meson factories the two-pion production in nucleon-nucleon collisions has been studied systematically at the proton storage rings CELSIUS and COSY. At energies near threshold the single-nucleon excitation is favored — as it is the case in the photo- and pion-induced reactions. Since single-Δ excitation is highly suppressed, single-Roper excitation dominates the near-threshold $\pi\pi$ production. In fact, the respective measurements at T_p = 800 MeV conducted at **COSY-TOF** and carried out with polarized proton beam give results for the Roper resonance properties, which agree with most recent results from the analyses of photo- and pion-induced reactions.

At higher energies double-nucleon excitations come into play solely for proton-induced $\pi\pi$ production. For $T_p >$ 1 GeV the $\Delta\Delta$ excitation becomes the leading process as observed in the respective $N\pi$ invariant mass spectra. Whereas this is in qualitative agreement with theoretical predictions, we find from the full information present in the data that the $\Delta\Delta$ system behaves very differently from what has been predicted.

In order to shed more light onto this problem, a long-standing puzzle in $\pi\pi$ production has been reexamined: the so-called ABC-effect. This acronym stands for an unexpected enhancement at low masses in the invariant $\pi\pi$ mass spectrum $M_{\pi\pi}$ first observed by **A**bashian, **B**ooth and **C**rowe in the double pionic fusion of deuterons and protons to ^{3}He. Follow-up experiments revealed this effect to be of isoscalar nature and to show up in cases, when the two-pion production process leads to a bound nuclear system. With the exception of low-statistics bubble-chamber measurements all experiments conducted on this issue have been inclusive measurements carried out preferentially with single-arm magnetic spectrographs for the detection of the fused nuclei.

Initially the low-mass enhancement had been interpreted as an unusually large $\pi\pi$ scattering length and evidence for the σ meson, respectively. Since the effect showed up particularly clearly at beam energies corresponding to the excitation of two Δs in the nuclear system, the ABC effect was interpreted later on as a t-channel $\Delta\Delta$ excitation in the course of the reaction process leading to both a low- and a high-mass enhancement in isoscalar $M_{\pi\pi}$ spectra.

With **WASA at COSY** we have measured the double-pionic fusion processes to d, ^{3}He and ^{4}He exclusively and kinematically complete with many orders of magnitude higher statistics than in previous measurements. For the most basic fusion process, the one leading to deuterium, first results from the data analysis are now available, see Fig. 2: At the top the spectrum of the $\pi^0\pi^0$-invariant mass $M_{\pi^0\pi^0}$ is shown as a function of the total energy in the center-of-mass system. Our data exhibit an enormeous low-mass enhancement, however, no apparent high-mass enhancement as predicted by conventional $\Delta\Delta$ calculations. Moreover, in the total cross section (Fig. 2, bottom) we observe an unexpected and narrow resonance-like structure — again in contradiction to the conventional $\Delta\Delta$ process (dotted curve for the $\pi^0\pi^0$ channel). As we see from Fig. 2, the ABC-effect, *i.e.* the low-mass enhancement is present only at energies within this narrow resonance strcucture, which has its maximum 90 MeV below the $\Delta\Delta$ mass and a width of only 50 MeV, *i.e.* five times smaller than expected from the conventional t-channel $\Delta\Delta$ excitation. Indeed, describing this structure by a s-channel ansatz leads to a surprisingly good description of both the total and the differential distributions including the ABC effect in the $M_{\pi^0\pi^0}$ spectra. A corresponding resonance has been predicted by various theoretical calculations, some of which even predict this resonance to be a member of a dibaryon multiplet.

From the fact that the ABC effect is observed also for double-pionic fusion processes to heavier nuclei, we conclude that this resonance is obviously robust enough to survive even in nuclei.

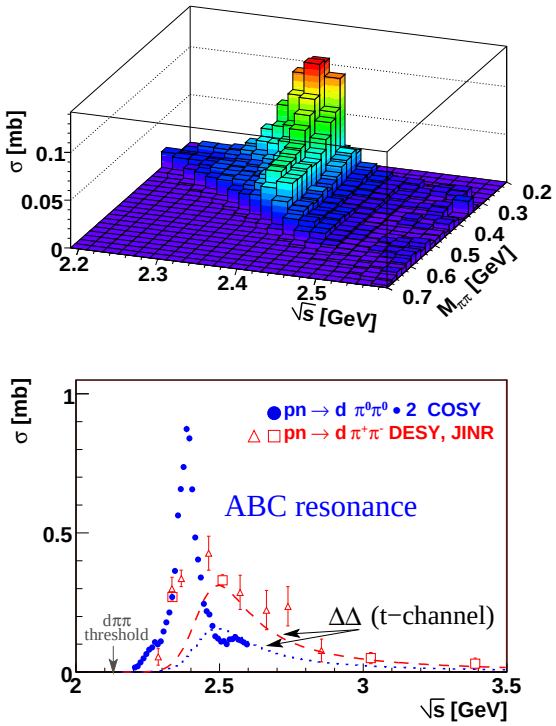

Fig. 2: Top: (Preliminary) energy dependence of $\pi^0\pi^0$ invariant mass $M_{\pi^0\pi^0}$ shown by a 3D-plot of $M_{\pi^0\pi^0}$ versus the total energy in the center-of-mass system $\sqrt{s}$. Bottom: Energy dependence of the total cross section for the $pn \to d\pi^+\pi^-$ reaction from threshold up to $\sqrt{s}$ = 3.5 GeV. Data for the $d\pi^+\pi^-$ channel are from JINR Dubna (squares) and DESY (open triangles). The (preliminary) results of this work for the $\pi^0\pi^0$ channel — scaled by the isospin factor of two — are given by the full circles. Dashed and dotted lines represent t-channel $\Delta\Delta$ calculations for $\pi^+\pi^-$ and $\pi^0\pi^0$ channels, respectively.

1.2.3 Kaon pair production

The analysis of kaon pair production in **ANKE** has revealed yet further interesting physics. In the 2007 Annual Report it was shown that the bulk of the observed distributions in $pp \to ppK^+K^-$ can be understood in terms of pp and K^-p final state interactions. In particular, the K^-p final state interaction (*fsi*) distorts strongly the relative K^-p/K^+p distributions for non-ϕ events. Similar effects have now been seen in the $pn \to dK^+K^-$ reaction which was measured in quasi-free kinematics using a deuterium target. By reconstructing the full kinematics on an event-by-event basis, this allowed several excess energies ε to be investigated simultaneously.

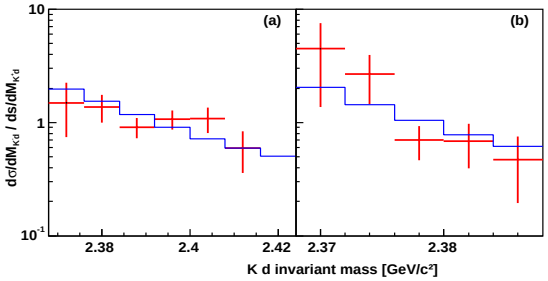

Fig. 3: Ratios of the $K^{\pm}d$ invariant mass distributions for (a): $42 < \varepsilon < 52$ MeV, (b): $12 < \varepsilon < 22$ MeV. The histograms are simulations with a K^-d scattering length of $a_{Kd} = (-1.0 + i1.2)$ fm.

Figure 3 shows the ratio R_{Kd} of the differential cross sections, $\mathrm{d}\sigma/\mathrm{d}M_{K^-d}$ divided by $\mathrm{d}\sigma/\mathrm{d}M_{K^+d}$. This has a very strong preference for low Kd invariant masses, M_{Kd}, arising from the K^-d *fsi*. If this is paramaterised in terms a K^-d scattering length a_{Kd}, one expects $R_{Kd} \propto |1 - ika_{Kd}|^{-2}$, where k is the relative momentum in the K^-d system. The simulation shown in Fig. 3 used $a_{Kd} = (-1.0 + i1.2)$ fm, which is a typical value from the literature. This is one more confirmation that the $\bar{K}$ is strongly attracted to nucleons and that this can be investigated through the study of *fsi* following kaon pair production.

The analysis of the experiment also allowed one to extract the energy dependence of the total $pn \to dK^+K^-$ production cross section. The results shown in Fig. 4, which exclude the ϕ contribution, illustrate also the available data on the $pp \to ppK^+K^-$ and $pp \to dK^+\bar{K}^0$ reactions. It is clear from a comparison of these different data sets that, after correcting for the different phase spaces, the total cross sections for the $pp \to ppK^+K^-$, $pn \to dK^+K^-$, and $pp \to dK^+\bar{K}^0$ reactions are very similar in magnitude. A common theoretical model to describe all three channels is highly desirable.

The K^-p and pp *fsi* alone do not describe the $pp \to ppK^+K^-$ data at low K^+K^- masses and this indicates that an *fsi* is also needed in this channel. The effects are smaller here and, to illustrate them, the experimental data at all three ANKE energies have been divided by the simulations that included K^-p and pp *fsi*, see Fig. 5. The enhancement is most prominent between the K^+K^- and $K^0\bar{K}^0$ thresholds so that it is also influenced by virtual $K^0\bar{K}^0$ production and its subsequent con-

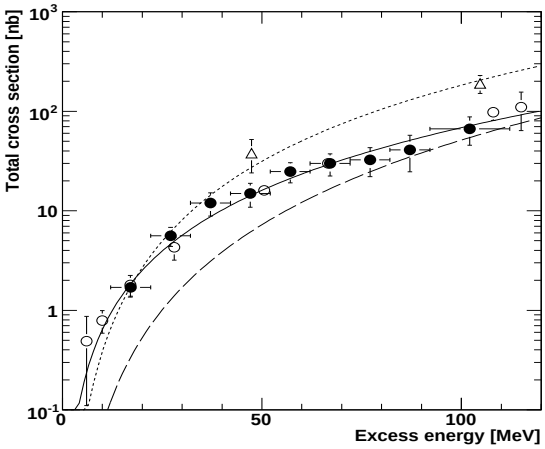

Fig. 4: Total cross section for non-ϕ $K\bar{K}$ production in nucleon-nucleon collisions near threshold. The data are for $pn \to dK^+K^-$ (closed circles), $pp \to dK^+\bar{K}^0$ (open triangles), and $pp \to ppK^+K^-$ (open circles). The dotted curve is the best fit for $pp \to dK^+\bar{K}^0$ data, whereas the solid curve describes the energy dependence of the $pn \to dK^+K^-$ total cross section. The dashed curve represents the subsequent prediction for $pn \to \{pn\}_{I=0}K^+K^-$.

version into K^+K^- through a charge-exchange *fsi*. This might generate a cusp at the $K^0\bar{K}^0$ threshold. Describing the coupled-channel *fsi* in a K-matrix formalism, the necessary inputs are the $K\bar{K}$ scattering lengths for isospin $I = 0$ and $I = 1$ and also the relative amplitudes for undistorted $I = 0/I = 1$ production. The best agreement shown in Fig. 5 is achieved with the kaon pairs being produced dominantly in isospin-zero. This manifests a cusp at the $K^0\bar{K}^0$ threshold, though the data themselves are not yet sufficiently precise to distinguish this effect unambiguously from a smoother threshold enhancement.

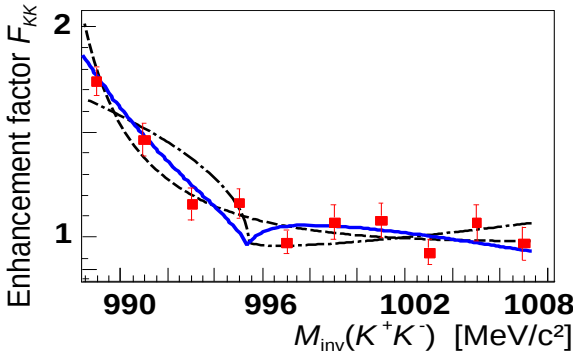

Fig. 5: Ratio of the K^+K^- invariant mass spectra from the $pp \to ppK^+K^-$ reaction to a simulation that includes K^-p and pp *fsi*. The experimental points correspond to the weighted average of data taken at 2.65, 2.70, and 2.83 GeV. The solid curve is the best theoretical fit; the dot-dashed curve neglets elastic rescattering and the dashed is obtained when charge-exchange is omitted.

1.2.4 Λ- Nucleon interactions

The Λp interaction has been investigated with the high-resolution **Big Karl** magnetic spectrograph. Like for the np system, the Λp pair can be a spin singlet $^3S_1$ and a triplet $^3S_1$ state. The total cross section of Λp scattering had been observed in bubble chambers down to 130 MeV/c momenta. The bubble chamber method suffers from the meager statistics. In addition, statistical error bars are largest for the smallest Λ momenta. However, this range is the only one which is sensitive to effective range parameters. Even neglecting the singlet state completely gives a good fit.

Another way to reach smaller energies is provided by a three body final state $p+p \rightarrow K^+ + \Lambda + p$ known as associated strangeness production. Siebert *et al.* measured this reaction at SATURNE for laboratory energies of 2.3 GeV and 2.7 GeV by detecting the kaon at cm angles 18.5° to 71°. They found a steep raise of the cross section at the Λp threshold and another one at the $\Sigma^0 p$ threshold. These data were analysed in terms of effective range parameters by Hinterberger and Sibirtsev, including the bubble chamber measurements into the analysis. The cross section for the $p+p \rightarrow K^+ + \Lambda + p$ reaction was assumed to have the form

$$\frac{d^2\sigma}{d\Omega_K dM_{\Lambda p}} = \left(\frac{1}{4}|f_{Bs}|^2 \frac{q^2+\beta_s^2}{q^2+\alpha_s^2} + \frac{3}{4}|f_{Bt}|^2 \frac{q^2+\beta_t^2}{q^2+\alpha_t^2}\right) \Phi_3 \quad (2)$$

with Φ_3 the three body phase space. f_B are the production amplitudes and α and β are the parameters of the Bargmann potential

$$V(r) = -\frac{8\alpha^2}{\alpha^2-\beta^2}\left(\frac{e^{\alpha r}}{\alpha-\beta} + \frac{e^{-\alpha r}}{\alpha+\beta}\right)^{-2},$$

which has the effective range expansion as exact solution. The fractions in Eq. (2) are the enhancement factors in terms of inverse Jost functions. The results are allowed ranges for the effective ranges as function of the scattering lengths.

In order to study the Λp interaction further the $p+p \rightarrow K^+ + \Lambda + p$ reaction has been measured at a beam momentum of 2.735 GeV/c corresponding to 1953.2 MeV, which is 133.2 MeV above threshold. This is closer to the threshold than the SATURNE study. Kaons were detected by Big Karl under forward angles. Suppression of protons and pions was achieved by means of time-of-flight and a dedicated threshold Cherenkov detector using silica aerogel. The obtained missing mass spectrum is shown in Fig. 6 sorted in 1.0 MeV wide bins. The resolution achieved of 0.32 MeV can be compared to 2 MeV at SATURNE. This resolution together with the high statistics rule out a narrow strangeness -1 dibaryon in the measured range especially at 2.0965 and 2.098 GeV.

We make use of the calculations by adjusting only $|f_{Bs}|^2$. By doing so it is guaranteed that also the SATURNE data

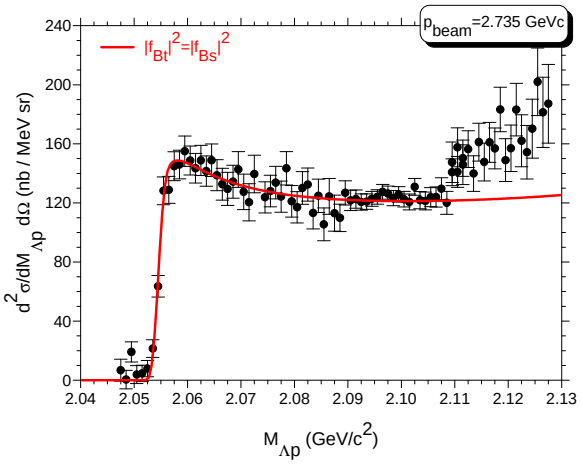

Fig. 6: Missing mass spectrum of the associated strangeness production. The data are a compilation of several spectrometer settings with different statistics. Shown is the sum for singlet and triplet final state interaction between the Λ and the proton taken from Hinterberger and Sibirtsev for the ratio of the matrix elements indicated in the figure. Only one matrix element is fitted to the present data.

as well as the elastic cross section data are accounted for. Figure 6 shows as an example the case $|f_{Bs}|^2 = |f_{Bt}|^2$. The shape of the experimental missing mass function is well reproduced up to 2.11 GeV/c^2, where the well known enhancement below the $\Sigma^0 p$ threshold shows up. This is an indication that the assumption $|f_B| = const.$ holds well. It should be mentioned that the sharp rise of the cross section above threshold is here within 4.5 MeV compared to 9 MeV in the SATURNE work, because of the less smearing due to the higher resolution.

The allowed area of effective range parameters can be compared with those from another reaction, which is $K^- + d \rightarrow \pi^- + \Lambda + p$. Several experiments were performed absorbing the kaon in flight. Tan studied this process with kaons at rest. In the entrance channel the deuteron wave function is known and hence the amplitude. Also the low energy $\bar{K}p$ interaction is known. One can then extract the Λp final state interaction. At low energies the dominant partial wave can be expected to be the s wave. Then from angular momentum and parity conservation it follows that the Λp system will be produced in the same state as the deuteron, *i.e.* the $^3S_1$ state. The parameters extracted overlap only within error bars with the range given by Sibirtsev and Hinterberger.

Also the enhancement in the cross section with a peak at 2.129 GeV/c^2 was seen in the spectra from kaon absorption at rest as well as in flight. Our present result is in nice agreement with these experimental findings. Various theoretical interpretations are in the literature for this peak.

1.2.5 Study of the $d+d \to \eta+\alpha$ reaction close to threshold

There has been a long standing interest whether η mesons can be bound to nuclei. In contrary to pionic atoms, where the binding is due to the Coulomb force, the binding occurs via the strong interaction and hence such systems are mesic nuclei. There are indications that already ^{3}He may be heavy enough to bind the η. If this is so then ^{4}He should bind even stronger. A good candidate to study this problem is the $d+d \to \eta+\alpha$ reaction. The idea is that the s-wave amplitude can be factorised in a weak production amplitude and a strong final state enhancement factor.

Based on the existing close-to-threshold data the s-wave was extracted as

$$\frac{\mathrm{d}\sigma}{\mathrm{d}\Omega} = \frac{p_\eta}{p_d}|f_s|^2 = \frac{\sigma}{4\pi}$$

with f_s the spin averaged s-wave amplitude. This assumption is, however, not appropriate for higher energies, although still applied in the literature. To overcome this problem differential cross sections as well as analysing powers have been measured for the reaction with a tensor polarised beam. The polarisation was measured by comparing elastic dp backward scattering with earlier results from Saclay. This is the first work which measured qualitatively new data employing a tensor polarised deuteron beam at **Big Karl**.

The experiment was performed in two stages. First an unpolarised deuteron beam with high intensity has been used to measure the differential cross section. In the second stage polarised beams with spin up, spin down and also unpolarised have been used. The latter was produced in the ion source by three transitions, so some polarisation may have remained. We, therefore, did not use this beam and developed a method to extract the analysing power A_{xx} without making use of unpolarised cross sections. The resulting angular distributions for the differential cross section and the analysing power are shown in Fig. 7. Because both observables are even functions of $\cos\theta$ they are plotted as function of $\cos^2\theta$. The knowledge of these distributions allows a partial wave analysis and/or spin-amplitude decomposition. First, the symmetries in this reaction have been used, *i.e.* bosons in the entrance and exit channel, parity and total angular momentum conservation to show that only s-, p-, and two d-waves can occur, if one truncates after d-waves.

The results are also shown in Fig. 7. When expressing the partial wave amplitudes in terms of the spin amplitudes it becomes clear why in the latter frame fewer parameters exist. The two d-waves are strongly correlated. In case of the spin amplitudes it becomes even possible to decouple the amplitudes into two groups and fit them separately. The latter shows that a possible p-wave is negligibly small. Therefore the deviation from anisotropy seen in previous experiments is only due to s-d wave interference. Since the amplitudes of the d-waves vary with p_η^2 the amplitudes can be extracted at the momenta of previous experiments from the present result and a corrected spin-averaged amplitude is derived.

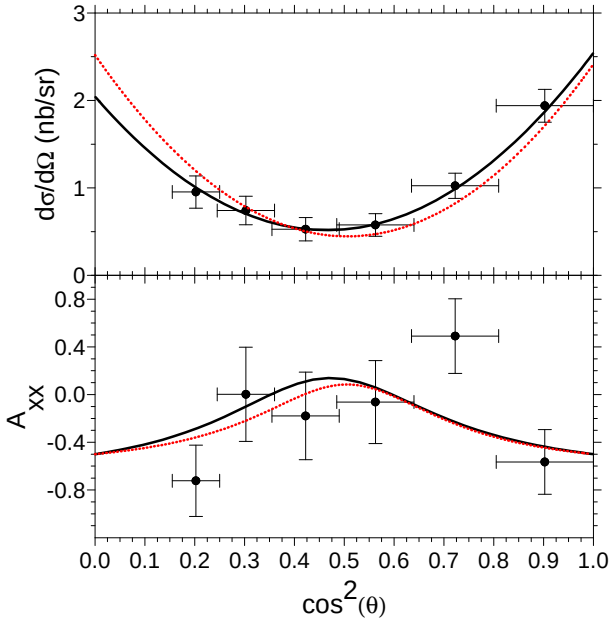

Fig. 7: Upper frame: angular distribution of the differential cross sections. The fits with partial wave amplitudes are shown as black solid curve, those with spin amplitudes as red dotted curve. Lower frame: same but for the analysing power A_{xx}.

The extracted spin averaged amplitude can be expressed as

$$|f_\varsigma|^2 = \frac{|f_B|^2}{1+p_\eta^2(a_r^2+a_i^2)+2p_\eta a_i}$$

with f_B the production amplitude, assumed to be a constant in the range of interest and $a = a_r + ia_i$ the complex scattering length. When fitting the effective range expansion the number of fit parameters went up from three to five. This leads to strong correlations because of the quality of the data.

The extracted complex scattering length is $|a_r| = 3.1 \pm 0.5\,\mathrm{fm}$ and $a_i = 0 \pm 0.5\,\mathrm{fm}$ corresponding to a quasi-bound or virtual state with $|Q_0| \approx 4$ MeV. Unitarity demands that the imaginary part of the scattering length be positive, *i.e.* $|a_i| < |a_r|$. Finally, in order that the pole lie on the bound- rather than the virtual-state plane, one needs also $a_r < 0$. The above-threshold data are, of course, insensitive to the sign of a_r so that they could never tell whether the system is quasi-bound or virtual. However, one can argue that the system is likely to be quasi-bound, because $|Q_0(^3\mathrm{He})| < |Q_0(^4\mathrm{He})|$.

1.2.6 Inverse diproton photodisintegration at intermediate energies

Photoabsorption on two-nucleon systems in nuclei at several hundred MeV allows one to probe fundamental properties of nuclei at short distances. The photodisintegration of the simplest nucleus, the deuteron, through the $\gamma d \to pn$ reaction is widely used as a testing ground for different theoretical ideas of the nucleon-nucleon interaction. However, much less is known, both experimentally and theoretically, on the other simplest process,

$$\gamma + \{pp\}_s \to p + p \,, \tag{3}$$

where $\{pp\}_s$ is a proton pair in the $^1S_0$ state. In this case, due to selection rules and in contrast to photodisintegration of the deuteron, there is no direct contribution from S-wave ΔN intermediate states, and M-odd multipoles are forbidden. Furthermore, since the diproton has no electric dipole moment, only the spin-flip contribution to the $E1$ operator survives. Therefore, features of the underlying dynamics, which are not visible in the photodisintegration of the deuteron, may reveal themselves.
In the absence of a free bound diproton, reaction (3) has only been investigated for a $^1S_0$ diproton bound within a nucleus, the lightest of these being ^{3}He. However, in reactions with light nuclei the total cross section for photon absorption by two protons is only a small part of the total rate, and extraction of the process suffers from large backgrounds. These contaminations are absent in the inverse reaction with the production of a free $^1S_0$ diproton

$$p + p \to \gamma + \{pp\}_s \,. \tag{4}$$

At excitation energies E_{pp} of the final pp pair less than 3 MeV, the system is almost exclusively in the $^1S_0$ state.
The experiment was performed at **ANKE** for proton beam energies of T_p=0.353, 0.500, and 0.550 GeV. The determination of the four-momenta of the two final protons allows a full kinematical reconstruction of $pp \to ppX$ events and the derivation of the missing-mass spectra for the pairs with $E_{pp} < 3$ MeV. While in our previous studies at T_p = 0.625 and 0.8 GeV only a hint of reaction (4) could be seen, for the present energies a clear peak is revealed around $M_x^2 \approx 0$ (Fig. 8). This is well separated from the π^0 signal at 0.353 GeV, whereas at 0.5 and 0.55 GeV the two structures partially overlap because of broadening of the pion peak away from the production threshold. The E_{pp} spectrum of events from the γ peak is consistent with pure $^1S_0$ production.
The differential cross sections $\mathrm{d}\sigma/\mathrm{d}\Omega_{pp}$ as a function of the diproton polar angle θ_{pp} were obtained for events with $E_{pp} < 3$ MeV in the γ peak of the M_x^2 distributions after subtraction of the background contamination. The differential cross section as a function of $cos^2\theta_{pp}$, shown in Fig. 9a, indicates a very strong dependence upon this variable. The cross sections for the $pp \to \{pp\}_s\gamma$ reaction are compared in Fig. 9b with those of $np \to d\gamma$ deduced from the Mainz data on inverse reaction. The absolute values of the small-angle cross section for $pp \to$

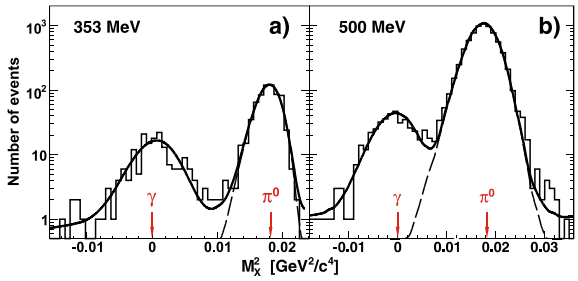

Fig. 8: Missing-mass-squared distributions for the $pp \to ppX$ reaction for events with $E_{pp} < 3$ MeV.

$\gamma\{pp\}_s$ are about two orders of magnitude lower than for $np \to d\gamma$ and its unexpected rise with energy may be related to $\Delta(1232)$ excitation. The rapid variation of the cross section with angle allows an estimate to be made of the ratio of the $E1$ and $E2$ multipole intensities.

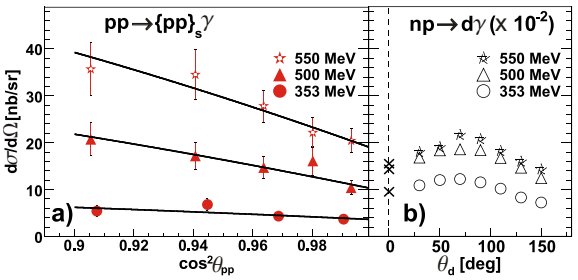

Fig. 9: (a) Angular dependence of the c.m. differential cross section of the $pp \to \{pp\}_s\gamma$ reaction. The full curves represent the quadratic fits. (b) Differential cross section for the $np \to d\gamma$ reaction deduced from the Mainz data on the inverse reaction. Crosses at $\sigma_d = 0^\circ$ are theoretical expectations for energies (down to up) of 353, 500, 550 MeV.

It is crucial that the reaction studied, $pp \to \{pp\}_s\gamma$, does not suffer from the drawbacks inherent in photoabsorption on ^{3}He, *i.e.* the presence of multinucleon absorption. A detailed study of this fundamental reaction might open up a new way to investigate the properties of the pp system at high momentum transfers under conditions that allow a clean interpretation.

1.2.7 np charge-exchange amplitude studies

An understanding of the NN interaction is fundamental to the whole of nuclear and hadronic physics. The database on proton-proton elastic scattering is enormous and the wealth of spin-dependent quantities measured by EDDA collaboration has allowed the extraction of NN phase shifts in the isospin $I = 1$ channel up to a beam energy of at least 2 GeV. The situation is far less advanced for the isoscalar channel where the much poorer neutron-proton data only permit the $I = 0$ phase shifts to be evaluated up to at most 1.3 GeV but with significant ambiguity above about 800 MeV.

The **ANKE** collaboration has been embarked on a systematic programme to measure the differential cross section and analysing powers of the $dp \to \{pp\}n$ reaction up to the maximum energy at COSY of 1.15 GeV per nucleon, with the aim of deducing information on the np amplitudes. Higher energies per nucleon will be achieved through the use of a proton beam and deuterium target. Spin correlations will also be studied with a polarised beam and target. However, for these to be valid objectives, the methodology has to be checked in a region where the np amplitudes are reasonably well known.

The charge-exchange amplitude of $np \to pn$ scattering may be written in terms of five scalar amplitudes (cf. Annual Report 2006): the spin-independent amplitude α between the initial neutron and final proton, a spin-orbit contribution γ, and the spin-spin terms β, δ, ε. The one-pion-exchange pole is contained purely in the δ amplitude and this gives rise to its very rapid variation with momentum transfer, which influences very strongly the deuteron charge-exchange observables.

Within the limits of impulse approximation applied to $dp \to \{pp\}_{^1S_0}n$ a measurement of the differential cross section, and the spherical tensor analysing powers t_{20}, and t_{22} would allow one to extract values of $|\beta(q)|^2 + |\gamma(q)|^2$, $|\delta(q)|^2$, and $|\varepsilon(q)|^2$ for small values of the momentum transfer $\vec{q}$ between the initial proton and final neutron. However, even if a sharp cut of 1 MeV is placed upon E_{pp}, there still remain small contributions from proton-proton P-waves that dilute the analysing power signal. Such effects must be included in any analysis aimed at providing quantitative information on the neutron-proton amplitudes.

The variation of the cross section with q can be found in Fig. 10 for $E_{pp} < 3$ MeV. The impulse approximation describes well the dependence on this variable out to $q =$ 140 MeV/c.

The experimental values of the two tensor analysing powers are shown in Fig. 11 as a function of the momentum transfer. The rapid rise of t_{22} with q is mainly a result of the fall in the $\delta(q)$ amplitude which, in a simple absorbed one-pion-exchange model, should vanish for $q \approx m_\pi c$. The much smoother variation of t_{20} is also expected, with a gentle decline from the forward value, once again being mainly driven by the fall in the $\delta(q)$ amplitude. All these features are well reproduced by the impulse approximation model using reliable np amplitudes.

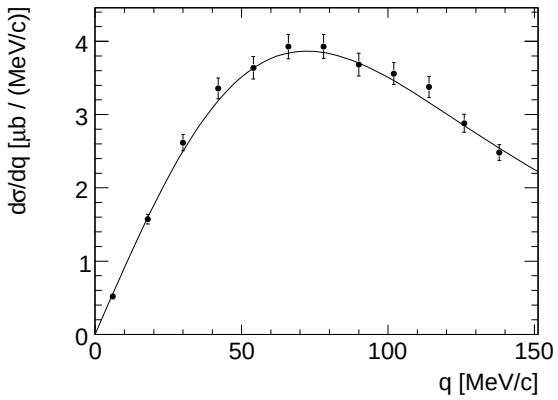

Fig. 10: Unpolarised differential cross section at $T_d = 1.17$ GeV for the $dp \to \{pp\}n$ reaction of $E_{pp} < 3$ MeV compared with the impulse approximation.

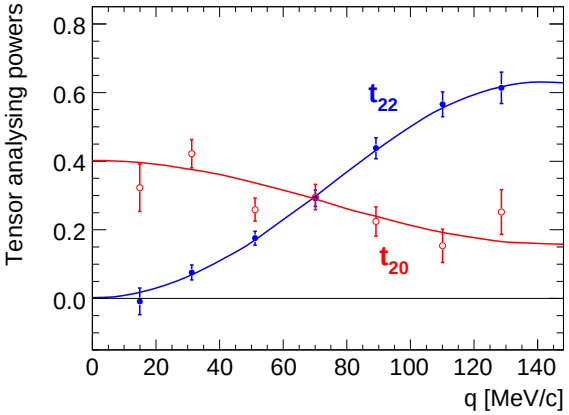

Fig. 11: Spherical tensor analysing powers t_{20} (open symbols) and t_{22} (closed) for the $\vec{d}p \to \{pp\}n$ reaction at $T_d/2 = 585$ MeV for $E_{pp} < 1$ MeV. The solid curves are the impulse approximation predictions.

Although all the experimental data agree with the impulse approximation model one could, invert the question. How well one could determine the amplitudes if there were no information available from the np phase shifts? Although the data reported here were obtained over short run, these are already sufficient to determine quite well the ratio of the $|\varepsilon(0)|/|\beta(0)|$ in the forward direction. Since little dilution of the t_{20} signal is expected at $q = 0$, all the data for $E_{pp} < 3$ MeV were fitted to a quadratic in q^2 for $q \leq 100$ MeV/c. The value obtained at the origin gives $t_{20} = 0.37 \pm 0.02$, where the error is purely statistical. The uncertainty introduced by the beam polarisation would, however, contribute less than ± 0.01 to this. Since there is little or no dilution of the analysing power by the P-waves at $q = 0$, this result translates into an amplitude ratio of $|\varepsilon(0)|/|\beta(0)| = 0.61 \pm 0.03$.

The proof-of-principle achieved here for the method suggests that measurements at higher energies will provide useful information in regions where the existing np database is far less reliable.

1.2.8 Do unpolarized electrons affect the polarization of a stored beam?

The QCD physics potential of experiments with high energy polarized antiprotons is enormous, but up to now high-luminosity experiments have been impossible. The situation would change dramatically with the production of stored polarized antiproton beams, and the subsequent realization of a double-polarized high-luminosity antiproton-proton collider. The list of fundamental physics issues to be addressed with such a collider includes the measurement of transversity, the quark transverse polarization inside a transversely polarized proton, which constitutes the last missing leading twist piece of the QCD description of the partonic structure of the nucleon. The transversity can be directly accessed only via double-polarized antiproton-proton Drell-Yan production. Without a measurement of the transversity, the spin tomography of the proton will remain incomplete. Other items of interest are the measurement of the phases of the timelike form factors of the proton, and double-polarized hard antiproton-proton scattering.

The PAX collaboration (**P**olarized **A**ntiproton e**X**periments) has formulated its ambitious physics program and a Technical Proposal has recently been submitted for the new Facility for Antiproton and Ion Research (FAIR) to be built at GSI in Darmstadt, Germany. The uniqueness and the strong scientific merits that would become available with the advent of stored beams of polarized antiprotons have been well received, and there is now an urgency to convincingly demonstrate experimentally that a high degree of antiproton beam polarization can be reached. The suggested collider aims at luminosities in excess of 10^{31} cm^{-2}s^{-1}. An integral part of such a machine is a dedicated large-acceptance Antiproton Polarizer Ring (APR), for which a basic design has been developed.

The original idea of PAX to use polarized electrons to produce a polarized beam of antiprotons has triggered further theoretical work on the subject, which led to a new suggestion by a group from Mainz to use co-moving electrons (or positrons) at slightly different velocities than the orbiting protons (or antiprotons) as a means to polarize the stored beam. The cross section for $e\vec{p}$ spin-flip predicted by the Mainz group in a *numerical* calculation is as large as about $2 \cdot 10^{13}$ barn, if the relative velocities between proton (antiproton) and electron (positron) are adjusted to $v/c \approx 0.002$. At the same time, *analytical* predictions for the same quantity by a group from Novosibirsk range well below a mbarn.

In order to provide an experimental answer for this puzzle, the ANKE and PAX collaborations joined forces at COSY and mounted an experiment, where for the first time, electrons in the electron cooler have been used as a target, and in which the effect of electrons on the polarization of a 49.3 MeV proton beam orbiting in COSY was determined. Instead of studying the buildup of polarization in an initially unpolarized beam, here the inverse situation was investigated by observation of the depolarization of an initially polarized beam. The proton beam polarization has been measured by making use of the analyzing power of $\vec{p}d$ elastic scattering on a deuterium cluster jet target. The experimental setup of the polarimeter consisting of two telescopes, each of them containing two 300 μm thick layers of Silicon. The energy deposit in the first detector layer is plotted as a function of the energy deposit in the second layer in Fig. 12. The upper band corresponds to deuterons and the lower one to protons from pd elastic scattering.

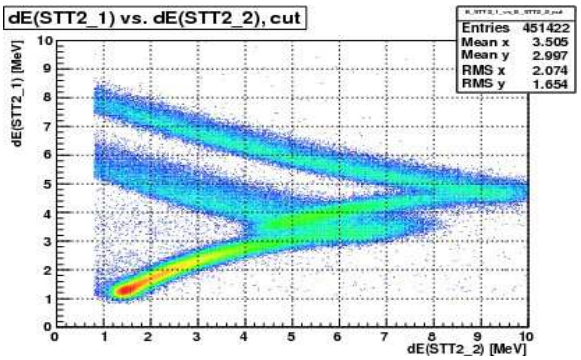

Fig. 12: Identification of pd elastic scattering in the detector system.

The depolarizing cross section is determined from the ratio of the measured beam polarizations P_{detuned} and P_{tuned}. These polarizations correspond to well-defined changes of the electron velocity with respect to the protons, which were achieved by detuning the accelerating voltage in the electron cooler by a specific amount.

The depolarizing cross section (see cover page) is plotted as a function of the magnitude of the electron velocity in the proton rest frame. The measurement shows that the predictions by the Mainz group were too large by at least six orders of magnitude. It should be noted that very recently, the Mainz group has submitted two errata to their original publications stating that because of numerical problems in the calculation their theoretical estimates were too large by about 15 orders of magnitude.

The depolarization study is the first step of investigations at COSY, shedding light on the ep spin-flip cross sections with unpolarized target electrons. The experimental finding rules out the practical use of polarized leptons to polarize a beam of antiprotons with present-day technologies. This leaves us with the only proven method to polarize a stored beam in situ, namely *spin filtering* by strong interaction. At present, we are lacking a complete quantitative understanding of all underlying processes, therefore the PAX collaboration aims at high-precision polarization buildup studies with transverse and longitudinal polarization using stored protons in COSY. In contrast to the pp system, the experimental basis for predicting the polarization buildup in a stored antiproton beam by spin filtering is practically non-existent. Therefore, it is of high priority to perform, subsequently to the COSY experiments, dedicated spin-filtering experiments using stored antiprotons at the AD of CERN.

1.3 Developments for the Experimental Facilities

1.3.1 Commissioning of the COSY-TOF Straw Tracker

The new COSY-TOF Straw Tube Tracker (STT) is an essential upgrade of the existing TOF apparatus for the future program *Strangeness Physics* at COSY-TOF. Mandatory for this program which contains for instance the measurement of the Λ-Nucleon scattering length to an accuracy better than 0.3 fm, is excellent tracking and vertex reconstruction of the primary and delayed decay tracks of the $pp \rightarrow pK^{+}\Lambda$ reaction.

Technically, the operation of a large-volume gas chamber in the surrounding TOF vacuum is an outstanding challenge. Only very few similar detector systems are currently operated or planned in future. The STT consists of 3120 straws with 10 mm inner diameter and 1050 mm length, close-packed in 15 double-layers at 6 different azimuthal alignments (see Fig. 13). The mylar film thickness of each straw is 30 μm, resulting in a very low radiation length of $X/X_0 \simeq 1.5\%$ of the whole detector. All straws are operated at an overpressure of 1.25 bar Ar/CO_2(10%) which provides a strong wire- and film-tube stretching for all straws equivalent to 125 kg and 3100 kg, respectively. With this self-supporting feature of the straw layers no reinforcement or heavy frame structures are necessary. The layer arrangement guarantees sufficient space for tube elongation by short-term pressure changes due to evacuation or a sudden venting incident of the TOF vacuum barrel.

The readout electronics inside the TOF vacuum barrel consists of low-power transimpedance preamplifiers directly connected to each straw, followed by 5.5 m long coaxial signal cables. A dedicated flange at the TOF front cap provides the connection of the 3120 signal lines, 75 high-voltage channels and 30 gas lines from the vacuum to outside. The flange was designed and constructed by IKP/ZAT. The detector signals are readout by leading-edge discriminators based on the ASD8-chip and TDCs based on the GPX-chip. Four TDC crates, placed near the COSY-TOF apparatus, and are readout in parallel via optical link. The TDC readout was developed by ZEL-FZJ.

The STT was installed in the COSY-TOF spectrometer during summer 2008. The apparatus had to be opened and the straw tube layers were mounted at the inner side of the removed front cap (see Fig. 13). A gas system with mixing unit and pressure control was set up outside the TOF beam area to provide permanent user access. Up to six 50 m long stainless steel pipes provide the gas support from the control rack to the STT detector. Concerning the readout in total 40.5 km signal cables were mounted and more than 5000 connectors had to be plugged.

A two days commissioning beam time with 3 GeV/c protons in August 2008 was used to setup and check the operation of the detector and electronic readout. Events from the reactions $pp \rightarrow pp$ and $pp \rightarrow d\pi^{+}$ were recorded and will be used for a calibration and performance tests of the detector like spatial resolution and efficiency.

Fig. 13: The Straw Tube Tracker at the COSY-TOF front-cap before its final mounting to the TOF vacuum barrel (at left side). The tracker consists of a stack of 15 straw double-layers.

Fig. 14 shows a sum spectrum of the raw TDC data of one double-layer consisting of 208 straws. The rising edge of the drift time spectrum starting at about 640 ns corresponds to particle crossings close to the straw wire. The falling edge at about 770 ns maximum drift time is related to tracks close to the straw tube wall. The background induced by additional beam particle interactions shows a broad time spread recuring every 600 ns. As can be seen this background is below the 1% level.

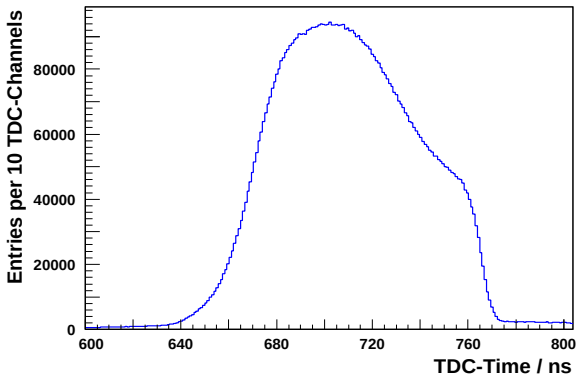

Fig. 14: Drift time distribution of one straw double-layer. The minimum and maximum drift times are at about 640 ns and 770 ns, respectively. The drift times are not offset corrected.

1.3.2 Achievements with the WASA Detector

In 2008, WASA-at-COSY has successfully continued its physics programme focussing on the study of symmetries and symmetry breaking mechanisms in η decays and the charge symmetry violating $dd \to {}^4\mathrm{He}\,\pi^0$ reaction. Exclusive data have also been taken on the manifestation of the ABC effect in the simplest two-pion production reaction leading to a bound nuclear system, $pn \to d\,\pi\pi$. In preparation of experiments in 2008, the scintillator material both for the Plastic Scintillator Barrel and for the Forward Trigger Hodoscope (FTH) has been exchanged, to ensure full detection efficiency, and during the year an additional layer of the Forward Veto Hodoscope (FVH) has been mounted. The long-term stability in deuterium pellet target operation achieved during a four week production run in autumn with a pellet target duty factor well above 90 % marks one of the major milestones in operation of the WASA facility this year.

Detector upgrades

The three-layer Forward Trigger Hodoscope (FTH) was in operation for more than twelve years at the WASA-PROMICE and CELSIUS/WASA experiments. Comparing non-uniformity parameters for different periods in time showed severe aging effects and radiation damage of the detector material. The FTH is crucial for the WASA trigger system, since, in addition to the presently used multiplicity information, it is intended to exploit the position information in a future upgrade of the trigger system to be able to increase the trigger selectivity and operate WASA at higher luminosities. In addition, an optimum performance of the detector is mandatory especially for the identification and separation of helium isotopes needed for the $dd \to {}^4\mathrm{He}\,\pi^0$ programme. Thus, the scintillator material was completely exchanged at the beginning of 2008, to ensure high efficiency operation during the next years and to optimize the intrinsic energy resolution especially in view of helium identification.
The Plastic Scintillator Barrel (PSB) provides both fast signals for the trigger logic to separate charged and neutral tracks and analog signals for particle identification in combination with the electromagnetic calorimeter and/or the central straw chamber (MDC). Since aging of the scintillator material had reduced the light attenuation length in the central part by typically a factor of four, and for some elements the signal from minimum ionizing particles was already close to the noise level, the scintillator material was echanged beginning of 2008 considerably improving the detector performance.
For the tagging of heavier mesons (*e.g.* ω, η') in the $pp \to ppX$ reaction via the missing mass with respect to the detected two-proton system several measures have been initiated: Already in 2007, two additional layers were added to the Forward Range Hodoscope system improving the resolution of the presently used energy loss measurement for forward scattered ejectiles of higher energy. In future, this technique can be supplemented by the installation of a DIRC detector and an additional time-of-flight measurement.
Since after the extension of the FRH system the Forward Veto Hodoscope had to be moved downstream and did not cover the whole range of forward scattering angles any more, a larger second FVH layer was installed and put into operation in autumn. In combination with the Forward Window Counter as a "start counter" first data from the new FVH are presently being analyzed to check the applicability of the time-of-flight measurement at WASA.
A DIRC detector at WASA, with a velocity resolution for high energy protons better than 1 %, would significantly improve the missing mass resolution and thus the signal-to-background ratio for the tagging of heavier mesons. On the other hand, construction of a DIRC detector for the WASA-at-COSY experiment, and operation of the detector under realistic experimental conditions gives at the same time the opportunity to contribute to the necessary R&D work for the future use of the DIRC concept at the PANDA detector at HESR.
The COSY beam was extracted to the COSY-TOF area for testing two different completely assembled DIRC prototype elements with protons in the range of kinetic energies relevant for the tagging of high-energy protons at WASA. Figure 15 shows the experimental setup in the TOF area.

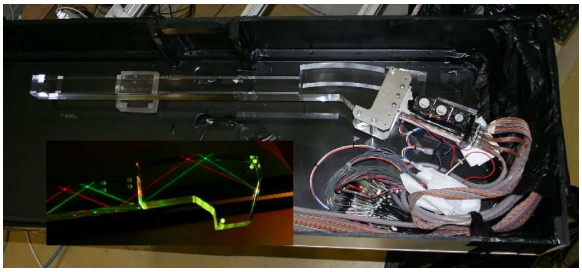

Fig. 15: DIRC prototype radiator with focusing element based on a polynom shaped surface during beam tests at the COSY-TOF area. The surface treatment was completely done at the Jülich workshop.

Prototype radiators have been prepared in the mechanical workshops at the universities of Erlangen and Tübingen, and at the Institut für Kernphysik at the Research Centre Jülich, where also the optical elements were prepared and glued to the radiators. Details and first test results are described in more detail elsewhere in this Annual Report.

Solenoid and pellet target operation

While warming up and cooling down the LHe system during maintenance work at the end of 2007, a leak with a corresponding heat bridge in the transfer line connecting the WASA solenoid to the cryogenic plant increased significantly. As a consequence, the cooling power was

insufficient to provide LHe to the superconducting magnet during the first half of 2008, and measurements with the WASA detector focussing on neutral final states were scheduled earlier to make optimum use of accelerator running time. After installation of a new transfer line in summer 2008 the cryogenic system is fully working again, and the solenoidal field is available for data taking.

During first experimental runs at COSY with deuterium, the nozzle of the pellet target typically blocked after 32 to 40 hours of operation, requiring a following warmup to room temperature for regeneration, and thus limiting the target duty factor to typical values of 80 %. This behaviour was already well-known from operation at CELSIUS, and indicated the presence of water in the gas system. Regeneration cycles warming up to 150 K that can be done in less than three hours, removing *e.g.* frozen nitrogen from the gas system, have been tried before, but with limited success. During a four week production run in autumn 2008 it became possible to operate the deuterium pellet target with short regeneration cycles, most likely due to considerable improvements to the cleanliness of the gas system, As a result the duty factor rises to values above 93 % (Fig. 16).

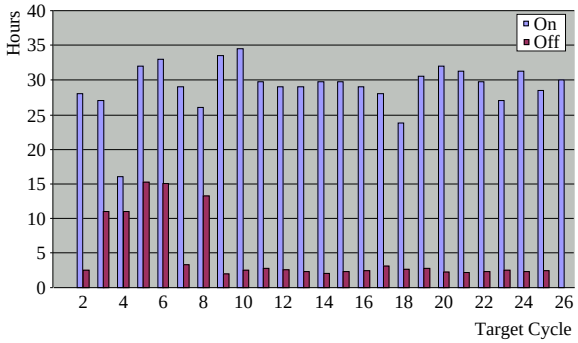

Fig. 16: Deuterium pellet target duty cycle in October 2008. After the last long warmup to room temperature, the duty cycle reaches a value $\geq 93\,\%$. Three "Target-ON" periods were cut short for better coordination in time with the DIRC tests in the COSY-TOF area.

η decays in pd $\rightarrow {}^3$He η

In October 2008, a first four-week long production run focussed on decays of η mesons produced in the reaction $pd \rightarrow {}^3\mathrm{He}\,\eta$ close to threshold. Experimentally, using the reaction $pd \rightarrow {}^3\mathrm{He}X$ allows to trigger and tag η mesons purely by the detection of ^{3}He nuclei in the forward detector, *i.e.* without any trigger bias on the decay system (and thus to determine absolute branching ratios). Figure 17 shows the η signal in the ^{3}He missing mass spectrum.

The data shown in Fig. 17 correspond to $\approx 7.5\%$ of the overall statistics. With a typical counting rate of 800 Hz at a luminosity of about $4 \cdot 10^{31}\mathrm{cm}^{-2}\mathrm{s}^{-1}$ an average of 4.5 η events per second have been recorded. In total, a sample

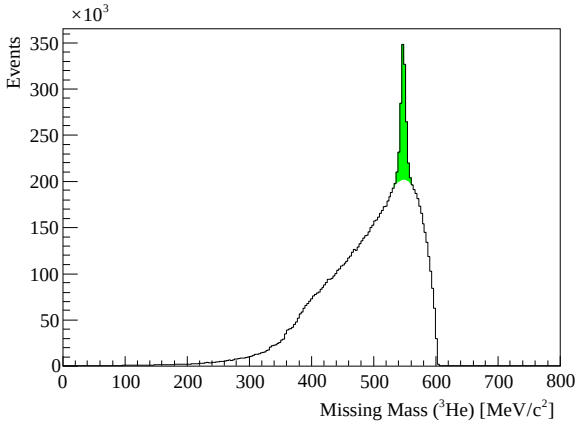

Fig. 17: Online ^{3}He missing mass spectrum determined from the forward detector. The figure is based on 40 hours of data taking and has 660000 events in the peak. With a tuned analysis algorithm, this number can be increased by at least 30 %.

of more than 10^7 η decays was collected on disk during the experiment, enhancing the statistics collected with the WASA detector by more than an order of magnitude.

Charge symmetry breaking in dd $\rightarrow {}^4$He π^0

One of the key experiments for WASA-at-COSY is a measurement of $\vec{d}d \rightarrow {}^4\mathrm{He}\,\pi^0$ to extract the p-wave contribution to the Charge Symmetry (CS) breaking amplitude. In preparation of data taking with polarized deuteron beam, the reaction has been measured with unpolarized beam at a momentum of $\mathrm{p}_d = 1.2\,\mathrm{GeV/c}$ ($\mathrm{T}_d = 351\,\mathrm{MeV}$) to establish the so far unknown cross section, that can only be estimated based on data available at much lower excess energy and to demonstrate the separation of the helium isotopes after installation of the new FTH. Data analysis is presently in progress, and from first checks of the data a total statistics of 500 to 1000 events is expected for the CS symmetry breaking reaction.

Outlook

To enlarge the statistics of η decays, tagged in $pd \rightarrow {}^3\mathrm{He}\,\eta$, eight weeks of beam time have been granted by the PAC for 2009. With this running period a data sample comparable in statistics to the recent data set collected for neutral decay channels by the Crystal Ball and TAPS experiment at MAMI is expected for WASA-at-COSY. Even larger statistics and the study of very rare η decays require η tagging in the $pp \rightarrow ppX$ reaction, and this will become possible with a more selective trigger system for WASA-at-COSY. While efforts to improve both the trigger selectivity and the resolution for high energy protons are the focus of near-future development work, WASA-at-COSY will continue to take competitive data in 2009.

2 COSY Operation and Developments

2.1 Overview

At the COSY accelerator facility concurrent to the reliable routine operation, methods and components for the HESR are now being examined in operation. This research and development benefits greatly from the unique capabilities of COSY providing all the features to investigate the demands to realize the High-Energy Storage Ring (HESR) of the future International Facility for Antiproton and Ion Research (FAIR) at GSI in Darmstadt. The following topics were treated in detail with high priority:

- Further details for the High Energy Storage Ring (HESR) have been worked out. The efforts aimed to advance the design of proposed systems and to increase the knowledge base through beam dynamic simulations and investigations. A new normal conducting lattice has been designed and detailed stochastic cooling simulations have been carried out to demonstrate the cooling capabilities in the new lattice. Studies of beam behaviour with pellet target, barrier bucket and stochastic cooling have been performed in 2008. A first successful demonstration took place in 2008 at COSY.

- The HESR lattice was redesigned with normal conducting magnets. The physical properties of all components are specified and for most of them technical specifications are being developed or are even completed. Prototypes of the accelerating cavity and of the barrier bucket cavity are ready, and performance tests at the COSY beam are in progress. In addition a prototype of a stochastic cooling tank for tests of the newly developed pick-ups could be installed and tested in COSY.

- Two RF cavities will be installed in the High-Energy Storage Ring (HESR) of the future International Facility for Antiproton and Ion Research (FAIR) in Darmstadt. One large cavity will be used for beam acceleration, deceleration and for bunch rotation. Additionally a barrier bucket (BB) with $h = 1 \ldots 5$ will be formed by this large cavity to combine the decelerated bunch with a new injected RESR bunch in the high luminosity mode (HL). During the experiment a small cavity will provide a low noise barrier-bucket signal. Both prototype cavities are manufactured and first RF-measurements were carried out at COSY. The recent results are presented.

- The HESR is planned as an anti-proton cooler ring in the momentum range from 1.5 to 15 GeV/c. An important and challenging feature of the new facility is the combination of highly dense phase space cooled beams with internal targets. A detailed numerical and analytical approach to the Fokker-Planck equation for longitudinal filter cooling including the beam-target interaction has been carried out to demonstrate the stochastic cooling capability. To gain confidence in the model predictions a series of experimental stochastic cooling studies with the internal target at ANKE have been carried out. A remarkable agreement between model and experiment was achieved. On this basis longitudinal stochastic cooling simulations were performed to predict the possibilities and limits of cooling when the newly installed WASA Pellet-target is operated.

- The EDM collaboration started the study for polarimeter development this year. Very high efficiencies in the order of 0.1 to 2% have been reached. Also high precision monitoring of the polarization of a polarized deuteron beam during resonance crossing has been demonstrated in an impressive way.

- SPIN@COSY continued to study the polarization behavior of stored beams of spin-1/2 fermions and spin-1bosons and how to best accelerate polarized protons to higher energy. An experimental test of a new technique to overcome spin-depolarizing resonances shows the potenial of the Kondratenko Crossing proposal.

- Investigation of polarization-loss mechanisms and recovery of proton polarization. Study of beam and polarization life time and dynamic apertures with the PAX collaboration.

- New insights in loss mechanisms in operation of electron cooling showed potential for an intensity increase.

- COSY also contributed its expertise in the context of EU projects and assisted the research of in- and outside users for instance by performing irradiations at the cyclotron and external detector areas.

2.2 Barrier-bucket RF tests

Theoretical investigations of stochastic momentum cooling for the HESR clearly reveal that the strong mean energy loss induced by the interaction of the beam with an internal pellet target cannot be compensated by cooling alone. A promising method to compensate the mean energy loss and thus to provide an antiproton beam with a significantly reduced momentum spread is the application of the broadband barrier bucket (BB) cavity in the HESR which will also be used to avoid detrimental antiproton beam neutralization. Starting from the broadband COSY cavity the design production and assembly of the barrier bucket cavity has finished using one COSY tank with minor changes.

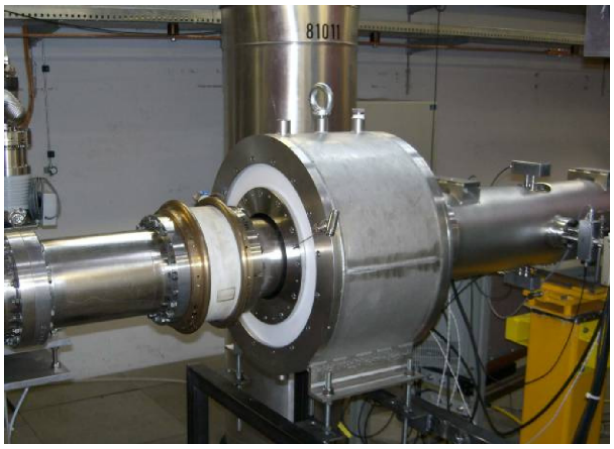

Fig. 18: Barrier bucket cavity with its asymmetric layout is installed in one arc of COSY. The shielding is dismounted to make the gap visible.

The asymmetric layout of the cavity with one gap results in a very compact design (length of cavity without gap: 28 cm). The length from flange to flange including the gap is in the order of 50 cm. The basic parameters of the cavity are summarized in Table 1. After measuring the impedance of the cavity with and without cooling water the cavity was installed in the COSY ring (Fig. 18).

Table 1: Basic parameters of the barrier bucket cavity.

The barrier bucket cavity	
Frequency range	1...20 harmonics (0.4 – 10 MHz)
Gap voltage	10...600 V
Mode of operation	cw
Cooling	Water cooled*
Material	VitroPerm 500F

*Design work started to build a forced airflow solution.

COSY allows for many HESR relevant experiments such as the operation of the prototype barrier bucket cavity together with a pellet target and a stochastic cooling system. During a WASA beam time the barrier bucket operation was tested together with stochastic cooling and a thick hydrogen pellet target. Figure 19 shows the barrier bucket voltage at the gap limited by the available RF power (upper blue curve) and the phase monitor proportional to the bunch distribution of the particles.

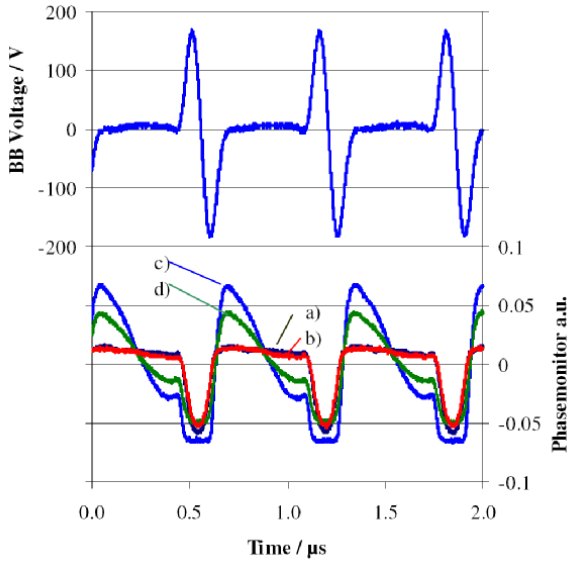

Fig. 19: First barrier bucket operation together with stochastic momentum cooling at COSY.

Curve a) (black) represents the nearly rectangular bunch at the beginning of the cycle formed by the barrier bucket. There is only a small time gap showing that the beam is nearly a DC-beam. Without cooling and without target the rectangular shape remains constant over the whole cycle length of 160 s (curve b) (red)).

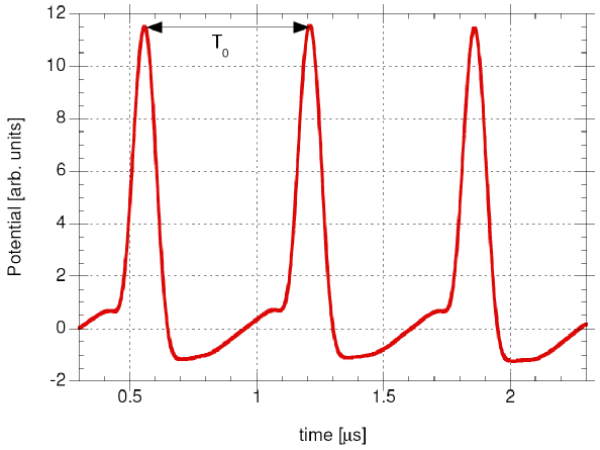

Fig. 20: Potential of the synchrotron motion for the barrier bucket cavity voltage of Fig. 19. The small bank of the voltage between the sinusoidal boundaries is clearly visible as a valley in the potential where a large fraction of the particles can be captured if the momentum spread is sufficiently cooled down.

The voltage in the region between the sinusoidal barrier signals is not identically zero as required for a flat bunch. A small bank of about 3% results in a valley in the potential of the synchrotron motion (Fig. 20). The stochastic cooling collects the particles in this valley so that the bunch now exhibits a hump (Fig. 19, curve c) (blue). The thick pellet target counteracts the stochastic cooling which is directly visible (Fig. 19, curve d)) in a lower asymmetry of the bunch shape. The experiments thus have shown that a flat BB potential is absolutely necessary for a good cooling efficiency and a flat beam distribution. Even a small DC-offset of the voltage may be harmful in as much it induces a small acceleration or deceleration of the beam. The influence of barrier bucket and stochastic cooling is presented in Fig. 21 where the longitudinal spectrum measured at the 1000$^{\text{th}}$ harmonic is plotted.

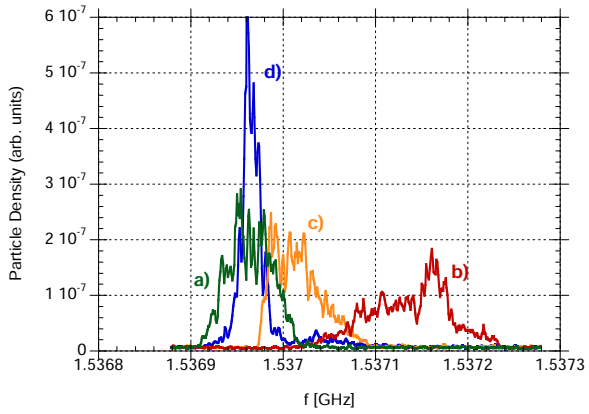

Fig. 21: Schottky spectra of COSY beam measured at the 1000$^{\text{th}}$ harmonic: a) starting distribution, b) final distribution after 160 s only pellet-target, c) final distribution with longitudinal stochastic cooling and d) final distribution with cooling and barrier bucket.

Curve a) represents the momentum distribution at the beginning of the cycle. Without stochastic cooling and barrier bucket, the energy loss and the longitudinal heating by the pellet target is clearly visible over the cycle length of 160 s (curve b)). The momentum in COSY was 2.6 GeV/c. The working point of the machine was above gamma-transition. Thus energy losses result in a shift of the spectra to higher revolution frequencies. Even with the relatively low numbers of particles $N = 8 \times 10^8$ the stochastic cooling (band 2; 1.8–3 GHz) alone is not able to compensate the whole energy loss by the target (curve c)). Curve d) shows the case where the mean energy loss is compensated by the barrier bucket system and the momentum spread is significantly reduced by stochastic cooling. Nevertheless some particles were lost due to the barrier height of $\pm$175 V limited by the available RF-power.

From the frequency shift during the whole cycle yield-

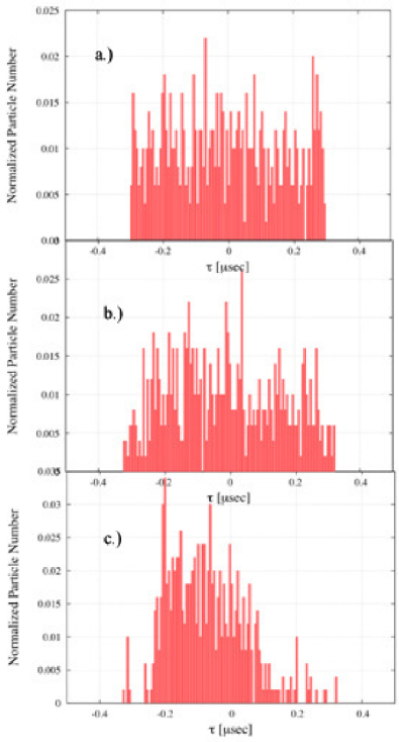

Fig. 22: Tracking results for the bunch shape in the barrier bucket with the measured voltage. The initial bunch is shown in a) When the target and cooling is switched off the initial rectangular bunch shape remains as shown in b) after 160 s. The simulation reproduces the hump after 160 s in the bunch shape when the beam momentum is cooled as shown in c).

ing a mean energy loss of $\approx$ 25 meV/turn we estimated a target thickness of $N_T \approx 3 \times 10^{15}$ atoms/cm^2 which corresponds to the expected PANDA target thickness. The mean energy loss can also be compensated with the normal RF-cavity. Since the voltage is much larger than that of the BB all particles were captured and no losses occurred. However due to the large bunching factor stochastic momentum cooling was rather poor, *i.e.* no cooling effect was visible.

The synchrotron motion of particles in a barrier bucket has been investigated with a numerical tracking code including the beam-target interaction and stochastic momentum cooling. The following figures represent the first results which predict the measurements already quite well. The measured barrier voltage of Fig. 19 resulting in the potential displayed in Fig. 20 was included in the code. Figure 22 shows the simulation results of the initial bunch in the barrier bucket (a)) and after 160 s (b)). In both cases stochastic cooling and target are switched off. The model predictions correspond to the measured bunch shape displayed in Fig. 20b). When the target is switched on together with stochastic momentum cooling the track-

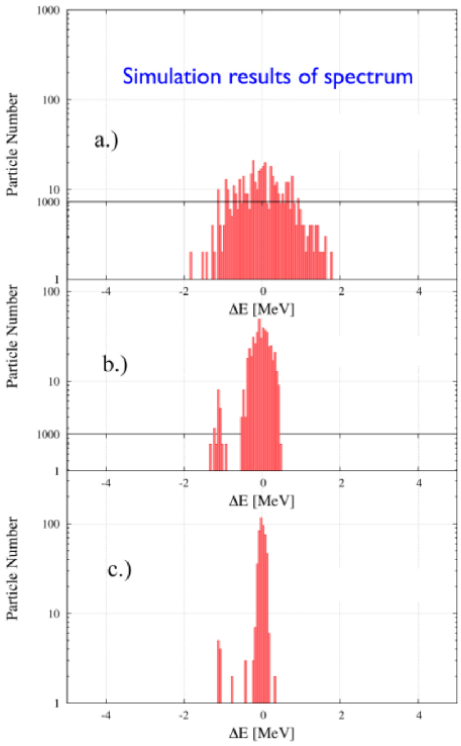

Fig. 23: Simulated beam spectra at initial time (a)), after 60 s (b)) and after 160 s (c)). Stochastic cooling and target are on.

ing results after 160 s, Fig. 23c), reproduce the hump in the bunch due to the valley in the potential.

Figure 23 represents beam spectra at initial time after 60 s and 160 s during stochastic cooling and beam-target interaction. The calculated spectra correspond to the measured distributions as shown in Fig. 21 and show the cooling effect when the target is on. The mean energy is kept constant by the barrier bucket. The first barrier bucket simulations including beam cooling and beam-target interaction already produce beam energy spectra that are in close agreement with the experimental results. The calculated bunch shape after 160 s is in accordance with the measured one. The simulations make clear that the particles are trapped in the potential valley resulting in a more sharply bunched beam.

The simulations indicate that a higher barrier voltage with a flat potential minimum will be necessary to confine all particles in the barrier. Strong cooling is necessary to reduce the momentum spread especially for a larger number of particles. Further improvements of the barrier bucket model including momentum cooling and beam-target interaction are envisaged and predictions will be tested in beam dynamics studies at COSY.

2.3 Polarimeter development to search for a permanent EDM of the Deuteron

The **dEDM** Collaboration intends to search for an electric dipole moment (EDM) in the deuteron using a polarized deuteron beam in a storage ring, where one hopes to achieve sensitivity levels approaching 10^{-29} e·cm. If an EDM is present, the polarization, which would initially lie in the plane of the storage ring, would rotate and lead to a growing vertical polarization component. This signature of the EDM would be recorded by a polarimeter based on deuteron-carbon scattering that operates continuously during this process. The goal of the first part of the EDM program at COSY is to use the EDDA detector and demonstrate that such an efficient polarimeter can be realized and to show that there are no barriers to eliminating any systematic polarimeter errors that might arise in the search down to a level of 50 ppm.

The initial horizontal polarization needed for the deuteron EDM search is inherently unstable to any spin decoherence mechanism; thus it must be injected into the ring or created there at the start of the experiment. To further improve the understanding of this part of the experiment, one hopes to create such horizontal polarization using the beam in the COSY ring, despite the fact that there is no way to slow the precession of the polarization in the vertical magnetic fields of the bending magnets.

First calculations show that a horizontal polarization might live on the order of 100 ms using cooled, bunched beam and the current magnetic field lattice of the ring. Once created, one wants to measure that horizontal polarization and investigate any procedures for increasing the polarization lifetime, such as by cooling the beam, removing high emittance parts of the beam, or adjusting the sextupole fields of the ring. For the EDM search, a polarization lifetime of hundreds of seconds is required and we plan to use these tests at COSY as a way to demonstrate control of that lifetime. The first run in June 2008 concentrated on the polarimeter development. A separate set of electronics for the EDDA detector was installed while leaving the original electronics in place for routine use by the COSY staff and other experiments. Five polarization states were selected for use: unpolarized, Vector Plus ($p_z = 2/3$, $p_{zz} = 0$), Vector Minus ($p_z = -2/3$, $p_{zz} = 0$), Tensor Plus ($p_z = -1$, $p_{zz} = 1$), and Tensor Minus ($p_z = 1/2$, $p_{zz} = -1/2$). Figure 24 shows a scatter plot of the measured vector and tensor asymmetries.

The momentum for the June run was $p = 1.2$ GeV/c, a value selected to accommodate the testing of Multi-Resistive-Plate Chambers provided by Frascati and the University of Rome. This proved to be too large an energy for the effective observation of near-elastic events from the targets since most particles exited the bar detectors without stopping. Thus, the pulse height spectra were featureless falling exponentials in shape and the effective analyzing power did not depend strongly on threshold. However, with white noise extraction, most of the deuterons penetrated far enough through the target material to generate efficiencies of the order of

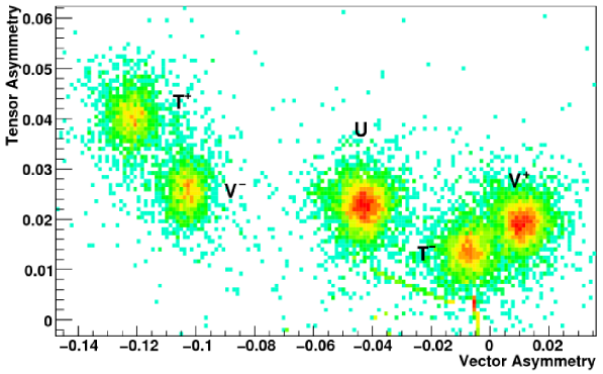

Fig. 24: Scatter plot showing polarimeter asymmetries for each of the polarization states.

1.5…2.0% , which is the ratio of events above threshold that were used for a polarization measurement to the number of deuterons lost from the circulating beam. The high value of this number indicated that breakup protons as well as elastic deuterons and a number of reaction products were a part of the included spectrum of events. The effective analyzing power was measured to be $A_y = 0.048$, based on values of the beam polarization from the Low Energy Polarimeter.

A number of scans was made of horizontal beam position and angle. In each case, changes to the asymmetries of a few percent (absolute) were recorded. For some beam positions, these asymmetries appeared to vary with time during the store, a situation that would be extremely problematic for an EDM search.

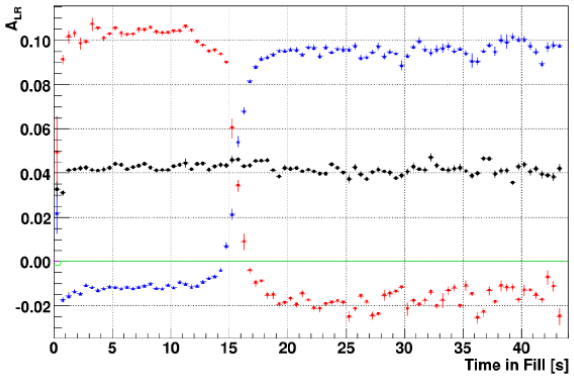

Fig. 25: Measurements made during a store of the polarization reversal created by crossing a depolarizing resonance using an RF solenoid. Red and blue data are spin up and down; the black data are for an unpolarized beam.

Figure 25 illustrates a test of the continuous monitoring feature of the EDDA detector readout. In this set of stores for spin up (red), spin down (blue), and unpolarized states (black), the RF solenoid is being ramped through the $1 - G\gamma$ depolarizing resonance (bunched beam). The

strength is large enough that the polarized states flip the sign of their polarization. The approach to and retreat from resonance is recorded. The errors represent the overlay of 2–3 stores for each polarization state.

Graphs of the analyzing power (A_y), efficiency (E), and figure of merit ($EA_y{}^2$) are shown in Fig. 26 as a function of threshold. The ring detectors were divided into two groups. Rings 2–4 showed evidence for the elastic scattering peak, Rings 5–8 (the most that were instrumented) still contained a significant analyzing power, but without an elastic peak, corresponding to an angle range where the deuterons did not stop in the ring detectors. There was no appreciable deuteron signal in ring 1. The results shown here are separated into the two response groups, those with an elastic peak in circles and without in plus signs. In both cases, the analyzing power is about five times larger than the one observed in the June run. At the same time, typical efficiencies have dropped to about 0.1%. This is a desirable compromise since the statistical reach of the measurements is the same and the sensitivity to systematic errors is less owing to the larger analyzing power. The figure of merit measures the statistical sensitivity; we chose to operate with a threshold of 85 mV. For most of the September run, we made studies of the operation of the target and extraction system, and measured the response of the polarimeter to deliberately introduced systematic errors. Mainly, we were interested in the response to changing the position or angle of the beam passing through the tube target. In addition, we studied the effects of pileup at high rates and included polarization states with a large tensor component that we wish to remove with the next run.

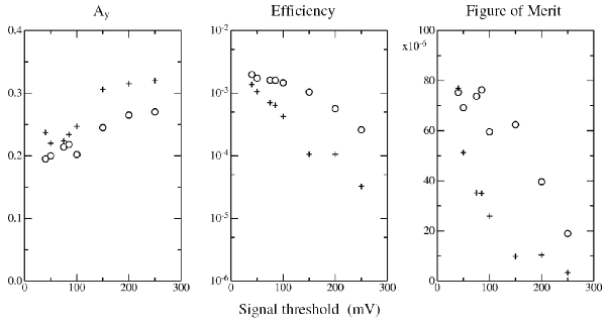

Fig. 26: Graphs of the vector analyzing power (A_y), efficiency (E), and figure of merit ($EA_y{}^2$) for the forward angle (rings 2–4, open circles) and backward angle (rings 5–8, plus signs) contributions to the EDDA detector as a polarimeter. The final signal threshold chosen for the September run was 85 mV.

2.4 Overcoming spin-depolarizing resonances

The **SPIN@COSY** collaboration recently tested a new spin resonance crossing technique, Kondratenko Crossing (KC), by sweeping an rf solenoid's frequency through an rf-induced spin resonance with both the KC and traditional fast crossing (FC) patterns. Using both rf bunched and unbunched 1.85 GeV/c polarized deuterons stored in COSY, the parameters of both crossing patterns were varied. Compared to FC with the same crossing speed, KC reduced the depolarization by measured factors of 4.7 ± 0.3 and 19^{+12}_{-5} for unbunched and bunched beams, respectively. This clearly showed the large potential benefit of Kondratenko Crossing over fast crossing.

The recently tested KC pattern using an rf solenoid is shown in Fig.27. Its frequency f_{rf} was ramped through several f ranges in times t. One can use the Chao matrix formalism to calculate analytically the polarization for this crossing pattern.

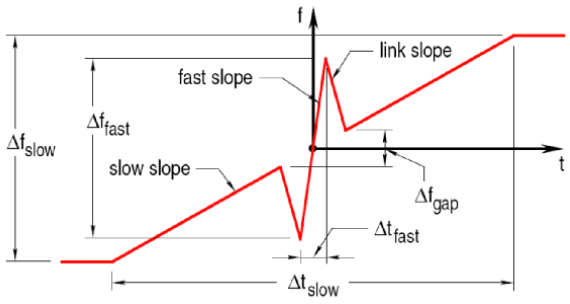

Fig. 27: Kondratenko Crossing (KC) pattern defining the parameters Δf_{fast}, Δt_{fast}, Δf_{slow}, and Δt_{slow}. The KC pattern is centered at f_{KC} (zero point on the vertical axis).

The resulting vertical polarization data are plotted in Fig. 28 for both bunched and unbunched beam and for both KC and fast crossing (FC). The peak's central frequency was shifted by 5 Hz for bunched KC relative to unbunched KC; this small shift was probably due to the rf cavitys bunching. Moreover, the bunched KC data have a broad flat-top. For unbunched beam, the $P_{\mathrm{V}}/P^{i}_{\mathrm{V}}$ ratio, measured at the KC peak, was: 0.966 ± 0.004 for KC, and 0.839 ± 0.005 for FC. For bunched beam, it was: 0.990 ± 0.002 for KC, and 0.848 ± 0.003 for FC. By minimizing the KC unbunched data's χ^2, we obtained f_{r} of 916999.1 ± 0.1 Hz and Δf of 24.4 ± 0.2 Hz.

The resonance strength was 1.067×10^{-5}; Δf_{fast} was 185 Hz; Δt_{fast} was 12 ms; Δf_{slow} was 400 Hz; and Δt_{slow} was 160 ms. The KC unbunched solid curve is the Chao formalism prediction for these parameters; the long-dashed line through these unbunched points is a Chao formalism fit with parameters f_{r} and f. The KC bunched solid curve is an empirical 2nd-order Lorentzian fit; the horizontal dashed line fit to the five highest points gives the peak KC bunched value of 0.990 ± 0.002. The errors are smaller than the data symbols.

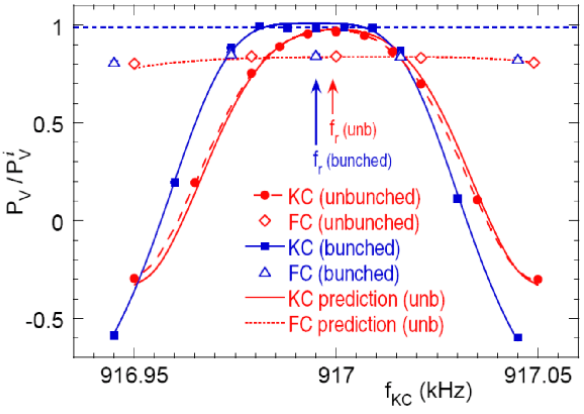

Fig. 28: Measured 1.85 GeV/c deuteron vector polarization ratios $P_{\mathrm{V}}/P^{i}_{\mathrm{V}}$ averaged for all nonzero spin states, plotted *vs.* the KC pattern's center frequency f_{KC}.

Thus, Fig. 28 clearly shows that beam bunching significantly decreased both KC's sensitivity to f_{KC} and KC's polarization loss.

2.5 Acceptance studies

The PAX collaboration studied polarization at injection momentum and depolarizing and beam lifetime processes. The beam time for beam acceptance studies gave new insights into loss mechanisms within COSY:

- The electron beam size limits the dynamic acceptance of COSY.
- The beam lifetime (dynamic aperture) is strongly tune dependant.
- Initial losses due to the electron cooling can be reduced by slowly increasing the electron current

These acceptance studies give new insights into loss mechanisms in COSY. The beam lifetime is strongly tune dependent due to dynamic apertures. The dynamic acceptance of COSY is limited by the electron beam size. With reduced proton beam size the initial losses dissapear, which are related to non linear focussing of outside protons by the electron beam. During set-up for these experiments it was observed that the initial losses due to electron cooling can be reduced by slowly increasing the electron current of the electron cooler. Initial losses disappear at smaller injected proton beam emittance because protons outside the electron beam see a non-linear focussing by the electron beam.
While increasing the electron current and proper timing of providing electrons for cooling the losses can be reduced. With a stepwise increase of the electron current an increase of the stored beam intensity has been demonstrated (see Figs. 29 and 30).
Ion losses may occur if the ion beam size is larger than the electron beam size. The method of magnetic expansion of the electron beam size to reduce these losses will be developed and tested in the near future.

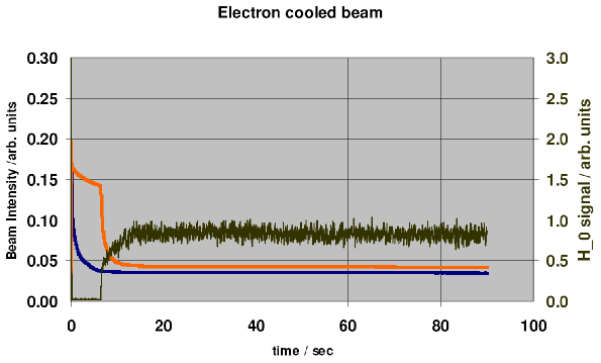

Fig. 29: Beam intensity *vs.* time. Less initial losses with 10ms (blue trace, stored) injection compared to 20 ms (orange) injection. The H_0-signal (brown) and the intensity is comparable for both cases.

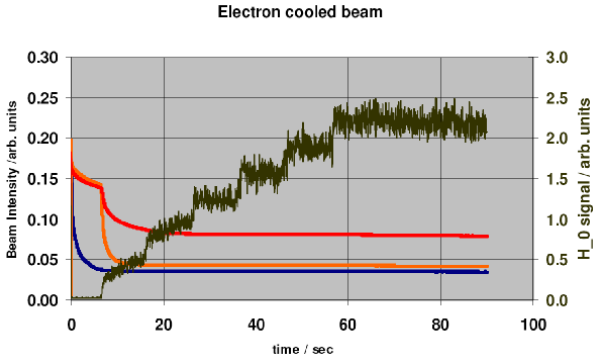

Fig. 30: Beam intensity in COSY *vs.* time. With stepwise increased electron current the H_0-signal (brown) increases accordingly and the final intensity (red line) is doubled. For comparision the intensities from Fig. 29 are included.

3 Further Experimental Activities

3.1 X-rays identify electron depletion in antiprotonic atoms

Antiprotons slowed down to atomic scale kinetic energies are captured into the Coulomb field of nuclei at about the outermost electron shell. Due to the large mass of the antiproton, this corresponds to main quantum numbers n above 100 for medium Z atoms. Consequently, the number of de-excitation steps in the subsequent quantum cascade becomes exceedingly large.

The de-excitation is determined by the competition of X-ray emission and depletion of electron shells by radiationless Auger transitions. Auger emission favours $\Delta n = 1$ steps, *i.e.*, minimum kinetic energy for the ejected electron, and dominates whenever energetically possible for $n > 9$. The preference of radiative de-excitation for $\Delta n \gg 1$ (maximum energy gain) leads to an accumulation in the highest-angular momentum states. There the cascade continues only by slow $\Delta n = 1$ X-ray transitions, as long as the energy gain does not exceed the binding energy of not yet ejected electrons.

An undisturbed cascade can be studied by using low density noble gases, where electron refilling is suppressed and chemical effects are absent. A shell-by-shell depletion up to complete ionisation for Argon and Krypton (Fig. 31) is revealed by appearance and disappearance of antiprotonic X-ray lines.

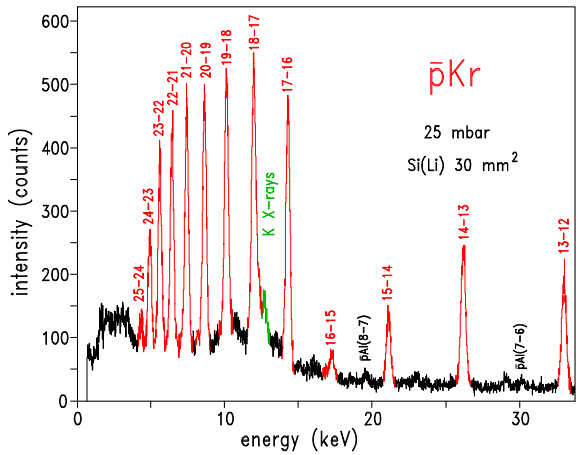

Fig. 31: X-ray spectra of antiprotonic Krypton show numerous and mostly saturated antiprotonic $\Delta n = 1$ transitions (red). Auger emission of L and K electrons becomes possible for de-excitation steps larger than 2.7 and 17 keV, respectively, leading to a suppression of X-ray emission until depletion of the electron shell is completed. In a few cases an electronic K X-ray (green) is emitted from a Krypton atom during the antiproton's descent through the electron shells. The spectrum was recorded with a 3.5 mm thick Si(Li) detector.

In the case of Xenon (Fig. 32), the number of de-excitation steps is no longer sufficient for complete ionisation, which is seen from the not saturated line yield of the (14–13) transition. Several electronic L and K X-rays per atom are emitted when refilling holes created by Auger ejection of inner shell electrons. The energy distribution of the electronic X-rays is correlated to the ionisation status and to the antiprotonic level reached.

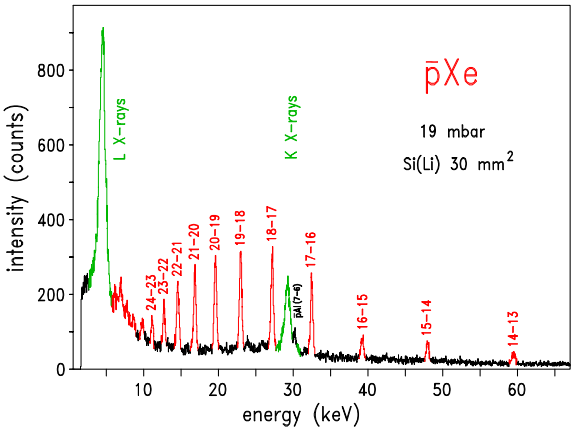

Fig. 32: The X-ray spectrum of antiprotonic Xenon exhibits besides the antiprotonic $\Delta n = 1$ transitions (red) strong L and K X-ray emission (green) from the partially depleted electron shell. More than 10 L and about 2 K X-rays are emitted during the de-excitation cascade.

The energy gain necessary for Auger emission leads to a strong correlation of the antiproton orbit $R_{\bar{p}}$ and the electron shell possibly affected. Furthermore, the remaining electrons determine the screening of the nuclear charge. The onset of depletion for the various shells is shown in Fig. 33.

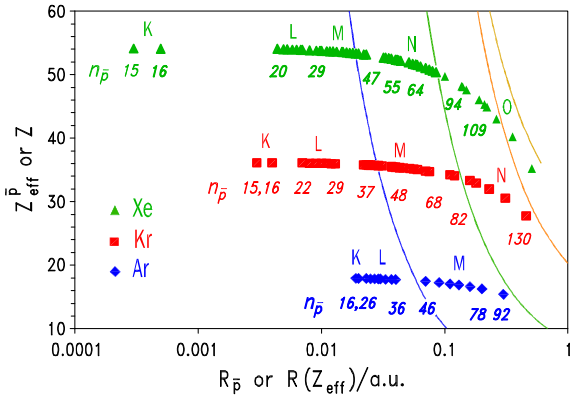

Fig. 33: Effective nuclear charge $Z^{\bar{p}}_{\text{eff}}$ acting on the antiproton as a function of its distance $R_{\bar{p}}$. K, L, M, N, and O indicate the regions where these shells can be ionised by antiprotonic $\Delta n_{\bar{p}} = 1$ transitions. Solid lines show the average radii of the electron shells K, L, M1 – M3, and M4 – M5 (from left) for the screened nuclear charge Z.

3.2 Laser-induced particle acceleration

The physics of laser-plasma interactions has undergone a revolution in recent years. By directing a high-power, ultrashort laser pulse onto a thin foil, it is now possible to produce high-energy proton and ion beams. However, for realizing reliable table-top accelerators one must still overcome fundamental and technological limitations. As the beams are poly-energetic and divergent at the source, reduction and control of these parameters is essential. Via special target engineering quasi mono-energetic protons can be generated due to the spatial reduction of the accelerating field.

A challenge for building continuously operating laser-based accelerators is that the plasma-generating target is destroyed when hit by the laser. Liquid drops with diameters down to 10 μm have been used as a promising alternative. They have the advantage of charge confinement, are relatively debris-less, and can easily be re-supplied into the interaction zone. However, for the acceleration of protons conventional drop generators cannot be operated with the pure target material (*i.e.* Hydrogen) and chemical compounds like water have to be used instead. Another drawback of drop targets is that the distance between the drop generating nozzle (which must be only a few Kelvin cold if pure Hydrogen is to be used) and the hot and radiating plasma is limited to a few cm. Such limitations can be overcome with a frozen pellet target.

Both necessary technologies are now at hand — a 100 TW laser at the Institute for Laser- and Plasma Physics (ILPP), University Düsseldorf, and a frozen pellet target at the IKP, see Sect. 6.3. A project has been established to furnish the target for its use at the ILPP laser and carry out first measurements with Hydrogen pellets.

The Düsseldorf 100-TW laser system PULSAR is actually one of the most powerful university lasers worldwide. It delivers laser pulses in the near infrared (800 nm) with a duration of 25 femtoseconds and a pulse energy of about 2.5 J at 10 Hz. A key feature of the system is its high intensity contrast of the pulse with respect to pre-pulses (better than 1:10^8 on a picosecond time scale), which particularly allows one to study fundamental physics of laser-plasma interactions by effective suppression of pre-plasma hydrodynamics.

As a first step — in order to develop particle detection techniques and to better understand the ion-acceleration mechanisms — measurements are carried out with conventional gas and foil targets. Figure 34 shows the experimental setup when the laser is fired into a pulsed Helium gas jet under high pressure. The development of the plasma and that of the acceleration channel within the gas was probed optically using a time synchronized, ultrashort probe pulse.

The probe pulse was generated by splitting of a part of the main beam before the last amplifier stage. The interaction zone of the main pulse with the target was imaged at high resolution onto a CCD camera. By tuning the delay between both beams, snapshots of the interaction were taken at different times by using the probe pulse as

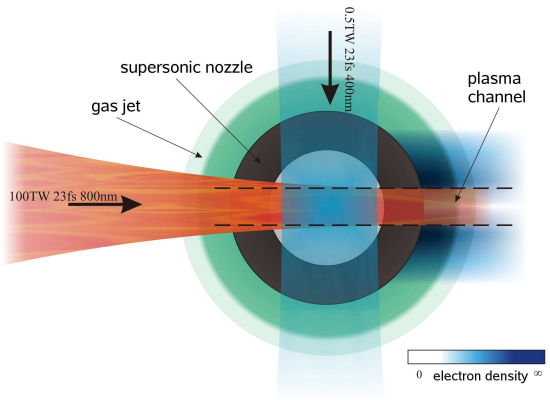

Fig. 34: Schematic top view of main beam (red) and probe beam (blue) at the interaction zone.

a backlighter in pump-probe geometry. The optical self-emission of the plasma was suppressed via interference filters. The data show the plasma formation and self-focusing of the pulse leading to a narrow plasma channel in which electrons are accelerated to MeV energies. Filamentary structures seen in shadowgrams like Fig. 35 are ascribed to electrons emitted from the laser focus during breaking of the wake field waves. The channel structure itself was diagnosed quantitatively using high-resolving interferometry, see Fig. 36.

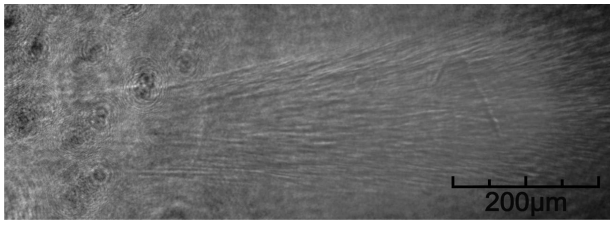

Fig. 35: Shadowgram showing filamentation.

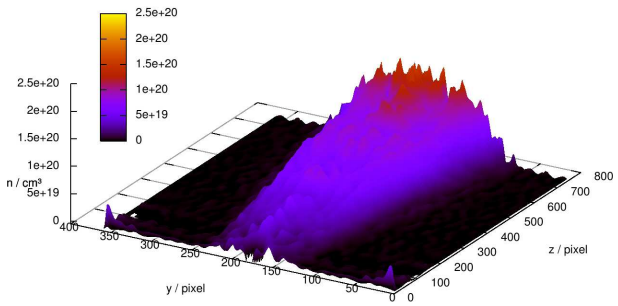

Fig. 36: Electron density distribution in a plasma produced in a Helium gas jet by an 60 TW laser pulse focused approximately at $y = 200$, $z = 0$.

Optical spectroscopy of light bursts emitted from the inner of the relativistic channel was performed as well. The data are currently under analysis and compared with 2- and 3-dimensional particle-in-cell simulations. This work is theoretically supported by P. Gibbon (JSC, FZ Jülich) and A. Pukhov (HHU Düsseldorf).

3.3 Precision Spectroscopy of Hydrogen with a Lamb-shift Polarimeter

For the Breit-Rabi diagram of the hydrogen states $2S_{1/2}, 2P_{1/2}$ and $2P_{3/2}$ (Fig. 37) high precision experimental data exist only for weak magnetic fields about a few mG, which allow to check the results of advanced bound-state QED calculations. These experimental data stem from 2-photon laser-spectroscopy and the separated-oscillatory-field method. At higher magnetic fields, the crossing of the β and the e states around 570 G were measured decades ago.

The g-factors of those states can be determined from the Breit-Rabi diagram the classical Lamb shift, the hyperfine splittings and, from the slope of the energy levels. The calculation of these values by bound-state QED is on a very accurate level, so that the uncertainty now is dominated by effects like the charge distribution of the proton. A test of the bound-state QED seems possible with a very precisely measured Breit-Rabi diagram. This is expected to contribute *e.g.* in the determination of the charge distribution in the proton.

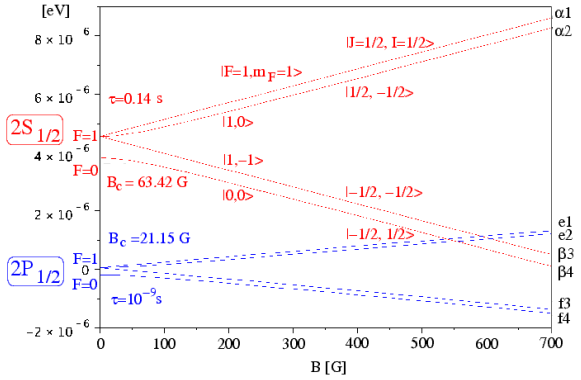

Fig. 37: The Breit-Rabi diagrams for the metastable $2S_{1/2}$ and the short-lived $2P_{1/2}$ hyperfine states.

A spin filter, the most important component of a Lamb-shift Polarimeter, is able to produce a beam of metastable hydrogen (deuterium) atoms in only one hyperfine state ($\alpha 1$, $\alpha 2$ or $\beta 3$). From these states, $M1$ transitions into the other hyperfine states can be induced at different transverse magnetic fields and the population of these states can be measured with a second spin filter. Based on the expected error of $\Delta f = 10$ kHz for a single measurement, 100 measurements between 0 and 100 G should lead to a relative error of 10^{-6} for the g-factors. Increasing of the magnetic field range will decrease the size of the error substantially. But it has to be taken into account, that the g-factors will change for large magnetic field. In addition, the hyperfine splitting of the $2S_{1/2}$ state corresponds to the difference of the $\alpha 1 \rightarrow \beta 4$ and the $\alpha 2 \rightarrow \beta 3$ transition energies or the sum of the transitions energies $\alpha 1 \rightarrow \alpha 2$ and $\beta 3 \rightarrow \beta 4$ independent of the magnetic field strength. Therefore, it is possible to average the values, measured at different fields to obtain an error of the hyperfine splitting of less than 1 kHz. The error is dominated by the Heisenberg uncertainty relation $\Delta\nu \times \Delta t \sim 1$, which will broaden the half with of the resonance. This problem can be solved by exciting the slow hydrogen beam of an atomic beam source (ABS) by electron bombardment before the hyperfine states are separated with the spin filter. In a proof-of-principle measurement $E1$ transitions into the single Zeeman states of the $2P_{1/2}$ state were induced with a Lecher TEM (transverse electromagnetic) transmission line. Because of the short lifetime (10^{-9}s) of the $2P_{1/2}$ state the atoms will decay immediately into the ground state and the produced Lyman-α photons are detected with a photomultiplier as a function of the radio frequency at a stable power level (see Fig. 38).

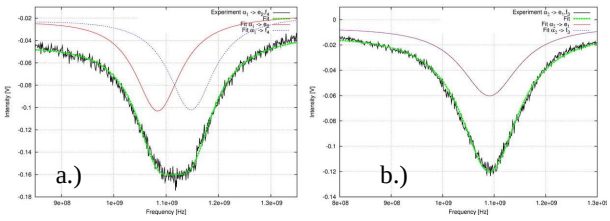

Fig. 38: The observed transitions $\alpha 1 \rightarrow f4$ and $\alpha 1 \rightarrow e2$ (a.) or $\alpha 2 \rightarrow f3$ and $\alpha 2 \rightarrow e1$ (b.) at a small vertical magnetic field ($B \sim 0.5$ G) in the transition region.

From the observed transitions at small magnetic fields the hyperfine splitting of the $2P_{1/2}$ state can be directly determined to 59.98 (2.03) MHz, which fits to the best known value of 59.22 (14) MHz. A much better precision of $\Delta f_{hfs} < 10$ kHz can be obtained, because similar to the M1 transitions the combination of the transition $[(\alpha 1 \rightarrow f4) - (\alpha 2 \rightarrow f3) - (\alpha 1 \rightarrow e1) + (\alpha 2 \rightarrow e2)]$ corresponds to the hyperfine splitting f_{hfs} independent of the magnetic field at the interaction region. Another outcome of these measurements is a value of 1057.34 (1.11) MHz for the classical Lamb shift. This agrees with other measurements, but the error is at least two orders of magnitude larger.

With this setup an error of $\Delta f = 100$ kHz for a single measurement is expected. This means, that the relative error of the g-factor for 100 measurements between 0 and 100 G will be around 10^{-5} and can be decreased further by increasing the magnetic field range. A 1.5 T dipole magnet exits in the COSY test hall which may lead to a relative error of $\sim 10^{-8}$ for the g-factor of the $2P_{1/2}$ states. In addition, $E1$ transitions into the single Zeeman states of the $2P_{3/2}$ state can be induced with a modified TEM waveguide for radio frequencies around 10 GHz. The same method is applicable for deuterium, too. In this case, three Zeeman states ($\alpha 1$, $\alpha 2$ and $\alpha 3$) are selected by the spin filter. In general this method may be useful for antihydrogen, because during the recombination of the antiproton and the positron $\sim 30\%$ of the antihydrogen will populate the metastable $2S_{1/2}$ state.

4 Theoretical Investigations

The IKP theory group studies the strong interactions in their various settings — spanning topics in hadron structure and dynamics, the nuclear many-body problem and high-energy Quantum Chromodynamics (QCD). The main focus is on the formulation and application of effective field theories for precision hadron and nuclear physics based on the symmetries of QCD. Within the virtual institute on "Spin and strong QCD" work focuses on applications for physics at COSY and FAIR. Some of the highlights of these activities are discussed in the following.

4.1 Three-nucleon forces in chiral EFT with deltas

In the last years, we have systematically analyzed the forces between two, three and four nucleons in the framework of a chiral effective field theory (EFT) of nucleons and pions. This approach has reached a very high precision and is fruitfully applied in nuclear structure and reaction calculations. The effects of resonances are encoded in the so-called low-energy constants (LECs). To improve the convergence of the chiral expansion and to achieve an understanding of the underlying physics, it is advantageous to include the $\Delta(1232)$ as an active degree of freedom in the EFT, counting the nucleon-delta mass difference as an additional small parameter. Within this scheme, we have analyzed the forces between three nucleons (3NFs). The leading 3NF appears at next-to-leading oder (NLO). Due to the vanishing of the lowest-order $NN \to N\Delta$ and $N\Delta \to NN$ contact interaction, the complete effect due the Δ is given by a single two-pion (2π) exchange diagram – which is nothing but the P_{33} contribution to the pion-nucleon scattering amplitude considered by Fujita and Miyazawa already in 1957. The corrections at NNLO are given entirely in terms of diagrams involving only pions and nucleons, that fall in three categories: a 2π-exchange graph proportional to some dimension two LECs $\tilde{c}_i$ of natural size, a 1π-$4N$-contact term and a local six fermion interaction. While the $\tilde{c}_i$ have already been determined in an analysis of πN scattering, the LECs accompanying the latter two topologies must be fixed from three-body data. We have further investigated the isospin-violating (IV) 3NFs in this theory. As it turns out, the leading IV effects can all be expressed in terms of the splittings in the pertinent hadron multiplets, i.e. the nucleon doublet, the pion triplet and the delta quartet. The new ingredient in our investigation is the first quantitative analysis of the delta quartet splitting. The Lagrangian that parameterizes the splittings within the quartet contains two independent operators $\mathscr{L} = -\bar{T}_i^\mu \left[-\delta m_\Delta^1 \frac{1}{2} \tau^3 \delta_{ij} - \delta m_\Delta^2 \frac{3}{4} \delta_{i3} \delta_{j3} \right] g_{\mu\nu} T_j^\nu$, where the LECs $\delta m_\delta^{1,2}$ are combinations of strong and electromagnetic dimension-two LECs. We have determined these LECs from the available (though not very precise) delta mass data. The calculation of the IV violating 3NF in the delta-full theory can then be done straightforwardly. The estimated size of the charge-symmetry breaking 3NF using $\delta m_\Delta^1 = -5.3\,\mathrm{MeV}$ is $|\delta m_\Delta^1 - 3\delta m_N| (g_A^2 h_A^2 M_\pi^6)/(432\pi^2 F_\pi^4 \Delta^2) \sim 3$ keV, which is comparable to the typical size of the leading CSB 3NF obtained based on EFT without explicit deltas, $\delta m_N g_A^4 M_\pi^4/(256\pi^2 F_\pi^4) \sim 7$ keV. It remains to apply these 3NFs in exact calculations of few-nucleon systems.

4.2 Nuclear lattice simulations with three-body forces

Lattice QCD has made considerable progress in describing the properties of nucleons and their interactions from first principles. However, so far only the two-baryons system could be studied at limited precision. Thus, to explore systematically the influence of the QCD symmetries on the nuclear few- and many-body problem, we have started a long term effort in nuclear lattice simulations. After first simulations of nuclei with $A = 2,3,4$ and neutron matter close to the unitary limit based on the leading (LO) and next-to-leading (NLO) order effective potential derived from chiral effective field theory gave some promising results, we have now extended these simulations to NNLO. At this order the first contributions from three-body forces appear. These depend on two constants. To describe the neutron-deuteron scattering in the finite volume, we use the standard Lüscher formula. The finite volume spectrum was generated with the Lanczos diagonalization method. The two free parameters were determined from a fit to the S-wave phase-shift in spin-$1/2$ doublet channel (see Fig. 39) and the triton binding energy. One observes a very natural convergence pattern in our simulations with increasing chiral order.

In Fig. 39 we also show the S-wave phase-shifts in the spin-$3/2$ quartet channel versus the square of relative momentum. This channel was not taken into account in the fit procedure. Again we observe a very nice convergence with increasing chiral order. Our predictions are located between the proton-deuteron and neutron-deuteron experimental data. Since isospin-breaking was not taken into account in our simulations the results are very satisfactory. As a first Monte-Carlo simulation of N^{2}LO lattice EFT we studied the binding energy of ^{4}He,given by $\langle E_{^4\mathrm{He}} \rangle = \langle \Psi_4 | \exp(-tH/2) H \exp(-tH/2) | \Psi_4 \rangle / \langle \Psi_4 | \exp(-tH) | \Psi_4 \rangle$. The length of the box was chosen to be $L = 16$ fm. Our Monte-Carlo simulations over-predict the physical binding energy (with Coulomb effects subtracted) by 5%. This is consistent with the expected theoretical accuracy of our simulations. In the next years, we plan to perform N^{2}LO Monte-Carlo simulations of light nuclei and probe neutron matter with larger number of neutrons in a box.

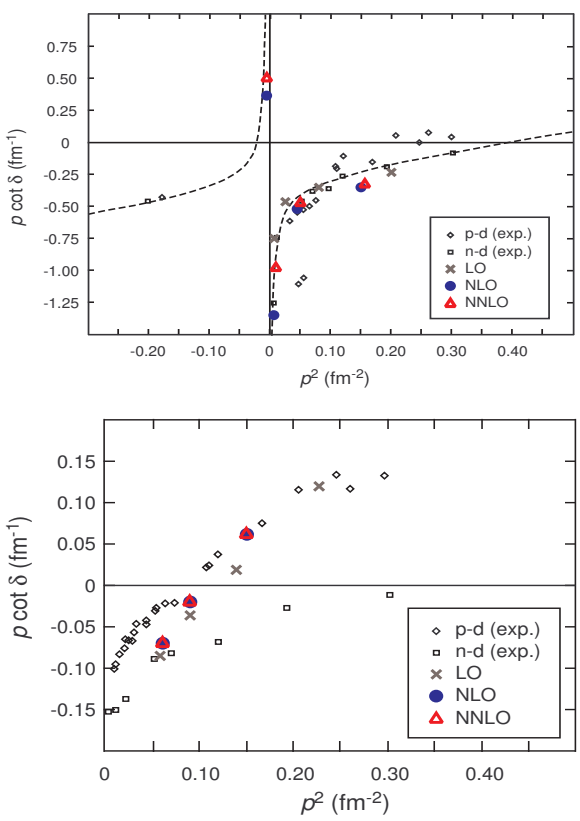

Fig. 39: Neutron-deuteron S-wave scattering phase-shifts in the spin-1/2 doublet channel *vs.* the square of relative momentum in comparison to the experimental data for proton-deuteron and neutron-deuteron scattering. The points at negative values of p^2 are extracted from the asymptotic normalization of the corresponding bound state wave functions. The line represents the best fit to the neutron-deuteron experimental points. Lower panel: Neutron-deuteron scattering S-wave phase-shifts in the spin-3/2 quartet channel versus the square of relative momentum in comparison to the data for proton-deuteron and neutron-deuteron scattering.

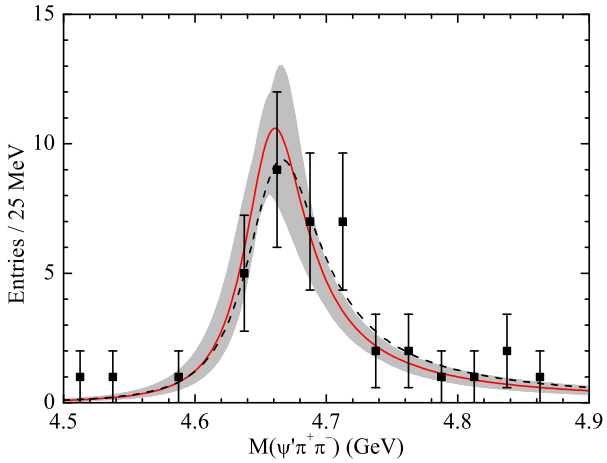

Fig. 40: Comparison of the line shape in the $\psi'\pi^+\pi^-$ invariant mass distribution derived from the molecular model with the data. The solid line shows the result of our best fit, while the shaded area shows the uncertainty that emerged from the fit. The dashed line shows the best fit result, if also the effective coupling is part of the fit.

4.3 On the nature of the Y(4660)

For a long time the non-relativistic quark model was believed to provide an accurate description of charmed mesons. However, in recent years experimental evidence has accumulated for a sizable number of states that seem to not fit into a standard $\bar{q}q$ assignment. Not only do their masses deviate significantly from most predictions, also their properties seem to be inconsistent with the expectations. A common feature of all those states is that they are located close to a threshold for the production of a particle pair in an *s*-wave. Because of this, it is frequently speculated that these states might well be born out of non-perturbative meson-meson interactions instead of interquark interactions. For that reason, those states were called hadronic molecules.

Based on an time-honored analysis by Weinberg a few years ago our group showed that the value of the effective coupling constant for the coupling of the resonance considered to the mentioned continuum state is a direct measure of the nature of that state. In addition, the value of that coupling constant is bounded from above taking its maximum taken if the state is of molecular nature. Since the effective coupling constant is an observable, this scheme allows one to quantify the molecular component of a state directly from experimental data. The only input needed are the masses of the continuum particles involved and the binding energy of the state. In a recent work we applied this idea to an investigation of the $Y(4660)$. This state was observed only in the $\pi^+\pi^-\psi'$ invariant mass distribution in $e^+e^- \to \gamma_{ISR}\pi^+\pi^-\psi'$ at BES, but not in various other open or hidden charm final states, clearly posing a problem to the conventional quark model. On the other hand the pole is located very close to the $\psi' f_0(980)$ threshold. We therefore investigated, if the empirical information available for the $Y(4660)$ is consistent with a molecular nature of this state. To do so we performed a fit to the $\psi'\pi^+\pi^-$ invariant mass distribution, leaving the mass of the state and the overall normalization as a free parameter. For any given mass of the Y the effective coupling could then be calculated using the method sketched above. The result of the fit is shown in Fig. 40. The fit is very good, in addition the theoretical spectrum automatically generates some asymmetry which is also seen in the data. To cross check our result we also performed a second fit, where also the effective coupling was treated as a free parameter. The fact that the best fit value for the coupling constant basically agrees in both fits we take as strong evidence that the $Y(4660)$ is indeed a $\psi' f_0$ bound state. The best fit result of this second fit is shown as the dashed line in the figure. Note

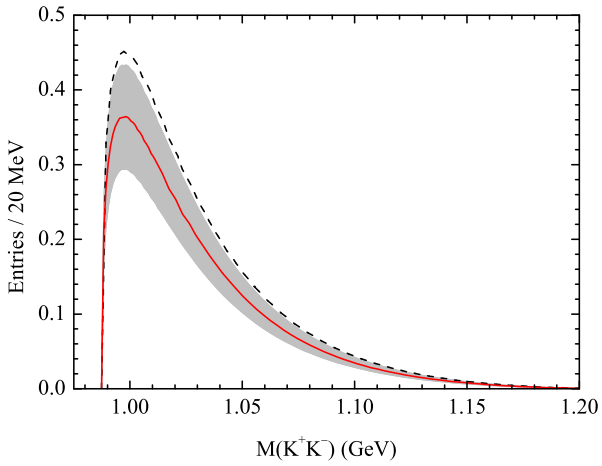

Fig. 41: Predictions for the $\bar{K}K$ invariant mass distributions.

that in this second fit, since now there was no connection anymore between coupling and mass of the state, even masses of the Y were consistent with the fit that were above the $\psi' f_0$ threshold, clearly at variance with a bound state scenario. In order to check our hypothesis we propose to measure the corresponding $\bar{K}K$ spectrum. Within our scheme it can be predicted without any free parameter. The result is shown in Fig. 41.

The hypothesis of the molecular nature of the $Y(4660)$ can be tested in future experiments like PANDA at FAIR or others. This is especially interesting, since the $f_0(980)$ qualifies as a $\bar{K}K$ molecule. In light of this the $Y(4660)$ might well be the first three-meson bound state ever observed.

4.4 The puzzle of the Σ_c masses resolved

Mass splittings within isospin multiplets of hadrons appear due to both the mass difference between u and d quarks and electromagnetic effects. Since the d quark is heavier than the u, usually the hadron with more d quarks is heavier within one isospin multiplet. For instance, the neutron (udd) is heavier than the proton (uud), and the $K^0(d\bar{s})$ is heavier than the $K^+(u\bar{s})$. There is only one exception to this pattern, the Σ_c iso-triplet ($\Sigma_c^{++}(cuu)$, $\Sigma_c^+(cud)$ and $\Sigma_c^0(cdd)$). The mass splittings within the Σ_c iso-triplet are measured

$$\begin{aligned} \Delta_{1c} &\equiv m_{\Sigma_c^+} - m_{\Sigma_c^0} = -0.9 \pm 0.4 \text{ MeV}, \\ \Delta_{2c} &\equiv m_{\Sigma_c^{++}} - m_{\Sigma_c^0} = 0.27 \pm 0.11 \text{ MeV}. \end{aligned}$$

Remarkably, the state with two u quarks has the largest and the one with a u and a d quark has the smallest mass. Only recently some of the bottom cousins of the Σ_c, $\Sigma_b^\pm$, were observed by the CDF Collaboration. Their masses are for the buu state $m_{\Sigma_b^+} = 5807.8 \pm 2.7$ MeV and for the bdd state $m_{\Sigma_b^-} = 5815.2 \pm 2.0$ MeV, respectively — their neutral partner Σ_b^0 has not been observed yet. Thus, here the natural ordering of the states seems to be restored. On the other hand, heavy quark symmetry relates baryons containing a b quark to those with a c quark. So there appears to be an additional effect beyond this symmetry that plays an important role in the generation of these mass patterns. We have analyzed the origin of these patterns, together with those in the $\Xi'_{c(b)}$ doublets, using chiral perturbation theory at leading one-loop order and heavy quark symmetry. We constructed both the strong and the electromagnetic Lagrangians at $\mathcal{O}(p^2)$ in the chiral expansion, that is the terms that are responsible for the mass corrections. In contrast to mass splittings in light quark baryon multiplets, there is an additional operator that describes the hard virtual photons exchanged between the heavy quark and light quarks accompanied by a low-energy constant β_{1h}. More precisely, since the heavy quark can be view as static, its charge acts as a static background field that transforms as a scalar under chiral $SU(3_L \times SU(3)_R$. At leading symmetry-breaking order, there is exactly one independent operator that describes this interaction. Remarkably, this term has a different sign for the charm baryons and the bottom baryons. This is due to the fact that the sign of the electric charge of the charm quark is different from that of the bottom quark. It is the different interference between this term and the other terms that drives the mass splittings within the Σ_c iso-triplet to have a different pattern compared to any other known isospin multiplet. This leads one to expect that the isospin mass splittings in the charm hadrons are always different from those in the bottom hadrons even if the heavy quark symmetry were exact. Furthermore, there is no loop contribution to the mass splitting between the two Ξ'_c baryons, and we predict $m_{\Xi_c'^+} - m_{\Xi_c'^0} = -0.2 \pm 0.6$ MeV. The present data for the masses of the Ξ'_c baryons are not accurate enough yet to test the prediction. For the Σ_b states, the β_{1h} term interferes constructively with the other terms and hence the loop corrections are less important. The mass of the Σ_b^0 and the mass difference $m_{\Xi_b'^0} - m_{\Xi_b'^-}$ are predicted to be 5810.3 ± 1.9 MeV and -4.0 ± 1.9 MeV, respectively, which can be tested in future experiments.

4.5 Near threshold $p\bar{p}$ enhancement in the $J/\psi \to \omega p\bar{p}$ decay

The study of the decays of mesons like the J/ψ, $\psi(2S)$, B, and Υ as pursued by the BES, Belle, BABAR and CLEO Collaborations is a rather powerful tool for examining systematically the spectrum of light as well as heavier hadrons. Specifically, exclusive measurements of decays into three-meson or meson-baryon-antibaryon channels play a very important role and have already led to the identification of several new structures.

Among the various three-particle channels explored those involving the proton-antiproton $(p\bar{p})$ system in the final state have caused considerable attention in the community. The excitement was initiated by the observation of a significant near-threshold enhancement in the $p\bar{p}$ invariant mass spectrum for the reaction $J/\psi \to \gamma p\bar{p}$ in

a high-statistics and high-mass-resolution experiment by the BES Collaboration.

The observed enhancement was interpreted as evidence for a $p\bar{p}$ bound state or baryonium, or for exotic glueball states. Alternatively, we (but also others) demonstrated that the near-threshold enhancement in the $p\bar{p}$ invariant mass spectrum from $J/\psi \to \gamma p\bar{p}$ could be simply due to the final state interaction (FSI) between the outgoing proton and antiproton.

Very recently the BES Collaboration presented a high-statistics measurement of the $J/\psi \to \omega p\bar{p}$ decay where, according to their own words, "no obvious near-threshold $p\bar{p}$ mass enhancement is observed". This supposed lack of any enhancement in the $\omega p\bar{p}$ channel was then seen as a hint that the FSI interpretation of the $p\bar{p}$ enhancement in $J/\psi \to \gamma p\bar{p}$ is disfavoured.

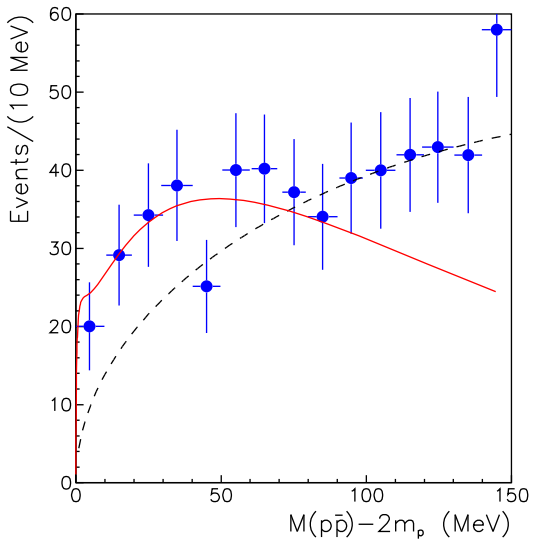

Fig. 42: The $p\bar{p}$ mass spectrum from the decay $J/\psi \to \omega p\bar{p}$. The circles show experimental results of the BES Collaboration, while the dashed line is the spectrum obtained by assuming a constant reaction amplitude. The solid line is a calculation that includes FSI effects based on the scattering amplitude predicted by the $N\bar{N}$ model A(OBE) of the Jülich group.

We have taken a closer look at those $J/\psi \to \omega p\bar{p}$ data by the BES Collaboration. Corresponding results are presented in Fig. 42, where the measured $p\bar{p}$ mass spectrum is shown. The dashed line represents a pure phase-space behaviour. The normalization of the phase space is done in the region $M(p\bar{p}) - 2m_p \approx$ 100-140 MeV, where the data indeed follow the phase-space distribution. The solid line is a calculation that includes FSI effects (in the $p\bar{p}$ partial wave relevant near threshold) based on the scattering amplitude predicted by the $N\bar{N}$ model A(OBE) of the Jülich group. Obviously, when such FSI effects are taken into account one can reproduce the dependence of the experimental mass spectrum on the invariant mass almost perfectly in the near-threshold region.

Thus, not only in $J/\psi \to \gamma p\bar{p}$ but also in the reaction $J/\psi \to \omega p\bar{p}$ there is indeed a noticeable enhancement in the $p\bar{p}$ invariant mass spectrum near threshold as compared to the phase-space behavior. Moreover, this enhancement is nicely reproduced by the final state interaction in the relevant $p\bar{p}$ partial wave as given by the Jülich $N\bar{N}$ model. Accordingly, and contrary to the statement by the BES Collaboration their new data on $J/\psi \to \omega p\bar{p}$ decay, in fact, strongly support the FSI interpretation of the $p\bar{p}$ enhancement seen in other decay reactions.

4.6 The DN and $\bar{D}N$ interactions

The distortion of charm in nuclear matter remains an heavily discussed issue since the first proposals to use charmonia and open charm as a probe of the early stage of heavy-ion collisions. Obviously, a reasonable understanding of scattering processes involving particles with charm in free space is a prerequisite for drawing conclusions on their behavior in the medium.

The basic problem here is the complete lack of relevant experimental data. This situation is expected to change with the operation of the future FAIR facility in Darmstadt (Germany). The PANDA Collaboration intends to investigate the distortion of open-charm mesons in *medium* and in the *vacuum*. In the latter case the measurements utilize the production of open-charm mesons by annihilating antiprotons on the deuteron and the subsequent rescattering of the produced D and $\bar{D}$ mesons on the spectator nucleon.

In this context we performed an exploratory study of the DN and $\bar{D}N$ interactions. In particular, we developed corresponding interaction models in close analogy to the meson-exchange $\bar{K}N$ and KN interactions of the Jülich group utilizing SU(4) symmetry constraints. The main ingredients of the interaction are provided by vector meson (ρ, ω) exchange and higher-order box diagrams involving D^*N, $D\Delta$, $D^*\Delta$ or $\bar{D}^*N$, $\bar{D}\Delta$, $\bar{D}^*\Delta$ intermediate states, respectively. Furthermore, in case of DN, where other channels with charm $C = +1$ are already open at its threshold, we take into account the coupling to the channels $\pi\Lambda_c(2286)$ and $\pi\Sigma_c(2455)$. The reaction amplitude is obtained by solving a Lippmann-Schwinger type (coupled-channel) scattering equation for the interaction potentials.

Predictions for reaction cross sections for the various channels are presented in Fig. 43. Evidently the cross sections in the DN channels (D^+p, D^+n) are substantially larger than those we obtain for $\bar{D}N$ (D^-n, D^-p). Furthermore, they exhibit a more pronounced momentum dependence.

Interestingly, our interaction model for DN generates several states dynamically. In view of the close analogy between our DN model and the corresponding $\bar{K}N$ interaction this is not too surprising, because also the latter yields a quasi-bound state which is associated with the $\Lambda(1405)$ resonance. In the $C = +1$ sector we find two S-wave states which we identify with the isospin $I = 0$

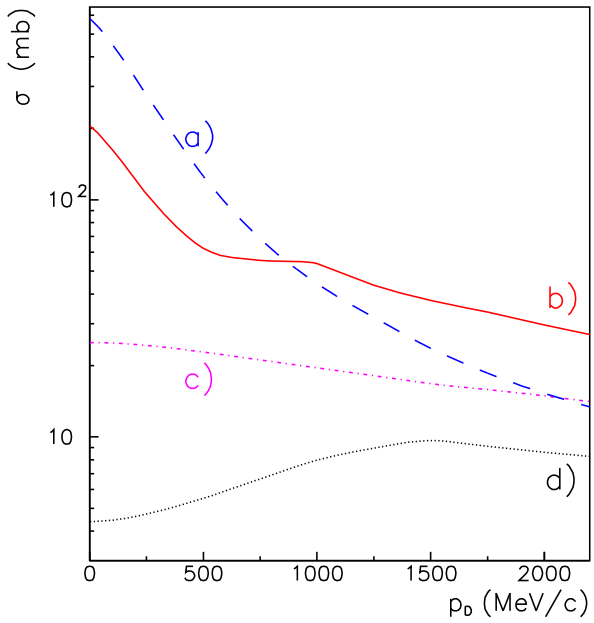

Fig. 43: Elastic cross sections for (a) D^+p (dashed line), (b) D^+n (solid line), (c) D^-n (dash-dotted line) and (d) D^-p (dotted line) as a function of the D-meson momentum.

resonance $\Lambda_c(2595)$ and the $I = 1$ resonance $\Sigma_c(2800)$, respectively. Our model generates also a P-wave state which lies at 2803 MeV, i.e. just below the DN threshold. We are tempted to associate this state with the $\Lambda_c(2765)$ resonance, whose quantum numbers are not yet established.

4.7 Scaling laws in Coulomb excitation of neutron halo nuclei

Exotic nuclei are available as secondary beams at many radioactive beam facilities around the world. These unstable nuclei are generally weakly bound with few, if any, excited states. A well developed method to study halo nuclei is Coulomb excitation. An instructive example is the excitation of the $1/2^-$ bound state in ^{11}Be from the $1/2^+$ ground state. Halo nuclei are a low-energy phenomenon and can be described effectively in terms of a few low-energy parameters. Let us consider the single-particle excitation of a neutron from a ground state $i = 0$ to a bound excited state $i = 1$ with neutron separation energies $E_i > 0$. (For ^{11}Be we have $E_0 = 504$ keV and $E_1 = 184$ keV.) The size of the single-particle wave functions is determined by the bound-state constants $q_i = \sqrt{2\mu E_i}/\hbar$ with the reduced mass $\mu = m_n m_c/(m_n + m_c)$ of the nucleon+core system. With the radius R of the core beyond which the nuclear interaction is assumed to vanish, it is possible to introduce dimensionless parameters $\gamma_i = q_i R$ that are a measure for the ratio of the core size to the size of the neutron wave functions. These parameters are small for halo nuclei, and can be used as convenient expansion parameters. In this spirit, we use this single-particle model for the $j_i^\pi = 1/2^+$ and $j_f^\pi = 1/2^-$ states

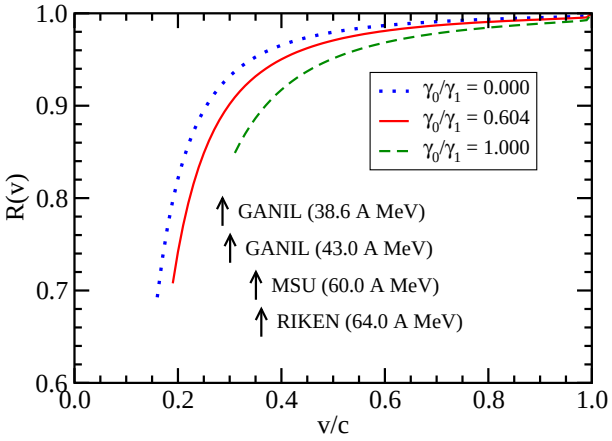

Fig. 44: Reduction factor R(v) as a function of the beam velocity v for values of 0 (blue dotted line), 0.604 (red solid line, the actual value) and 1 (green dashed line) of the ratio $\gamma_1/\gamma_0 = \sqrt{E_1/E_0}$. The beam velocities of the experiments at GANIL, MSU, and RIKEN are shown as arrows.

in order to evaluate the matrix element for the $E1$ electromagnetic excitation. It is dominated by the exterior contributions.

We treat electromagnetic excitation in the semiclassical approximation. For high beam velocities v the classical trajectory can be taken as a straight line with impact parameter b. In the sudden approximation one can take higher-order effects into account. Like the related Glauber or eikonal approximation it is applicable for high beam energies and low excitation energies. We obtain simple scaling laws for the excitation probabilities. Total cross sections are obtained by integration over the impact parameter, starting from a minimum impact parameter $b_{\min}$. We define a reduction factor $R(v) = \sigma^{(\infty)}/\sigma_{\rm LO}$ of the total excitation cross section $\sigma^{(\infty)} = \sigma_{\rm LO} + \sigma_{\rm NLO} + \ldots$ caused by higher-order effects. This factor $R(v)$ can be used to take higher-order effects into account in an analysis of the experimental data and is shown in Fig. 44. Our model is simple and realistic, appropriate for halo nuclei. The analytical results obtained are also very useful for benchmark tests of more involved numerical calculations.

5 Preparation of the HESR

5.1 Overview

Great progress has been achieved in developing a consistent operating scheme for the HESR to fulfill the numerous and to some extent conflicting user requirements. The previously developed normal conducting HESR lattice (see IKP Annual Report 2007) was refined to bring down the required quadrupole gradients to a level easily accessible to normal conducting quadrupole magnets. It could be verified that a satisfying performance within the required parameters is reached in every operating condition. All subsystems are now in the process of detailing the technical specifications. HESR work is more and more integrated into the FAIR project structure. All relevant documents for FAIR (and thus for HESR as well) from now on are stored using the electronic data management system EDMS of CERN to ensure a well defined flow of information between the participating laboratories. The HESR consortium led by the IKP now consists of members coming from Sweden, Poland, Romania, Georgia, Ukraine. The progress in the most relevant work packages for HESR is highlighted below.

5.2 RF Prototypes

Two RF cavities will be installed in the HESR. One large cavity will be used for beam acceleration, deceleration and for bunch rotation (see Fig. 45). Additionally a barrier bucket (BB) with $h = 1 \ldots 5$ will be formed by this large cavity to combine the decelerated bunch with a newly injected RESR bunch in the high luminosity mode (HL). During the experiment a small cavity will provide a low noise barrier-bucket signal (see Sect. 2.2). Both prototype cavities are manufactured and first RF-measurements were carried out at COSY. The parameters of the accelerating cavity are listed in Table 2.

Table 2: Basic parameters of the accelerating cavity.

The accelerating cavity	
HESR rev. frequencies	440 – 520 kHz
Frequency-range	1 – 10 harmonics (0.4 – 5 MHz)
Gap voltage	100 – 5000V peak
No of gaps	1
No of tanks	2
Mode of operation	cw
Cooling	water-cooled
Material	FineMet 3M

Fig. 45: Accelerating cavity for HESR installed on top of the former COSY tube amplifier.

5.3 Stochastic Cooling Prototypes

New pick-up structures for the HESR have been developed, namely a printed-loop coupler and a ring-slot coupler. With energies up to 2.5 GeV COSY is the ideal running accelerator to test the structures in an HESR like environment. The cooling tank which was designed to test the different structures with real beam (Fig. 46) is now installed in the COSY ring and measurements could be performed.

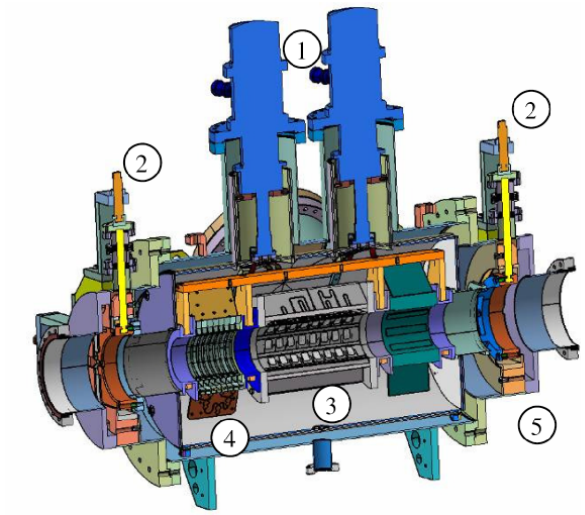

Fig. 46: Layout of the stochastic cooling test-tank: (1) cold heads, (2) *x*-*y* support, (3) printed loops, (4) ring slot coupler, (5) thermal shield. Tank length: 1.15 m flange to flange.

Selected results of tests with the COSY beam are illustrated in Fig. 47 and 48. Figure 47 compares two alternatives for the pick-up design that were developed in-house.

The red line shows the longitudinal signal of 6 rows of the lambda/4 structure, the blue line shows the same signal acquired by three electrode-rows of the slot coupler. It has to be pointed out that the higher signal could be gained with the shorter pick-up proving its higher sensitivity.

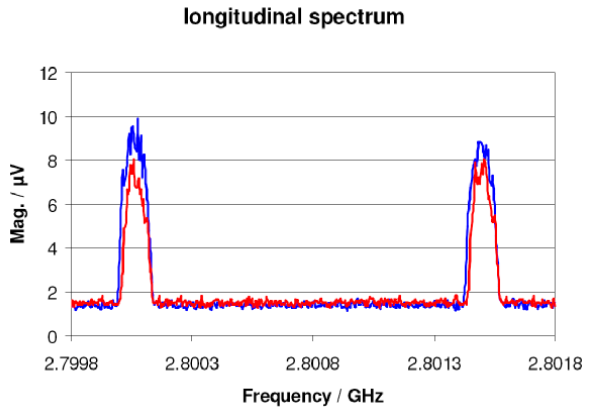

Fig. 47: Red: Longitudinal signal of 6 rows lambda/4 structure, blue: longitudinal signal of 4 electrode-rows slot coupler.

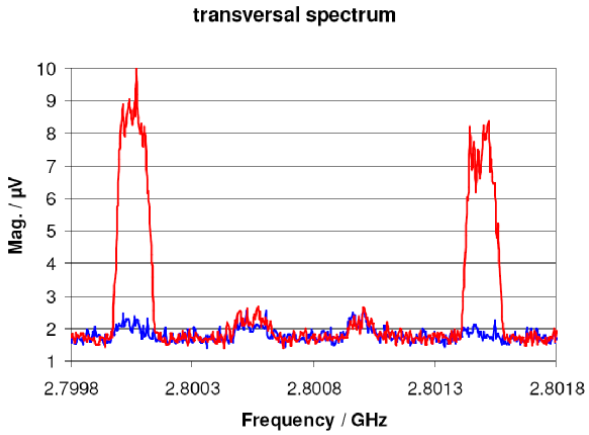

Fig. 48: Transverse spectra of slot coupler in horizontal direction, blue: centred beam, red: beam ~ 15 mm horizontally off center.

Figure 48 shows (i) that for an off-centered beam the signal at the harmonic frequencies is recorded properly proving the pick-ups to work as expected, and (ii) that betatron sidebands are visible with reasonable signal-to-noise ratio which could be used for transverse stoachastic cooling.

Apart from revealing the properties of the developed pick-ups the beam tests additionally proved the successful construction of the test tank including its cryogenic properties which are essential to obtain meaningful measurements.

5.4 Magnets

For all main magnets (dipole: Fig. 49, quadrupole: Fig. 50, sextupole: Fig: 51) blue prints are close to completion. Detailed lists of technical parameters are defined. For the case of the dipole magnet 3D magnetic field calculations are finished for field optimization (coil ends, harmonic analysis). For quadrupole and sextupole magnets these calculations are in progress. The sextupole magnets are designed with a wider gap to house the beam position monitors. Steering magnets are in the process of designing. A fruitful collaboration with colleagues from Romania could be set to investigate many aspects of the magnet design.

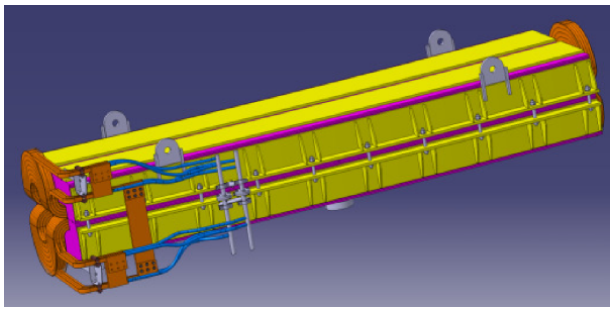

Fig. 49: HESR bent dipole magnet, length 4.2 m.

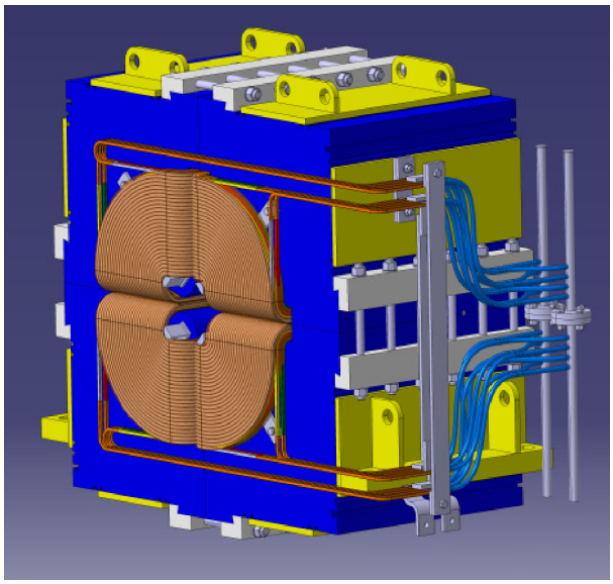

Fig. 50: HESR quadrupole magnet, length 60 cm.

5.5 Injection system

The injection beam line is inclined by 15° relative to the straight sections. Three elements are needed for the HESR injection (i) auxiliary dipole magnet, (ii) septum magnet, and (iii) fast kicker magnet. A combination of a septum magnet and an auxiliary dipole magnet will yield

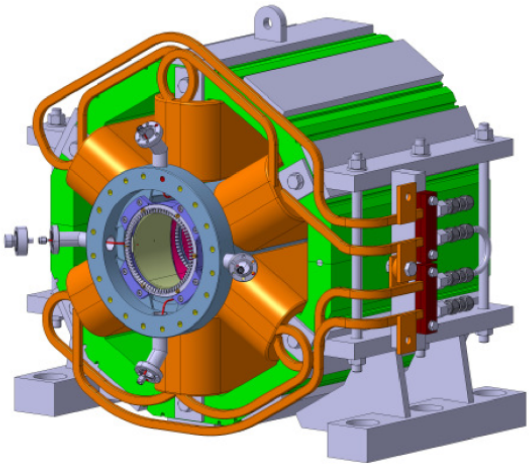

Fig. 51: HESR sextupole magnet with beam position monitor inserted, length 30 cm.

the total injection angle. Different combinations of the septum deflection angle and the auxiliary dipole magnet deflection angle are compared taking into account conventional electro-magnet designs and permanent magnet designs for the auxiliary dipole magnet. The final magnet in the injection chain is a fast kicker magnet. A dedicated design for HESR purpose has to be chosen, but the system is currently being optimized to make best use of standardized components of GSI kicker magnets. Characteristic parameters are summarized in Table 3. For all injection magnets the physics parameters are defined. Technical variations and financial impacts are being evaluated.

Table 3: Parameters of injection kicker magnet.

The injection kicker	
Total deflection angle	6 mrad
Number of modules	2
Max. kick angle per module	3.2 mrad
Rise time	200 ns
Time with constant field	550 ns
Fall time	200 ns
Repetition rate	< 0.1 Hz
Effective length of one module	0.96 m
Bending field	0.0814 T
Current	5833 A
Number of windings	1
Peak power dissipation for μs pulse	204 MW
Aperture of ferrite (h, v)	100 mm, 100 mm
Charge-up voltage	70 kV
Impedance of cable	6 Ω
Field in ferrite	0.102 T
Weight of ferrite	66.1 kg
Thickness of ferrite	40 mm

5.6 Electron cooling system

To ensure the high beam quality in HESR for precision experiments the HESR is equipped with a 4.5 MV electron cooler. The design is upgradeable to 8 MeV to reach the full energy of the HESR ring. It will be operated together with the stochastic cooling system to mutually benefit from the specific system advantages. The task to build the electron cooler is completely covered by our partners in Sweden (Uppsala University) and Poland (Soltan Institute, Warsaw). A conceptual layout is available for the complete list of sub-systems. A mechanical design is available for all major system components. Prototypes of critical components have been built and tested. A solenoid prototype for the high-voltage column, which will be gas-cooled, was tested for its thermal properties. Electron beam diagnostics is an important part to ensure the electron beam quality. A combined scraper and position pick-up will be used for diagnostics at the interaction section. In order to examine the sensitivity a scraper prototype was tested in the former CELSIUS electron cooler. The tests were successful showing that the sensitivity exceeded the specifications. The present work is directed towards tests of the electron gun and the electron collector prototypes. The electron gun is built by Uppsala University and the collector by the Soltan Institute. This work will continue in 2009.

6 The PANDA Experiment

6.1 Introduction

One major component of the **F**acility for **A**ntiproton and **I**on **R**esearch (FAIR) in Darmstadt is the **H**igh **E**nergy **S**torage **R**ing (HESR) with the "Anti**P**roton **AN**nihilations at **DA**rmstadt" - experiment ($\overline{\text{P}}$ANDA). The HESR will provide a phase space cooled antiproton beam of unsurpassed quality and precision. A momentum range up to 15 GeV/c together with an average interaction rate of 10 MHz will allow the detailed study of a wide variety of topics, like the structure of hadrons in the charmonium mass range, the spectroscopy of double hyper nuclei and electromagnetic processes. To serve this wide physics program the general purpose experiment $\overline{\text{P}}$ANDA is currently planned.

The basic concept of the detector is given by its division into two main parts, the central or target spectrometer and the forward spectrometer. This combines a nearly 4π coverage in the target region together with high acceptance of particles emitted at small polar angles in this fixed target kinematics.

The heart of the central spectrometer is a micro vertex detector located direct around the target for extremely precise tracking information. It is surrounded by the central tracker built either of straw tubes (STT) or a time projection chamber (TPC) in the barrel part, and a set of micro pattern gas detectors, so called triple gas electron multiplier detectors (GEM) in the forward direction. Particle identification is done by two ring imaging Cherenkov counters surrounded by a compact electromagnetic calorimeter made out of $PbWO_4$ crystals. The entire system is situated in a 2 T solenoidal magnet which is covered outside with detectors for muon identification and tracking.

The forward spectrometer consists of a 2 T·m dipole magnet with a set of multiwire drift chambers (MuDC) for tracking, a RICH detector for particle identification, calorimeters for charged and neutral particles and a layer of muon counters.

The ongoing activities of the IKP for the $\overline{\text{P}}$ANDA detector are focused in three parts: the micro vertex detector, the straw tube tracker and the simulation of the tracking detectors. Furthermore, the physics potential of the $\overline{\text{P}}$ANDA experiment for multistrange and charmed baryons has been evaluated.

6.2 Micro vertex detector

The Micro Vertex Detector (MVD) plays a key role in the $\overline{\text{P}}$ANDA experiment to identify open charm and strange hadrons by detecting secondary decays of particles displaced from the primary interaction point. These decay lengths range from a few 100 μm for charmed mesons and baryons up to several cm for strange hadrons.

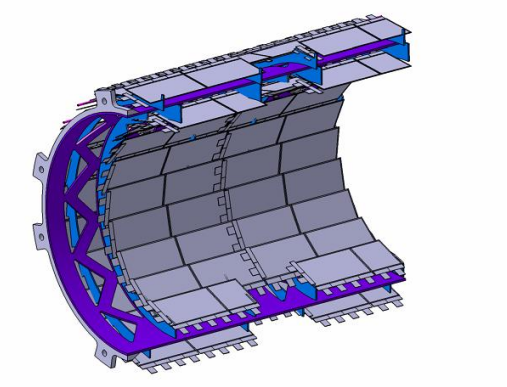

Fig. 52: CAD-Model of the two strip detector barrel layers.

6.2.1 Mechanical support structure

The vertex resolution of the MVD for low energetic particles is dominated by the multiple scattering of these particles as they go through the detector. To minimize the multiple scattering the overall radiation length of the detector has to be reduced. To achieve this the MVD has to be as lightweight as possible using only low-Z materials. Together with the INFN Torino, the IKV of the RWTH Aachen and the ZAT of the FZ-Jülich an intense design program has started to build a support structure for the MVD completely out of carbon sandwich structures. A first prototype of the support barrel for the strip sensors can be seen in Fig. 52. The basic structural component is a central barrel made out of two carbon fibre layers each 200 μm thin and a rohacell foam core. The two layers of strip readout sensors are connected to the central support structure via cogwheels which ensure a fan like overlapping of the sensors.

In Fig. 53 an enlarged picture of one sandwich structure can be seen which is used for the first prototype of the support structure which is under construction in Aachen and Jülich.

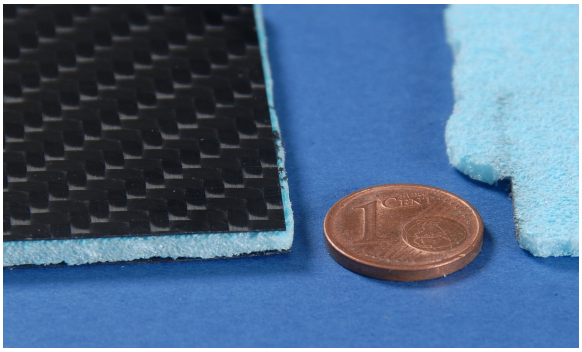

Fig. 53: Enlarged picture of the carbon sandwich structure used for the support structure of the MVD.

6.2.2 Readout system

To amplify, digitize and readout the hit data coming from the pixel sensors, two different custom made front-end electronic chips as options are foreseen. The first option is the FE-I3 front-end chip currently in use for the ATLAS pixel detector. This chip already features integrated analog-to-digital-converters (ADCs) via time-over-threshold (TOT) determination and a purely digital external interface eliminating the need for external analog circuitry. Its drawback are the pixel dimensions of 50x400 μm which give especially in the long direction a poor spatial resolution and the triggered readout architecture which is not optimal for the $\overline{\text{P}}$ANDA detector. Therefore, it is only considered as a fall back solution if the second option, a new custom made chip called ToPix fails. The ToPix chip is a development of the INFN Torino.
To verify the usability of the two readout chips a flexible test system was developed in Jülich which can easily be adopted to all kind of readout systems.
The tests on the FE-I3 are separated in two groups, basic functionality tests and performance tests: To test the basic functionality of the frontend chip, an automated register test which verifies data integrity can be executed with the digital readout system. In order to ensure that the subsequent tests yield reliable results, this basic check should be the first thing to be executed after connecting new hardware to the digital readout system.

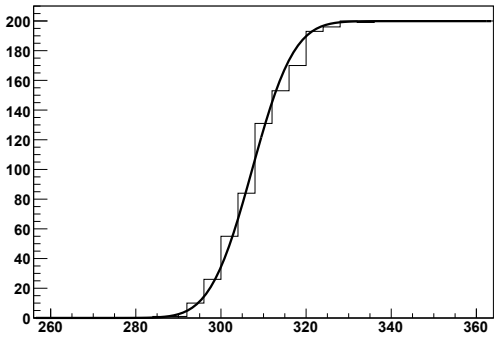

Fig. 54: Threshold scan results of a single pixel on an Atlas FE-I3. The response (total count of reported hits) of a single pixel to a threshold scan with 200 iterations per injected charge (in arbitrary units) is shown. An error function has been fit to the data.

The next step is determining the characteristics of the pixel cells found on the FE-I3. This is done by executing a threshold scan as follows. A known charge is injected repeatedly into the pixel's capacitor. The percentage of how often a hit is actually detected is recorded as a function of injected charge (Fig. 54). From these data, the pixel's threshold and noise can be extracted.
In Fig. 55, the threshold distribution of all the pixels on a frontend chip is shown. The large dispersion is a consequence of the individual thresholds not being tuned, but instead all being set to the same value. In practice, the data gained from this test is used to tune the individual thresholds in such a way that the observed pixel response to charge injection would be the same, or at least as similar as possible, for all pixels.

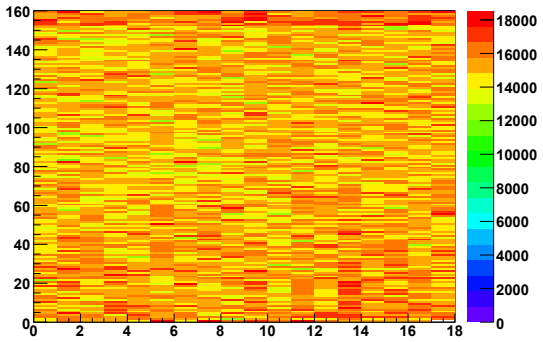

Fig. 55: Threshold scan results of all FE-I3 pixels arranged in 18 columns and 160 rows. The threshold distribution of the individual pixels for an uncalibrated frontend chip are plotted in arbitrary units.

The next application is the connection of the ToPiX frontend chip prototype to the digital readout system. This frontend chip is specifically designed for use in the $\overline{\text{P}}$ANDA MVD and currently under development at INFN Torino.

6.3 Frozen pellet target

Many technical and scientific applications, like experiments with internal targets at particle accelerators, require the transport of substances, which are gaseous at room temperatures, into an interaction zone. At the same time, the pressure in the surrounding vacuum chamber must be kept as small as possible. A solution of this technological challenge are so-called frozen pellet targets which provide fluxes of solid pellets from, *e.g.*, H_2, N_2, Ar or Xe with diameters in the 10 μ m range.
The central part of a pellet target is the triple-point chamber (TPC). In that chamber a jet of a cryogenic liquid is injected through a thin nozzle (with diameter roughly equal to the pellet diameter) into the same gaseous material close to triple-point conditions. Periodic excitation of the nozzle by a piezoelectric transducer imposes jet oscillations along its surface. The axially symmetric jet then disintegrates into drops downstream of the nozzle when the perturbation amplitude becomes equal to the jet radius. This domain is commonly denoted as the Rayleigh regime. From the TPC — which makes sure that an extremely regular drop flow can be produced under optimal conditions without disturbances from evaporation — the drops pass through a thin tube ("sluice") into vacuum. During that transition they cool, due to surface evaporation, by a few Kelvin below the freezing point, and a regular flux of very stable frozen pellets is produced.

The IKP has broad experience in building and operating pellet targets. A first generation pellet generator — originally build in Uppsala, Sweden — is being used at WASA for high-luminosity internal-target experiments. However, the pellet beam is too divergent to effectively employ that target for the $\overline{\text{P}}$ANDA experiment.
In order to produce the narrowest possible (diameters well below 1 mm), stable and mono-disperse pellet fluxes the drop-production process must be carefully optimzed and, in particular, the production of satellite drops of varying size must be supressed. That has recently been achieved at IKP, in close collaboration with two groups from ITEP Moscow and MPEI Moscow. The novel pellet generator (see Fig. 56) uses a patented cooling method that suppresses disturbing nozzle vibrations. Figure 57 shows an example for the extremely regular and satellite-free breakup of a cryogenic jet that can now be achieved.

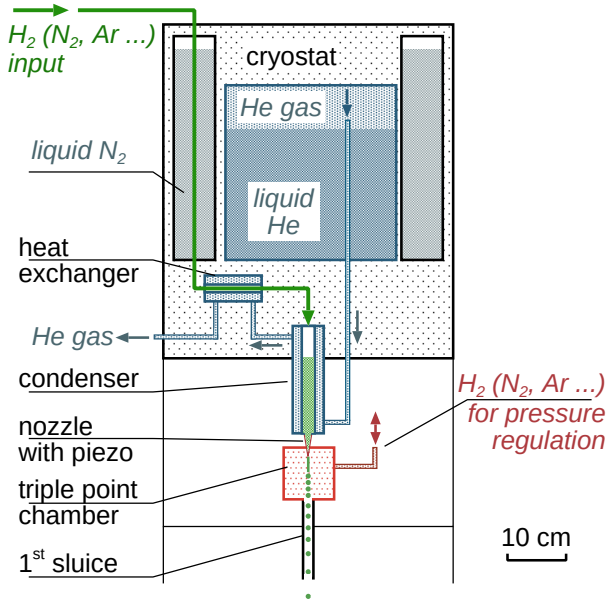

Fig. 56: Sketch of the drop generator. The cryostat (total height ∼0.8 m, not drawn to scale) comprises the cooling liquids (N_2 and He) as well as the heat exchanger and the upper part of the condenser. These are cooled by a stream of evaporated He gas. The condenser houses a few cm^3 of the cryogenic liquid which is driven through a nozzle into the TPC by overpressure. Constant pressure in the TPC is maintained by an auxiliary gas feeding.

So far, stable H_2, N_2 and Ar pellet production with diameters 20–40 μm and a pellet rate of a few 10 kHz has been observed. Deviations from the mean pellet diameter are below 1% (10%) over periods of few seconds (hours). The average velocity of 30 μm pellets is ∼70 m/s. The radial displacement of the pellets from their nominal flight path in a dummy scattering chamber (at a distance of more than one meter from the drop generator) of about $\pm$200 μm has been extrapolated from the angular pellet distributions measured behind the sluice from the TPC.

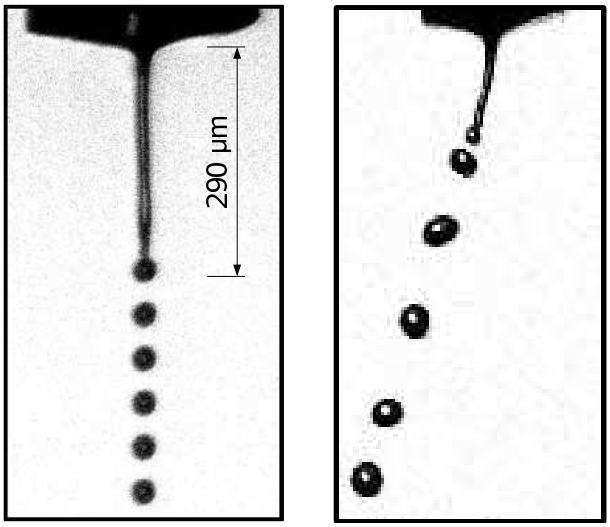

Fig. 57: Left: First observation of satellite-free disintegration of a cryogenic jet (here: N_2, diameter 17 μm) in the TPC. Right: At low pressures the jets bend, spontaneously breaking the axial symmetry of the setup.

This value is dominated by the experimental resolution. From the jet and drop parameters in the TPC together with the measured pellet velocity, the pellet-to-pellet distance in the scattering chamber can be calculated (assuming that all drops reach the chamber as pellets). For H_2 jets one obtains a value of 1.65 mm which will be experimentally verified during future tests at IKP.
Based on the layout of the prototype pellet generator the $\overline{\text{P}}$ANDA pellet target will be built. This target will comprise of a new adjustment system for the vibrating nozzle which will be installed and tested at the existing prototype in 2009.
The drop generator has also been used to study for the first time quantitatively the breakup of cryogenic jets into drops. Surprisingly, H_2 and N_2 jets reveal deviations from linear behavior, indicating that Rayleigh's well established theory formulated in 1878 is not appropriate for thin jets that exchange energy and/or mass with the surrounding medium. Another new phenomenon, for which so far not even a rudimentary theoretical explanation has been formulated, are jet modes where the axial symmetry of the dynamics is lost (Fig. 57).

6.4 Luminosity monitor

The $\overline{\text{P}}$ANDA experiment requires a very precise measurement of the luminosity to measure absolute branching ratios. Therefore a dedicated luminosity monitor is under development in IKP. The well known elastic antiproton-proton scattering process was taken as reference channel in which the forward outgoing antiproton is measured. The detector will be located at about 10.5 m downstream of the target of the $\overline{\text{P}}$ANDA detector. At this position the luminosity monitor measures particles at a radial dis-

tance between 3 cm and 8 cm from the beam axis, where the process is dominated by Coulomb interaction. The luminosity monitor consists of a sequence of four planes of double sided silicon strip detectors. The planes are separated by 20 cm along the beam direction. Each plane consists of 4 sensors 2 cm x 5 cm x 300 μm, with 50 μm pitch arranged radially to the beam axis and together placed in the vacuum. With this arrangement the particles can be tracked back to the target area to reduce the background of particles not coming from the primary interaction.
At the moment an intensive simulation program is ongoing under the use of the pandaRoot framework to optimize the detector layout which can be seen in Fig. 58.

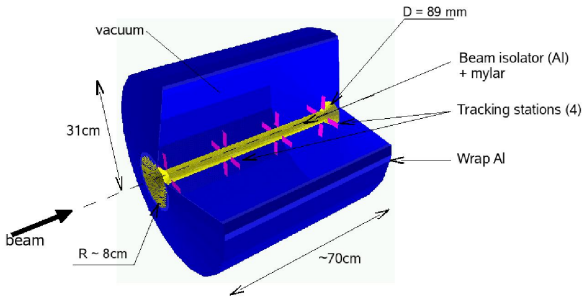

Fig. 58: Schematic overview of the luminosity monitor concept

A Councils

A.1 Hadron Physics Program Advisory Council

Prof. R. Beck	Universität Bonn	
Prof. J.-P. Blaizot	CEA Saclay, FR	
Prof. D.F. Geesaman	Argonne National Laboratory, U.S.A.	
Dr. P. Gianotti	Laboratori Nazionali di Frascati, I	
Prof. M. Harakeh	KVI Groningen, NL	
Prof. E. Jaeschke	Humboldt Universität Berlin	
Prof. K. Königsmann	Albert-Ludwigs-Universität Freiburg	
Prof. R. Kulessa	Jagellonian University Cracow, PL	
Prof. St. Paul	TU München	Chairperson
Prof. K. Peters	GSI Darmstadt	
Prof. U. Wiedner	Universität Bochum	
Prof. U.-J. Wiese	Universität Bern	

A.2 COSY Program Advisory Committee

Prof. M. Anselmino	L'Universita di Torino, IT	
Prof. D. Barber	DESY, DE	
Prof. J. Bijnens	Lund University, SE	
Prof. N. Herrmann	Universität Heidelberg, DE	
Prof. B. Kämpfer	FZ Dresden-Rossendorf, DE	
Prof. H. Löhner	KVI Groningen, NL	
Prof. A. Magiera	Jagellonian University Cracow, PL	
Prof. W. Meyer	Ruhr-Universität Bochum, DE	
Prof. W.T.H. van Oers	University of Manitoba, CA	Chairperson
Prof. A.K. Opper	George Washington University, USA	
Prof. E. Oset	Universitat de Valencia, ES	
Prof. U. Thoma	Universität Bonn, DE	

B Publications

1. Experiment

1. Abd El-Bary, S.; COSY-TOF, Collaboration
Two-pion production in proton-proton collisions with a polarized beam
European Physical Journal A **37** (2008) 267.

2. Abdel-Bary, M.; COSY-TOF, Collaboration
Analyzing power *Ay* for ω meson production in proton-proton collisions
Physics Letters B **662** (2008) 14.

3. Abdel-Bary, M.; COSY-TOF, Collaboration
Single pion production in *np* collisions for excess energies up to 90 MeV
European Physical Journal A **36** (2008) 7.

4. Bargholtz, Chr.; CELSIUS-WASA, Collab.
The WASA detector facility at CELSIUS
Nuclear Instruments and Methods in Physics Research Section A **594** (2008) 339.

5. Berlowski, M.; Bargholtz, Chr.; Bashkanov, D.; Bogolawsky, D.; Bondar, A.; Calén, H.; Cappellaro, F.; Clement, H.; Demirörs, L.; Ekström, C.; Fransson, K.; Geren, L.; Gustafsson, L.; Höistad, B.; Ivanov, G.; Jacewicz, M.; Jiganov, E.; Johansson, T.; Keleta, S.; Koch, I.; Kullander, S.; Kupsc, A.; Kuzmin, A.; Kuznetsov, A.; Laukhin, I.V.; Lindberg, K.; Marciniewski, P.; Meier, R.; Morosov, B.; Oelert, W.; Pauly, C.; Pettersson, H.; Petukhov, Y.; Povtorejko, A.; Ruber, R.J.M.Y.; Schönning, K.; Scobel, W.; Shafigullin, R.; Shwartz, B.; Skorodko, T.; Sopov, V.; Stepaniak, J.; Tegner, P.-E.; Thörngren Engblom, P.; Tikhomirov, V.; Turowiecki, A.; Wagner, G.J.; Wolke, M.; Yamamoto, A.; Zabierowski, J.; Zartova, I.; Złomanczuk, J.
Measurement of η meson decays into lepton-antilepton pairs
Physical Review D **77** (2008) 032004.

6. Boukharov, A.V.; Büscher, M.; Gerasimov, A.S.; Chernetsky, V. D.; Fedorets, P.V.; Maryshev, I.N.; Semenov, A.A.; Ginevskii, A.F.
Dynamics of Cryogenic Jets: Non-Rayleigh Breakup and Onset of Nonaxisymmetric Motions
Physical Review Letters **100** (2008) 174505.

7. Budzanowski, A.; Fidelus, M.; Filges, D.; Goldenbaum, F.; Hodde, H.; Jarczyk, L.; Kamys, B.; Kistryn, M.; Kistryn, St.; Kliczewski, St.; Kowalczyk, A.; Kozik, E.; Kulessa, P.; Machner, H.; Magiera, A.; Piskor-Ignatowicz, B.; Pysz, K.; Rudy, Z.; Siudak, R.; Wojciechowski, M.
Competition of coalescence and "fireball" processes in nonequilibrium emission of light charged particles from *p*+Au collisions
Physical Review C **78** (2008) 024603.

8. Covita, D.S.; Ay, M.; Schlesser, S.; Gotta, D.; Simons, L. M.; Le Bigot, E.-O.; dos Santos, J.M.F.
Accurate miscut angle determination for spherically bent Bragg crystals
Review of Scientific Instruments **79** (2008), 033102

9. Dzyuba, A.; Büscher, M.; Hanhart, C.; Kleber, V.; Koptev, V.; Ströher, H.; Wilkin, C.
Interpretation of $K\bar{K}$ pair production in *pp* collisions
European Physical Journal A **38** (2008) 1.

10. Dzyuba, A.; Büscher,M.; Hartmann,M.; Keshelashvili,I.; Koptev,V.; Maeda,Y.; Sibirtsev,A.; Ströher,H.; Wiklin,C.
Coupled-channel effects in the $pp \to ppK^+K^-$ reaction
Physics Letters B **668** (2008) 315.

11. Gabrielse, G.; Larochelle, P.; Le Sage, D.; Levitt, B.; Kolthammer, W. S.; McConnell, R.; Richerme, P.; Wrubel, J.; Speck, A.; George, M.C.; Grzonka, D.; Oelert, W.; Sefzick, T.; Zhang, Z.; Carew, A.; Comeau, D.; Hessels, E.A.; Storry, C. H.; Weel, M.; Walz, J.
First Antihydrogen Production within a Penning-Ioffe Trap
Physical Review Letters **100** (2008) 113001.

12. Gotta, D.; Rashid, K.; Fricke, B.; Indelicato, P.; Simons, L. M.
X-ray transitions from antiprotonic noble gases
European Physical Journal D **47** (2008), 11 - 26

13. Jayanti, R.; Machner, H.; Buhr, G.; Nolte, M.; Palarczyk, M.
Correlations of projectile like fragments in heavy ion reactions at Fermi energy
European Physical Journal A **38** (2008) 35.

14. Kleines, H.; Zwoll, K.; Wüstner, P.; Erven, W.; Kämmerling, P.; Kemmerling, G.; Loevenich, H.; Ackens, A.; Wolke, M.; Hejny, V.; Ohm, H.; Sefzick, T.; Nellen, R.; Marciniewski, P.; Fransson, K.; Gustafsson, L.; Kupsc, A.; Calén, H.
Performance Issues of the New DAQ System for WASA at COSY
IEEE Transactions on Nuclear Science **55** (2008) 261.

15. Komarov, V.; Azaryan, T.; Chiladze, D.; Dymov, S.; Hartmann, M.; Kacharava, A.; Keshelashvili, I.; Khoukaz, A.; Kulikov, A.; Kurbatov, V.; Macharashvili, G.; Merzliakov, S.; Mikirtytchiants, S.; Papenbrock, M.; Nekipelov, M.; Rathmann, F.; Serdyuk, V.; Ströher, H.; Tsirkov, D.; Uzikov, Yu.; Wiklin, C.
Observation of inverse diproton photodisintegration at intermediate energies
Physical Review Letters **101** (2008) 102501.

16. Kurbatov, V.; Büscher, M.; Dymov, S.; Gusev, D.; Hartmann, M.; Kacharava, A.; Khoukaz, A.; Komarov, V.; Kulikov, A.; Macharashvili, G.; Mersmann, T.; Merzliakov, S.; Mikirtytchiants, S.; Prasuhn, D.; Rathmann, F.; Schleichert, R.; Ströher, H.; Tsirkov, D.; Uzikov, Yu.; Wilkin, C.; Yaschenko, S.
Energy depence of forward $^1S_0$ diproton production in the $pp \to pp\pi^0$ reaction
Physics Letters B **661** (2008) 22.

17. Maeda, Y.; Hartmann, M.; Keshelashvili, I.; Barsov, S.; Büscher, M.; Drochner, M.; Dzyuba, A.; Hejny, V.; Kacharava, A.; Kleber, V.; Koch, H.R.; Koptev, V.; Kulessa, P.; Lorentz, B.; Mersmann, T.; Mikirtytchiants, S.; Mussgiller, A.; Nekipelov, M.; Ohm, H.; Prasuhn, D.; Schleichert, R.; Stein, H.J.; Ströher, H.; Valdau, Yu.; Wilkin, C.; Wüstner, P.
Kaon pair production in proton-proton collisions
Physical Review C **77** (2008) 015204.

18. Maeda, Y.; Segawa, M.; Ishida, T.; Kacharava, A.; Nomachi, M.; Shimbara, Y.; Sugaya, Y.; Tamura, K.; Yagita, T.; Yasuda, K.; Yoshida, H.P.; Wilkin, C.
Differential cross section and analyzing power of the $pp \to pp\pi^0$ reaction at a beam energy of 390 MeV
Physical Review C **77** (2008) 044004.

19. Murata, I.; Filges, D.; Goldenbaum, F.
A new approach to estimate importance for weight window in forward Monte-Carlo calculations
Nuclear Science and Engineering **159** (2008) 273.

20. Nünighoff, K.; Pohl, C.; Koulikov, S.; Cantargi, F.; Conrad, H.; Filges, D.; Glückler, H.; Goldenbaum, F.; Granada, F.; Hansen, G.; Matzerath, T.; Paul, N.; Petriw, S.; Schaal, H.; Soltner, H.; Stelzer, H.; Ninaus, W.; Wohlmuther, M.
Neutron experiments with cryogenic methane hydrate and mesitylene moderators
European Physical Journal A **38** (2008) 115.

21. Siudak, R.; Budzanowski, A.; Chatterjee, A.; Clemens, H.; Dorochkevitsch, E.; Ernst, J.; Hawranek, P.; Hinterberger, F.; Jahn, R.; Jarczyk, L.; Joosten, R.; Kilian, K.; Kirillov, Di.; Kliczewski, S.; Kolev, D.; Kravcikova, M.; Machner, H.; Magiera, A.; Martinska, G.; Massmann, F.; Munkel, J.; Piskunov, N.; Protic, D.; Ritman, J.; von Rossen, P.; Roy, B.; Sitnik, I.; Slepnev, I.; Smyrski, J.; Tsenov, R.; Ulbrich, K.; Urban, J.; Vankova, G.; Wagner, G. J.; Ziegler, R.
A threshold Cherenkov detector for K^+/π^+ separation using silica aerogel
Nuclear Instruments and Methods in Physics Research Section A **596** (2008) 311.

22. Skorodko, T.; Bashkanov, M.; Bogoslawsky, D.; Calén, H.; Cappellaro, F.; Clement, H.; Demirörs, L.; Doroshkevich, E.; Duniec, D.; Ekström, C.; Fransson, K.; Gustafsson, L.; Höistad, B.; Ivanov, G.; Jacewicz, M.; Jiganov, E.; Johansson, T.; Khakimova, O.; Kaskulov, M.; Keleta, S.; Koch, I.; Kren, F.; Kullander, S.; Kupsc, A.; Kuznetsov, A.; Marciniewski, P.; Meier, R.; Morosov, B.; Pauly, C.; Petterson, H.; Petukhov, Y.; Povtorejko, A.; Schönning, K.; Scobel, W.; Shwartz, B.; Sopov, V.; Stepaniak, J.; Thörngren Engblom, P.; Tikhomirov, V.; Wagner, G.J.; Wolke, M.; Yamamoto, A.; Zabierowski, J.; Złomanczuk, J.
Excitation of the Roper resonance in single- and double-pion production in nucleon-nucleon collisions
European Physical Journal A **35** (2008) 317.

23. Zychor, I.; Büscher, M.; Hartmann, M.; Kacharava, A.; Keshelashvili, I.; Khoukaz, A.; Kleber, V.; Koptev, V.; Maeda, Y.; Mersmann, T.; Mikirtychiants, S.; Schleichert, R.; Ströher, H.; Valdau, Yu.; Wilkin, C.

Lineshape of the $\Lambda(1405)$ hyperon measured through its $\Sigma^+\pi^0$ decay
Physics Letters B **660** (2008) 167.

2. Theory

24. Baltz, A. J.; Baur, G.; d'Enterria, D.; Frankfurt, L.; Gelis, F.; Guzey, V.; Hencken, K.; Kharlov, Yu.; Klasen, M.; Klein, S. R.; Nikulin, V.; Nystrand, J.; Pshenichnov, I. A.; Sadovsky, S.; Scapparone, E.; Seger, J.; Strikman, M.; Tverskoy, M.; Vogt, R.; White, S. N.; Wiedemann, U. A.; Yepes, P.; Zhalov, M.
The Physics of Ultraperipheral Collisions at the LHC
Physics Reports **458** (2008) 1.

25. Baru, V.; Haidenbauer, J.; Hanhart, C.; Kudryavtsev, A. E.; Lensky, V.; Meißner, U.-G.
Role of the $\Delta(1232)$ in pion-deuteron scattering at threshold within chiral effective field theory
Physics Letters B **659** (2008) 184.

26. Baur, G.; Typel, S.
Coulomb dissociation, a tool for nuclear astrophysics
Journal of Physics G **35** (2008) 014028.

27. Belushkin, M. A.; Hammer, H. W.; Meißner, U.-G.
Model-independent extraction of two-photon effects in elastic electron-proton scattering
Physics Letters B **658** (2008) 138.

28. Bernard, V.; Epelbaum, E.; Krebs, H.; Meißner, U.-G.
Subleading contributions to the chiral three-nucleon force I: long-range terms
Physical Review C **77** (2008) 064004.

29. Bernard, V.; Lage, M.; Meißner, U.-G.; Rusetsky, A.
Analysis of the Δ-resonance in a finite volume
European Physical Journal A **35** (2008) 281.

30. Bernard, V.; Lage, M.; Meißner, U.-G.; Rusetsky, A.
Resonance properties from the finite-volume energy spectrum
Journal of High Energy Physics **08** (2008) 024.

31. Bernard, V.; Meißner, U.-G.; Rusetsky, A.
The Δ-resonance in a finite volume
Nuclear Physics B **788** (2008) 1.

32. Bigi, I.I.; Devidze, G.G.; Liparteliani, A.G; Meißner, U.-G.
$B \to \gamma\gamma$ in an Appelquist-Cheng-Dobrescu model
Physical Review D **78** (2008) 097501.

33. Borasoy, B.; Bruns, P. C.; Meißner, U.-G.; Nißler, R.
A gauge invariant chiral unitary framework for kaon photo- and electroproduction on the proton
European Physical Journal A **34** (2008) 161.

34. Borasoy, B.; Epelbaum, E.; Krebs, H.; Lee, D.; Meißner, U.-G.
Chiral effective field theory on the lattice at next-to-leading order
European Physical Journal A **35** (2008) 343.

35. Bruns, P.C.; Meißner, U.-G.
Infrared regularization with vector mesons and baryons
European Physical Journal C **58** (2008) 407.

36. Döring, M.; Ajaka, J.; Assafiri, Y.; Bartalini, O.; Bellini, V.; Bouchigny, S.; Castoldi, M.; D'Angelo, A.; Didelez, J. P.; Di Salvo, R.; Fantini, A.; Fichen, L.; Gervino, G.; Ghio, F.; Girolami, B.; Giusa, A.; Guidal, M.; Hourany, E.; Kunne, R.; Lapik, A.; Sandri, P. L.; Moricciani, D.; Muskarenkov, A.; Nedorezov, V.; Oset, E.; Randieri, C.; Rudnev, N.; Russo, G.; Schaerf, C.; Sperduto, M.; Sutera, M.; Turinge, A.
Simultaneous Photoproduction of η and π^0 Mesons on the Proton
Physical Review Letters **100** (2008) 05200.

37. Döring, M.; Oset, E.
s wave pion nucleus optical potential
Physical Review C **77** (2008) 024602.

38. Döring, M.; Oset, E.; Jido, D.
Transition form factors of the $N(1535)$ as a dynamically generated resonance
Physical Review C **77** (2008) 065207.

39. Döring, M.; Oset, E.; Zou, B. S.
Role of the N(1535) resonance and the $\pi^- p \to KY$ amplitudes in the OZI forbidden $\pi N \to \phi N$ reaction
Physical Review C **78** (2008) 025207.

40. Entem, D.R.; Ruiz Arriola, E.; Pavon Valderrama, M.; Machleidt, R.
Renormalization of chiral two-pion exchange NN interactions. Momentum vs. coordinate space
Physical Review C **77** (2008) 044006.

41. Epelbaum, E.
Chiral dynamics of few-nucleon systems
Nuclear Physics A **805** (2008) 439.

42. Epelbaum, E.
Few-nucleon forces and systems in chiral effective field theory
Few-Body Systems **43** (2008) 57.

43. Epelbaum, E.
Isospin-breaking nuclear forces with Δ degrees of freedom
Few-Body Systems **44** (2008) 129.

44. Epelbaum, E.; Krebs, H.; Meißner, U.-G.
Δ-excitations and the three-nucleon force
Nuclear Physics A **806** (2008) 65.

45. Epelbaum, E.
Four-nucleon force using the method of unitary transformation
European Physical Journal A **34** (2008) 197.

46. Epelbaum, E.; Krebs, H.; Meißner, U.-G.
Isospin-breaking two-nucleon force with explicit Δ-excitations
Physical Review C **77** (2008) 034006.

47. Guo, F.-K.; Hanhart, Chr.; Krewald, S.; Meißner, U.-G.
Subleading contributions to the width of the $D_{s0}^*(2317)$
Physics Letters B **666** (2008) 251.

48. Guo, F.-K.; Hanhart, Chr.; Meißner, U.-G.
Evidence that the $Y(4660)$ is a $f_0(980)\Psi'$ bound state
Physics Letters B **665** (2008) 26.

49. Guo, F.-K.; Krewald, S.; Meißner, U.-G.
Hadronic-loop induced mass shifts in scalar heavy-light mesons
Physics Letters B **665** (2008) 157.

50. Guo, F.-K.; Hanhart, Chr.; Meißner, U.-G.
Mass splittings within heavy baryon isospin multiplets in chiral perturbation theory
Journal of High Energy Physics **09** (2008) 136.

51. Haidenbauer, J.
Meson production in nucleon-nucleon collisions
Few-Body Systems **43** (2008) 83.

52. Haidenbauer, J.; Krein, G.; Meißner, U.-G.; Sibirtsev, A.
Charmed meson rescattering in the reaction $\bar{p}d \to D\bar{D}N$
European Physical Journal A **37** (2008) 55.

53. Haidenbauer, J.; Meißner, U.-G.; Sibirtsev, A.
Near threshold $p\bar{p}$ enhancement in the $J/\Psi \to \omega p\bar{p}$ decay
Physics Letters B **666** (2008) 352.

54. Hanhart, C.
How and when can one identify hadronic molecules in the baryon spectrum
European Physical Journal A **35** (2008) 271.

55. Hanhart, Chr.; Pelaez, J. R.; Rios, G.
Quark mass dependence of the rho and sigma from dispersion relations and Chiral Perturbation Theory
Physical Review Letters **100** (2008) 152001.

56. Kalashnikova, Yu. S.; Kudryavtsev, A. E.; Nefediev, A. V.; Haidenbauer, J.; Hanhart, C.
Comment on 'Once more about the $K\bar{K}$ molecule approach to the light scalars'
Physical Review D **78** (2008) 058501.

57. Kistryn, St.; Stephan, E.; Kalantar-Nayestanaki, N.; Biegun, A.; Bodek, K.; Ciepal, I.; Deltuva, A.; Epelbaum, E.; Fonseca, A. C.; Glöckle, W.; Golak, J.; Kamada, H.; Kis, M.; Klos, B.; Kozela, A.; Nogga, A.; Mahjour-Shafiei, M.; Micherdzinska, A.; Sauer, P. U.; Skibinski, R.; Sworst, Z.; Witala, H.; Zejma, J.; Zipper, W.
Studies of the three-nucleon system dynamics: Cross sections of the deuteron-proton breakup at 130 MeV
Few-Body Systems **44** (2008) 11.

58. Lyutorovich, N.; Speth, J.; Avdeenkov, A.; GrÃƒÂ¼mmer, F.; Kamerdzhiev, S.; Krewald, S.; Tselyaev, V.I.
Self-consistent calculations within the Green's function method including particle-phonon coupling and the single-particle continuum
European Physical Journal A **37** (2008) 381.

59. Meißner, U.-G.; Rakhimov, A. M.; Wirzba, A.; Yakhshiev, U. T.
Neutron-proton mass difference in finite nuclei and the Nolen-Schiffer anomaly
European Physical Journal A **36** (2008) 37.

60. Pavon Valderrama, M.; Nogga, A.; Ruiz Arriola, E.; Phillips, D. R.
Deuteron form factors in chiral effective theory: Regulator-independent results and the role of two-pion exchange
European Physical Journal A **36** (2008) 315.

61. Polinder, H.
Strange two-baryon interactions using chiral effective field theory
Few-Body Systems **44** (2008) 113.

62. Polinder, H.
***S*=-1, -2 baryon-baryon interactions in chiral effective field theory**
Nuclear Physics A **805** (2008) 188.

63. Slifer, K.; Amarian, M.; Auerbach, L.; Averett, T.; Berthot, J.; Bertin, P.; Bertozzi, B.; Black, T.; Brash, E.; Brown, D.; Burtin, E.; Calarco, J.; Cates, G.; Chai, Z.; Chen, J.-P.; Choi, S.; Chudakov, E.; Ciofi degli Atti, C.; Cisbani, E.; de Jager, C.W.; Deur, A.; DiSalvo, R.; Dieterich, S.; Djawotho, P.; Finn, M.; Fissum, K.; Fonvieille, H.; Frullani, S.; Gao, H.; Gao, J.; Garibaldi, F.; Gasparian, A.; Gilad, S.; Gilman, R.; Glamazdin, A.; Glashausser, C.; Glöckle, W.; Golak, J.; Goldberg, E.; Gomez, J.; Gorbenko, V.; Hansen, J.-O.; Hersman, B.; Holmes, R.; Huber, G.M.; Hughes, E.; Humensky, B.; Incerti, S.; Iodice, M.; Jensen, S.; Jiang, X.; Jones, C.; Jones, G.; Jones, M.; Jutier, C.; Kamada, H.; Ketikyan, A.; Kominis, I.; Korsch, W.; Kramer, K.; Kumar, K.; Kumbartzki, G.; Kuss, M.; Lakuriqi, E.; Laveissiere, G.; Lerose, J.; Liang, M.; Liyanage, N.; Lolos, G.; Malov, S.; Marroncle, J.; McCormick, K.; McKeown, R.D.; Meziani, Z.-E.; Michaels, R.; Mitchell, J.; Nogga, A.; Pace, E.; Papandreou, Z.; Pavlin, T.; Petratos, G.G.; Pripstein, D.; Prout, D.; Ransome, R.; Roblin, Y.; Rowntree, D.; Rvachev, M.; Sabatie, F.; Saha, A.; Salme, G.; Scopetta, S.; Skibinski, R.; Souder, P.; Saito, T.; Strauch, S.; Suleiman, R.; Takahashi, K.; Teijiro, S.; Todor, L.; Tsubota, H.; Ueno, H.; Urciuoli, G.; Van der Meer, R.; Vernin, P.; Voskanian, H.; Witala, H.; Wojtsekhowski, B.; Xiong, F.; Xu, W.; Yang, J.-C.; Zhang, B.; Zolnierczuk, P.
^{3}He spin-dependent cross sections and sum rules
Physical Review Letters **101** (2008) 022303.

64. Sworst, R.; Kistryn, St.; Stephan, E.; Biegun, A.; Bodek, K.; Ciepal, I.; Epelbaum, E.; Glöckle, W.; Golak, J.; Kalantar-Nayestanaki, N.; Kamada, H.; Klos, B.; Kozela, A.; Nogga, A.; Skibinski, R.; Witala, H.; Zejma, J.;

Zipper, W.
Influence of three-nucleon force effects on polarization observables of the ^{1}H($\vec{d}$,$\vec{p}p$)n breakup reaction at 130 MeV
Acta Physica Polonica B **39** (2008) 401.

65. Typel, S.; Baur, G.
Scaling laws and higher-order effects in Coulomb excitation of neutron halo nuclei
European Physical Journal A **38** (2008) 355.

66. Wirzba, A.
The Casimir effect as a scattering problem
Journal of Physics A **41** (2008) 164003.

3. Accelerator (including conference proceedings)

67. An, S.Z.; Bongardt, K.; Maier, R.; Tang, J.; Zhang, T.J.
Collective effects for long bunches in dual harmonic RF Systems
Chinese Journal of Physics **32** (2008) 139.

68. An, S.Z.; Bongardt, K.; Maier, R.; Tang, J.; Zhang, T.J.
Emittance-dominated long bunches in dual harmonic RF System
Chinese Journal of Physics **32** (2008) 60.

69. Bongardt, K.
ESS Plans and Synergy with CERN
Beam07 Proceedings (CERN Yellow Report 2008-005), p. 152

70. Dietrich, J.; Böhme, C.; Kamerdzhiev, V.
Beam Profile Measurements Based on Beam Interaction with Residual Gas
Proceedings of the 8th International Topical Meeting on Nuclear Applications and Utilization of Accelerators (ACCAPP'07), p. 138

71. Garishvili, A.; Lorentz, B.; Nass, A.; Lehrach, A.; Lenisa, P.; Maier, R.; Martin, S.; Rathmann, F.; Statera, M.; Steffens, E.; Ströher, H.
Storage Ring Section for a Polarized Gas Target with High Angular Acceptance
Polarized Ion Sources, Targets and Polarimetry (PSTP2007), AIP Conference Proceedings **980**, p. 176

72. Morozov, V.S.; Chao, A.W.; Krisch, A.D.; Leonova, M.A.; Raymond, R.S.; Sivers, D.W.; Wong, V.K.; Garishvili, A.; Gebel, R.; Lehrach, A.; Lorentz, B.; Maier, R.; Prasuhn, D.; Stockhorst, H.; Welsch, D.M.; Hinterberger, F.; Ulbrich, K.; Schnase, A.; Stephenson, E.J.; Brantjes, N.P.M.; Onderwater, C.J.G.; da Silva, M.
Experimental verification of striking predicted oscillations near a spin resonance
Physical Review Letters **100** (2008) 054801.

73. Senichev, Yu.
The advanced HESR lattice for improved stochastic cooling
Proceedings of the Workshop on Beam Cooling and Related Topics (COOL07), p. 102

74. Smirnov, A. V.; Meshkov, I. N.; Sidorin, A. O.; Dietrich, J.; Noda, A.; Shirai, T.; Souda, H.; Tongu, H.; Noda, K.
Necessary Condition for Beam Ordering
Proceedings of the Workshop on Beam Cooling and Related Topics (COOL07), p. 87

C Invited Talks and Colloquia

1. Baur, G.
   Pair production and ionization in relativistic ion-ion collisions
   WE-Heraeus-Seminar — Highly Charged Ions and Antiprotons
   Bad Honnef, Germany: 04.04.2008 – 12.04.2008

2. Baur, G.
   Exchange of high and low energy photons in ultraperipheral relativistic heavy ion collisions
   Workshop on High Energy Photon Collisions at the LHC
   Geneva, Switzerland: 22.04.2008 – 25.04.2008

3. Baur, G.
   Coherent photon-photon interactions in very peripheral relativistic heavy ion collisions
   Workshop and School on Fundamental Physics with Ultra-high Field
   Frauenwoerth: 29.09.2008 – 02.10.2008

4. Büscher, M.
   The Light Scalar Mesons $a_0/f_0(980)$ at COSY-Jülich
   Workshop on Scalar Mesons and Related Topics (Scadron 70)
   Lisboa, Portugal: 11.02.2008 – 16.02.2008

5. Büscher, M.
   Target TDR for PANDA: The Moscow-Jülich Pellet Target
   Plenary talk at the PANDA collaboration meeting
   Darmstadt, Germany: 11.12.2008

6. Czerwinski, E.
   Study of the Properties of the η' Meson at COSY-11
   CANU 2008 and JCHP-FFE Workshop
   Bad Honnef, Germany: 15.12.2008 – 16.12.2008

7. Dietrich, J.
   Beam Profile Measurements Based on Beam Interaction with Residual Gas
   Goethe-Universität Frankfurt am Main, Winterseminar Beschleunigerphysik
   Riezlern, Germany: 03.03.2008

8. Dietrich, J.
   Status 2 MeV Electron Cooler
   22nd HESR-Consortium
   Jülich, Germany: 11.03.2008

9. Dietrich, J.
   2 MeV Elektronenkühler für COSY-Jülich
   Johannes-Gutenberg-Universität Mainz
   Mainz, Germany: 23.10.2008

10. Dietrich, J.
    COSY — Status and Future
    University of Witwatersrand and iThemba LABS Gauteng
    Johannesburg, South Africa: 10.11.2008

11. Dietrich, J.
    COSY — Status and Future
    iThemba LABS
    Faure, South Africa: 20.11.2008

12. Dymov, S.
    Hadron Physics with Diproton Final States at ANKE-COSY
    MESON 2008
    Cracow, Poland: 06.06.2008 – 10.06.2008

13. Dymov, S.
Hadron Interactions with Diproton Final States at ANKE-COSY
STORI08
Lanzhou, China: 14.09.2008 – 18.09.2008

14. Dzhygadlo, R.
Hyperon-Rekonstruktion im COSY-TOF Straw Tube Tracker
CANU 2008 and JCHP-FFE Workshop
Bad Honnef, Germany: 15.12.2008 – 16.12.2008

15. Engels, R.
Precision Spectroscopy of Metastable Hydrogen or Antihydrogen with a Lamb-Shift Polarimeter
LEAP 2008
Vienna, Austria: 16.09.2008 – 19.09.2008

16. Engels, R.
How we recently switched on the magnet
WASA-at-COSY Collaboration Meeting
Jülich, Germany: 22.09.2008 – 23.09.2008

17. Engels, R.
First experiments with the Polarized Internal Target at ANKE/COSY
SPIN2008
Charlottesville, Va., U.S.A.: 06.10.2008 – 11.10.2008

18. Engels, R.
Precision Spectroscopy of Metastable Hydrogen with a Lamb-Shift Polarimeter
SPIN2008
Charlottesville, Va., U.S.A.: 06.10.2008 – 11.10.2008

19. Engels, R.
The Lamb-Shift Polarimeter: How it works and what it can be used for
Technische Universität München, Physik Department E18
München, Germany: 20.10.2008

20. Engels, R.
Precision Spectroscopy of Hydrogen: History and Future Experiments
Universität Basel
Basel, Switzerland: 05.12.2008

21. Epelbaum, E.
Few nucleons in chiral effective field theory
Universität Basel, Seminar
Basel, Schweiz: 13.03.2008

22. Epelbaum, E.
Effective field theory for few-nucleon systems
Donnersberg Workshop 2008 (A1 Collaboration)
Dannenfels, Germany: 31.03.2008 – 03.04.2008

23. Epelbaum, E.
Chiral dynamics of few-nucleon systems
Universität Bonn, Physikalisches Kolloquium
Bonn: 09.05.2008

24. Epelbaum, E.
Chiral dynamics of few-nucleon systems: Recent developments
VIQCD Meeting
Ferrara, Italy: 01.06.2008

25. Epelbaum, E.
Chiral EFT for few-nucleon systems
INT Workshop on Soft Photons and Light Nuclei
Seattle, Wash., U.S.A.: 16.06.2008 – 20.06.2008

26. Epelbaum, E.
Chiral effective field theory: the status
X Workshop on Electron-Nucleus Scattering
Elba, Italy: 23.06.2008 – 27.06.2008

27. Epelbaum, E.
Subleading contributions to the chiral three-nucleon force
410. WE-Heraeus-Seminar
Bad Honnef, Germany: 28.07.2008 – 30.07.2008

28. Epelbaum, E.
Chiral dynamics of few-nucleon systems: recent developments
Conference on Quark Confinement and the Hadron Spectrum
Mainz, Germany: 01.09.2008 – 06.09.2008

29. Epelbaum, E.
Effective theory with singular long-range interactions
ECT* Workshop on Bound States and Resonances in Effective Field Theories
Trento, Italy: 29.09.2008 – 03.10.2008

30. Epelbaum, E.
Chiral dynamics in nuclei
International Conference on Particles and Nuclei (PANIC08)
Eilat, Israel: 09.11.2008 – 14.11.2008

31. Epelbaum, E.
Nuclear lattice simulations based on chiral effective field theory
Universität Giessen, Graduiertenkolleg-Kolloquium
Giessen: 20.11.2008

32. Fedorets, P.
Pellet target (current status)
XXIV PANDA Collaboration Meeting
Darmstadt, Germany: 03.03.2008 – 07.03.2008

33. Fedorets, P.
Production of hydrogen, nitrogen and argon pellets with the Moscow-Jülich pellet target
STORI08
Lanzhou, China: 13.09.2008 – 19.09.2008

34. Fedorets, P.
Analysis of the reaction $pd \to {}^3\mathrm{He}(\pi^0\pi^0)/(\pi^0\eta) \to 3\mathrm{He}\,4\gamma$
WASA@COSY Collaboration Meeting
Jülich, Germany: 25.09.2008

35. Fedorets, P.
Scalar Mesons at WASA status and perspectives
WASA@COSY Collaboration Meeting
Jülich, Germany: 23.09.2008

36. Fedorets, P.
Status of high energy pd and dd data analysis
WASA-at-COSY Collaboration Meeting
Jülich, Germany: 27.03.2008

37. Fedorets, P.
Status of $pd \to {}^3\mathrm{He}\,X$ at $p = 2.935$ GeV/c ($T = 2.143$ GeV) from November 2007
WASA-at-COSY Workshop on Analysis of η and η' Decays
Uppsala, Sweden: 29.02.2008 – 02.03.2008

38. Garishvili, A.
Lattice Studies for Spinfiltering Experiments at COSY and AD
EPAC'08
Genoa, Italy: 23.06.2008 – 27.06.2008

39. Gebel, R.
Status Report of the Injector Cyclotron JULIC at COSY/Jülich
European Cyclotron Progress Meeting
Berlin, Germany: 15.10.2008 – 18.10.2008

40. Gillitzer, A.
Charm in nuclei
LEAP 2008
Vienna, Austria: 16.09.2008 – 19.09.2008

41. Goldenbaum, F.
Experimental data on evaporation and pre-equilibrium emission in GeV p-induced spallation reactions
Advanced Workshop on Model Codes for Spallation Reactions
Trieste, Italy: 04.02.2008 – 08.02.2008

42. Gotta, D.
Conclusions for Recent Pionic-Atom Experiments
International Workshop on Cold Antimatter Plasmas and Application to Fundamental Physics (pbar08)
Okinawa, Japan: 20.02.2008 – 22.02.2008

43. Gotta, D.
X-ray Spectroscopy of Light Hadronic Atoms
International Conference on Exotic Atoms (EXA08)
Vienna, Austria: 15.09.2008 – 19.09.2008

44. Grigoryev, K.
The Polarized Internal Gas Target of ANKE at COSY
STORI08
Lanzhou, China: 14.09.2008 – 18.09.2008

45. Grzonka, D.
Study of the spin triplet proton-lambda interaction using the COSY-11 detector
Symposium on Meson Physics
Cracow, Poland: 01.10.2008 – 04.10.2008

46. Haidenbauer, J.
Hyperon-Nucleon Interaction: From meson exchange to effective field theory
Universität Gießen, Kolloquium
GieÃŸen, Germany: 08.05.2008

47. Haidenbauer, J.
Investigating the D meson interaction in antiproton-deuteron collisions
Hadrons at Fair, FIAS
Frankfurt/Main, Germany: 25.06.2008 – 27.06.2008

48. Haidenbauer, J.
$\bar{p}p$ and $\bar{p}d$ interactions at medium energies
409. WE-Heraeus-Seminar — Polarized Antiprotons
Bad Honnef, Germany: 23.06.2008 – 25.06.2008

49. Haidenbauer, J.
Strangeness $S = -2$ Baryon-Baryon Interaction in Chiral Effective Field Theory
XVIIIth International Conference on Particles and Nuclei (PANIC08)
Eilat, Israel: 09.11.2008 – 14.11.2008

50. Haidenbauer, J.
The Interaction of D-Mesons with Nucleons
XVIIIth International Conference on Particles and Nuclei (PANIC08)
Eilat, Israel: 09.11.2008 – 14.11.2008

51. Hanhart, C.
A method to identify hadronic molecules and its application to X(3872) and X(3875)
GSI Darmstadt, Seminar
Darmstadt, Germany: 30.01.2008

52. Hanhart, C.
How to find molecules in the meson and baryon spectrum
International Workshop on Bound States and Resonances in Effective Field Theory
Trento, Italy: 29.09.2008 – 03.10.2008

53. Hanhart, C.
How to identify hadronic molecules in the spectrum: method and applications
Universität Bonn, Seminar
Bonn, Germany: 10.04.2008

54. Hanhart, C.
How to identify hadronic molecules in the spectrum: method and applications
University of Uppsala, Seminar
Uppsala, Sweden: 23.05.2008

55. Hanhart, C.
How to identify hadronic molecules in the spectrum: method and applications
Institute of High Energy Physics (IHEP), Seminar
Beijing, China: 19.09.2008

56. Hanhart, C.
Meson production from hadronic probes
STORI08
Lanzhou, China: 14.09.2008 – 18.09.2008

57. Hartmann, M.
Hyperon Physics at COSY
Frühjahrstagung der Deutschen Physikalischen Gesellschaft
Darmstadt, Germany: 14.03.2008

58. Hartmann, M.
Some Experimental Techniques at Storage Rings
STORI08
Lanzhou, China: 14.09.2008 – 18.09.2008

59. Hejny, V.
Charge symmetry breaking in $dd \to {}^4\mathrm{He}\,\pi^0$
WASA-at-COSY Collaboration Meeting
Jülich, Germany: 27.03.2008 – 28.03.2008

60. Hejny, V.
Passive base test on the calorimeter
WASA-at-COSY Analysis Meeting
Jülich, Germany: 26.03.2008 – 27.03.2008

61. Hügging, F.
Frei konfigurierbares digitales Auslesesystem für den PANDA MVD
Frühjahrstagung der Deutschen Physikalischen Gesellschaft
Darmstadt, Germany: 10.03.2008 – 14.03.2008

62. Janusz, M.
Feasibility of $\eta \to \pi^+\pi^- e^+ e^-$
WASA-at-COSY Workshop on Analysis of η and η' Decays
Uppsala, Sweden: 29.02.2008 – 02.03.2008

63. Janusz, M.
Status Report from CDC group
WASA-at-COSY Workshop on Analysis of η and η' Decays
Uppsala, Sweden: 29.02.2008 – 02.03.2008

64. Janusz, M.
PID (electron-pion) in CD (purity and efficiency)
WASA-at-COSY Workshop on Analysis of η and η' Decays
Uppsala, Sweden: 29.02.2008 – 02.03.2008

65. Janusz, M.
Status of analysis of April 2007 data
WASA-at-COSY Analysis Meeting
Jülich, Germany: 09.06.2008 – 10.06.2008

66. Janusz, M.
Study of the $\eta \to \pi^+\pi^- e^+ e^-$ decays with WASA-at-COSY
Symposium on Meson Physics
Cracow, Poland: 01.10.2008 – 04.10.2008

67. Janusz, M.
Charged Decays of η with WASA-at-COSY
CANU 2008 and JCHP-FFE Workshop
Bad Honnef, Germany: 15.12.2008 – 16.12.2008

68. Jany, B.R.
Feasibility of $\eta' \to \pi^+\pi^-\eta$
WASA-at-COSY Workshop on Analysis of η and η' Decays
Uppsala, Sweden: 29.02.2008 – 02.03.2008

69. Jany, B.R.
Bayesian Likelihood based FD Kinetic Energy reconstruction
WASA-at-COSY Workshop on Analysis of η and η' Decays
Uppsala, Sweden: 29.02.2008 – 02.03.2008

70. Jany, B.R.
FD Kinetic Energy Reconstruction
WASA-at-COSY Collaboration Meeting
Jülich, Germany: 27.03.2008 – 28.03.2008

71. Jany, B.R.
Trigger conditions for η' run
WASA-at-COSY Analysis Meeting
Jülich, Germany: 26.03.2008 – 27.03.2008

72. Jany, B.R.
In search of an η' signal: Status of April 08 data
WASA-at-COSY Collaboration Meeting
Jülich, Germany: 22.09.2008 – 23.09.2008

73. Jany, B.R.
In search of η' – Analysis of η' feasibility run
WASA-at-COSY Analysis Meeting
Jülich, Germany: 09.06.2008 – 10.06.2008

74. Kacharava, A.
Physics Program at COSY-Jülich with Polarized Hadronic Probes
SPIN2008
Charlottesville, Va., U.S.A.: 06.10.2008 – 11.10.2008

75. Khoukaz, A.
Hadron Physics at COSY
MESON 2008
Cracow, Poland: 06.06.2008 – 10.06.2008

76. Khoukaz, A.
Hadron Physics at COSY
STORI08
Lanzhou, China: 14.09.2008 – 18.09.2008

77. Kowalczyk, A.
Pion production in proton induced spallation reactions in the energy range of few GeV order
MESON 2008
Cracow, Poland: 06.06.2008 – 10.06.2008

78. Kowalzcyk, A.
Strangeness Production with WASA-at-COSY
CANU 2008 and JCHP-FFE Workshop
Bad Honnef, Germany: 15.12.2008 – 16.12.2008

79. Krewald, S.
Determination of Resonance Poles in Pion Nucleon Scattering
Workshop on Pion-Nucleon Partial Wave Analysis
Washington, DC, U.S.A.: 17.03.2008 – 20.03.2008

80. Krzemien, W.
Search for the ^{3}He-η bound state at COSY-11
MESON 2008
Cracow, Poland: 06.06.2008 – 10.06.2008

81. Lehrach, A.
Anwendung von Petawatt-Lasern
Universität Bonn: Habilitationskolloquium
Bonn, Germany: 27.05.2008

82. Lehrach, A.
Siberian Snakes for Spin-Filter Experiments
409. WE-Heraeus-Seminar — Polarized Antiprotons
Bad Honnef, Germany: 23.06.2008 – 25.06.2008

83. Lehrach, A.
The High Energy Storage Ring (HESR) for FAIR
STORI08
Lanzhou, China: 14.09.2008 – 18.09.2008

84. Lehrach, A.
Antimaterie — die gespiegelte Welt
Universität Bonn: Antrittsvorlesung
Bonn, Germany: 03.12.2008

85. Leonova, M.A.
SPIN@COSY: Spin-Manipulating Polarized Deuterons and Protons
SPIN2008
Charlottesville, Va., U.S.A.: 06.10.2008 – 11.10.2008

86. Leonova, M.A.
Experimental Test of New Technique to Overcome Spin-Depolarizing Resonances
SPIN2008
Charlottesville, Va., U.S.A.: 06.10.2008 – 11.10.2008

87. Leonova, M.A.
Experimental Verification of Predicted Oscillations near a Spin Resonance
SPIN2008
Charlottesville, Va., U.S.A.: 06.10.2008 – 11.10.2008

88. Lorentz, B.
HESR Linear Lattice Design
EPAC'08
Genoa, Italy: 23.06.2008 – 27.06.2008

89. Lorentz, B.
Machine Aspects of Spin Filtering Experiments
RuPAC 08
Zvenigorod, Russia: 28.09.2008 – 03.10.2008

90. Luccio, A.U.
Simulation of Spin Resonances of Polarized Deuterons in COSY
EPAC'08
Genoa, Italy: 23.06.2008 – 27.06.2008

91. Luccio, A.U.
Simulation of deuteron polarization at COSY
SPIN2008
Charlottesville, Va., U.S.A.: 06.10.2008 – 11.10.2008

92. Machner, H.
New developments in NN and NY Interactions
Bhabha Atomic Research Centre, seminar
Mumbai, India: 14.02.2008

93. Machner, H.
Recent developments in NN and NY Interactions — News from an old field
IV DAE-BRNS: Workshop on Hadron Physics
Aligarh, India : 18.02.2008 – 23.02.2008

94. Machner, H.
Correleations of projectile-like fragments in heavy-ion reactions at fermi energy
International School of Nuclear Physics
Erice, Italy: 16.09.2008 – 24.09.2008

95. Machner, H.
Recent developments in NN and NY Interactions — News from an old field
XIX International Baldin Seminar on High Energy Physics Problems
Dubna, Russia: 29.09.2008 – 04.10.2008

96. Meißner, U.-G.
An introduction to chiral perturbation theory
XXI Heidelberg Physics Graduate Days of the Graduate School of Fundamental Physics
Heidelberg, Germany: 29.09.2008 – 02.10.2008

97. Meißner, U.-G.
Gauge invariance and chiral coupled-channel dynamics
Workshop on Quark Hadron Dynamics
Almunecar, Spain: 25.09.2008 – 28.09.2008

98. Meißner, U.-G.
Nuclear lattice Simulations
410. WE-Heraeus Seminar
Bad Honnef, Germany: 28.07.2008 – 30.07.2008

99. Meißner, U.-G.
Nuclear physics from simulations
CEA-FZJ Workshop on High Performance Computing
Jülich, Germany: 21.01.2008 – 22.01.2008

100. Meißner, U.-G.
Nucleon form factors from dispersion theory
ECT* Workshop on Hadron Electromagnetic Form Factors
Trento, Italy: 12.05.2008 – 23.05.2008

101. Meißner, U.-G.
Theory of nuclear forces
The 7th CNS-EFES Summer School
Riken, Tokyo: 26.08.2008 – 01.09.2008

102. Meißner, U.-G.
Topics in baryon chiral perturbation theory
International Conference on Quark Confinement and the Hadron Spectrum (Confinement08), plenary talk
Mainz, Germany: 01.09.2008 – 06.09.2008

103. Mertens, M.
A Versatile Digital Readout System for the PANDA MVD
IEEE Nuclear Science Symposium
Dresden, Germany: 19.10.2008 – 25.10.2008

104. Nass, A.
Spin Filtering Studies at COSY and AD
SPIN2008
Charlottesville, Va., U.S.A.: 06.10.2008 – 11.10.2008

105. Nass, A.
Studies on Beam Formation in an Atomic Beam Source
SPIN2008
Charlottesville, Va., U.S.A.: 06.10.2008 – 11.10.2008

106. Nogga, A.
Using light nuclei to probe chiral nuclear interactions
International Workshop XXXVI on Gross Properties of Nuclei and Nuclear Excitations
Hirschegg, Austria: 13.01.2008 – 19.01.2008

107. Nogga, A.
Few-body systems with chiral interactions
Workshop of the SFB 634
Bad Godesberg: 22.10.2008 – 24.10.2008

108. Oelert, W.
Auf dem Weg zu Antiwasserstoff in Ruhe
Frühjahrstagung der Deutschen Physikalischen Gesellschaft
Darmstadt, Germany: 10.03.2008 – 14.03.2008

109. Oelert, W.
Das Spiegelbild der Antimaterie
Ansbach Gymnasium, Schülerseminar
Jülich, Germany: 12.03.2008

110. Oelert, W.
Antimaterie, das Gegenüber der Materie
Haus Overbach, Seminar
Jülich, Germany: 25.03.2008

111. Oelert, W.
On the way to physics with anti-hydrogen
409. WE-Heraeus — Polarized Antiprotons
Bad Honnef, Germany: 23.06.2008 – 25.06.2008

112. Oelert, W.
Introduction to the COSY accelerator at Jülich/Germany and examples of typical experiments
York University, Physics Department, Colloquium
Toronto, Canada: 09.12.2008

113. Oellers, D.
Measurement of the Depolarizing *pe* Spin Flip Cross Section using co-moving electrons
Frühjahrstagung der Deutschen Physikalischen Gesellschaft
Darmstadt, Germany: 14.03.2008

114. Oellers, D.
Polarized Antiprotons
Physikzentrum Bad Honnef
Bad Honnef, Germany: 23.06.2008

115. Pauly, Chr.
News from WASA
Crystal Ball Collaboration Meeting
Mainz, Germany: 21.09.2008

116. Pauly, Chr.
Search for Symmetry Breaking Patterns with WASA-at-COSY
International Conference on Particles and Nuclei (PANIC08)
Eilat, Israel: 09.11.2008 – 14.11.2008

117. Pavon-Valderrama, M.
Deuteron Form Factors in Effective Field Theory
Workshop on Soft Photons and Light Nuclei
Seattle, U.S.A.: 16.06.2008 – 20.06.2008

118. Pavon-Valderrama, M.
Deuteron Form Factors in Effective Field Theory
410. WE Heraeus-Seminar
Bad Honnef: 28.07.2008 – 30.07.2008

119. Pavon-Valderrama, M.
Renormalization, Modified Effective Range Expansion and Deuteron Form Factors
Bound States and Resonances in EFT
Trento, Italy: 29.09.2008 – 03.10.2008

120. Podkopal, P.
Report on analysis of break-up reaction $dd \to \pi AN$ measured with WASA-at-COSY
Frühjahrstagung der Deutschen Physikalischen Gesellschaft
Darmstadt, Germany: 10.03.2008 – 14.03.2008

121. Podkopal, P.
Normalization with elastic and quasi-elastic channels for dd experiments
WASA-at-COSY Analysis Meeting
Jülich, Germany: 26.03.2008 – 27.03.2008

122. Podkopal, P.
Performance of PSC during Apr08 beam time
WASA-at-COSY Analysis Meeting
Jülich, Germany: 09.06.2008 – 10.06.2008

123. Przerwa, J.
Isospin dependence of the η' meson production in nucleon-nucleon collisions
MESON 2008
Cracow, Poland: 06.06.2008 – 10.06.2008

124. Rathmann, F.
Towards Polarized Antiprotons
LEAP 2008
Vienna, Austria: 16.09.2008 – 19.09.2008

125. Redmer, C.F.
Status and Future Plans for WASA-at-COSY
CANU 2008 and JCHP-FFE Workshop
Bad Honnef, Germany: 15.12.2008 – 16.12.2008

126. Ritman, J.
Charm Physics in PANDA: which components could be enhanced for optimal physics output
Interaction Meeting for Planning Indian Participation in PANDA at FAIR: DAE-BRNS Theme Meeting
Mumbai, India: 15.04.2008

127. Ritman, J.
WASA-at-COSY: PANDA's Little Brother is up and Running
B.A.R.C, Kolloquium
Mumbai, India: 17.04.2008

128. Ritman, J.
WASA-at-COSY & PANDA: 4π Detectors for Fixed Target Experiments on Hadron Structure and Dynamics
STORI08
Lanzhou, China: 17.09.2008

129. Ritman, J.
Hadron physics at COSY: a step towards PANDA@FAIR
IHEP, Kolloquium
Beijing, China: 23.09.2008

130. Ritman, J.
Wir sind Sternenstaub: Nukleosynthese nach dem Urknall
Saturday Morning Physics
Bochum, Germany: 15.11.2008

131. Ritman, J.
Hadron Physics at COSY: a Step Towards PANDA@FAIR
Cairo Cyclotron Project, Cairo, Kolloquium
Cairo, Egypt: 19.11.2008

132. Ritman, J.
Untersuchungen der starken QCD mit Antiprotonen
Komitee für Hadronen- und Kernphysik (KHuK), Jahrestagung
Bad Honnef, Germany: 17.12.2008

133. Röder, M.
Hyperon-Rekonstruktion im COSY-TOF Straw Commissioning of the Straw Tube Tracker for the COSY-TOF experiment
CANU 2008 and JCHP-FFE Workshop
Bad Honnef, Germany: 15.12.2008 – 16.12.2008

134. Salmin, R.
Omega Meson Production with WASA-at-COSY
CANU 2008 and JCHP-FFE Workshop
Bad Honnef, Germany 15.12.2008 – 16.12.2008

135. Schadmand, S.
Hadron Physics with WASA-at-COSY
Workshop on Hadron Dynamics
Almunecar, Spain: 25.09.2008 – 28.09.2008

136. Schadmand, S.
Hadrons in Nuclei with Elementary Probes
Justus-Liebig-Universität Gießen, Seminar
Gießen, Germany: 08.11.2008

137. Schröder, W.
Strangeness Production at COSY-TOF
MESON 2008
Cracow, Poland: 06.06.2008 – 10.06.2008

138. Schult, O.
Entfesselte Finanzmärkte – Physik trifft Kapital
Diskussionsveranstaltung
Vallendar: 01.07.2008

139. Senichev, Yu.
Magnetoopic Structures for Synchrotrons with Negative Momentum Compaction
RuPAC 2008
Zvenigorod, Russia: 28.09.2008 – 03.10.2008

140. Sibirtsev, A.
Charged Pion Photoproduction and High Mass Baryons
Duke University, Seminar
Durham, NC, U.S.A.: 14.02.2008

141. Sibirtsev, A.
Charged pion photoproduction at Jlab
Institute of High Energy Physics (IHEP), Seminar
Beijing, China: 26.09.2008

142. Sibirtsev, A.
Perspectives on Baryon spectroscopy at COSY
Institute of High Energy Physics (IHEP), Seminar
Beijing, China: 23.09.2008

143. Sibirtsev, A.
ϕ meson decay in pp collisions
MESON 2008
Cracow, Poland: 06.06.2008 – 10.06.2008

144. Sibirtsev, A.
ϕ meson production in pp interactions
Institute of High Energy Physics (IHEP), Seminar
Beijing, China: 24.09.2008

145. Sibirtsev, A.
Spectroscopy of Excited hyperons at PANDA
Institute of High Energy Physics (IHEP), Seminar
Beijing, China: 25.09.2008

146. Sibirtsev, A.
Strangeness production
STORI08
Lanzhou, China: 14.09.2008 – 18.09.2008

147. Smirnov, A.
Simulation of Pellet Target Experiments with BETACOOL Code
21st Russian Particle Accelerator Conference (RuPAC 2008)
Zvenigorod, Russia: 28.09.2008 – 03.10.2008

148. Sokolov, A.
The lightweight straw tube trackers for the COSY-TOF and PANDA experiments
Frühjahrstagung der Deutschen Physikalischen Gesellschaft
Darmstadt, Germany: 10.03.2008 – 14.03.2008

149. Stassen, R.
The HESR RF-System and tests in COSY
EPAC08
Genoa, Italy: 23.06.2008 – 27.06.2008

150. Stockhorst, H.
Stochastische Kühlung von Antiprotonen im HESR der FAIR-Anlage
Universität Frankfurt
Frankfurt, Germany: 30.05.2008

151. Stockhorst, H.
Stochastic cooling developments for the HESR at FAIR
EPAC 2008
Genoa, Italy: 23.06.2008 – 27.06.2008

152. Stockmanns, T.
The readout concept of the PANDA Micro-Vertex-Detector
Frühjahrstagung der Deutschen Physikalischen Gesellschaft
Darmstadt, Germany: 10.03.2008 – 14.03.2008

153. Strauch, Th.
Pionic Deuterium
Frühjahrstagung der Deutschen Physikalischen Gesellschaft
Darmstadt, Germany: 14.03.2008

154. Strauch, Th.
Pionic Deuterium
International Conference on Exotic Atoms (EXA08)
Vienna, Austria: 15.09.2008 – 19.09.2008

155. Ströher, H.
Towards Polarized Antiprotons
BARC
Mumbai, India: 15.02.2008

156. Ströher, H.
Hadron Physics with Hadronic Probes: Present and Future
Fourth DAE-BRNS Workshop on Hadron Physics
Aligarh, India: 18.02.2008 – 23.02.2008

157. Ströher, H.
Antiproton Polarization Studies for FAIR (How to polarize antiprotons and what to use them for?)
Transversity'08
Ferrara, Italy: 28.05.2008 – 31.05.2008

158. Ströher, H.
Towards Polarized Antiprotons
VI-QCD Seminar
Ferrara, Italy: 01.06.2008

159. Ströher, H.
Towards Polarized Antiprotons
MESON 08
Cracow, Poland: 06.06.2008 – 10.06.2008

160. Ströher, H.
Polarized Antiprotons (Summary-1)
409. WE-Heraeus-Seminar — Polarized Antiprotons
Bad Honnef, Germany: 23.06.2008 – 25.06.2008

161. Ströher, H.
Antiproton Polarization Studies for FAIR
Stockholm University, Department of Physics
Stockholm, Sweden: 12.06.2008

162. Ströher, H.
Double Pion Production in the $dd \rightarrow \alpha\pi\pi$ Reaction
Thesis opponent, Dissertation of Samson Kelata
Uppsala, Sweden: 13.06.2008

163. Ströher, H.
Summarizing Remarks
STORI08
Lanzhou, China: 14.09.2008 – 18.09.2008

164. Ströher, H.
Application to host SPIN2010: The Case for Jülich
SPIN2008
Charlottesville, Va., U.S.A.: 06.10.2008 – 11.10.2008

165. Ströher, H.
Spin Physics at COSY — Now and in Future
SPIN2008
Charlottesville, Va., U.S.A.: 06.10.2008 – 11.10.2008

166. Ströher, H.
Polarized Antiprotons
Dalpiaz-Symposium
Ferrara, Italy: 17.10.2008 – 18.10.2008

167. Tolba, T.
A Pellet Tracking System for WASA at COSY
Frühjahrstagung der Deutschen Physikalischen Gesellschaft
Darmstadt, Germany: 10.03.2008 – 14.03.2008

168. Urban, J.
The polarized $d+d \rightarrow \alpha+\eta$ reaction and search for η-nucleus bound states
MESON 2008
Cracow, Poland: 06.06.2008 – 10.06.2008

169. Vlasov, P.
$\eta \rightarrow 3\pi^0$ decay with WASA-at-COSY
Frühjahrstagung der Deutschen Physikalischen Gesellschaft
Darmstadt, Germany: 10.03.2008 – 14.03.2008

170. Weglorz, W.
WASA-at-COSY
Institute of Modern Physics, Seminar
Lanzhou, China: 21.06.2008

171. Weglorz, W.
Status of the CSB Program at WASA-at-COSY
CANU 2008 and JCHP-FFE Workshop
Bad Honnef, Germany: 15.12.2008 – 16.12.2008

172. Weidemann, Ch.
Chemical Shift of K transitions in Manganese
Frühjahrstagung der Deutschen Physikalischen Gesellschaft
Darmstadt, Germany: 14.03.2008

173. Welsch, D.M.
Closed Orbit Correction and Multipole Compensation Schemes for Normal-conducting HESR
EPAC'08
Genoa, Italy: 23.06.2008 – 27.06.2008

174. Wirzba, A.
The Casimir effect as a scattering problem
Universität Duisburg-Essen, Seminar
Duisburg, Germany: 28.05.2008

175. Wirzba, A.
Fermionic and Scalar Casimir Effect within the Scattering Approach
University of California, Kavli Institut for Theoretical Physics
Santa Barbara, CA, U.S.A.: 23.10.2008

176. Wirzba, A.
Fermionic Casimir Effect within the Scattering Approach
European Science Foundation 1st Network Meeting
Royaumont, France: 29.11.2008

177. Wolke, M.
Symmetries and Symmetry Breaking — First Experiments with WASA at COSY
Universität Mainz: Institutsseminar Kernphysik
Mainz, Germany: 14.01.2008

178. Wolke, M.
Fundamental Symmetries, Hadron Structure and Dynamics
Uppsala University: Department of Physics and Astronomy
Uppsala, Sweden: 28.08.2008

179. Yurev, L.
MDC calibration and e^+e^- reconstruction
WASA-at-COSY Workshop on Analysis of η and η' Decays
Uppsala, Sweden: 29.02.2008 – 02.03.2008

180. Yurev, L.
Feasibility of $\eta \rightarrow e^+e^-e^+e^-$
WASA-at-COSY Workshop on Analysis of η and η' Decays
Uppsala, Sweden: 29.02.2008 – 02.03.2008

181. Yurev, L.
MC studies on $\eta \to e^+e^-e^+e^-$ pair selection
WASA-at-COSY Analysis Meeting
Jülich, Germany: 26.03.2008 – 27.03.2008

182. Yurev, L.
Online Analysis and Trigger Preparation for the May08 η run
WASA-at-COSY Analysis Meeting
Jülich, Germany: 26.03.2008 – 27.03.2008

183. Yurev, L.
MDC layer efficiency studies
WASA-at-COSY Analysis Meeting
Jülich, Germany: 09.06.2008 – 10.06.2008

184. Yurev, L.
Status of $\eta \to e^+e^-e^+e^-$ from Apr07
WASA-at-COSY Analysis Meeting
Jülich, Germany: 09.06.2008 – 10.06.2008

185. Yurev, L.
MDC fit performance; Status of $\eta \to e^+e^-e^+e^-$ from Apr07
WASA-at-COSY Analysis Meeting
Jülich, Germany: 24.09.2008 – 25.09.2008

186. Zheng, C.
Analysis of matching trigger
WASA-at-COSY Analysis Meeting
Jülich, Germany: 26.03.2008 – 27.03.2008

187. Zheng, C.
Evaluation of the matching trigger in Apr08
WASA-at-COSY Analysis Meeting
Jülich, Germany: 09.06.2008 – 10.06.2008

188. Zheng, C.
Matching Trigger with High threshold for 'fHedwrH1'
WASA-at-COSY Analysis Meeting
Jülich, Germany: 24.09.2008 – 25.09.2008

189. Zychor, I.
Excited hyperons produced in pp collisions with ANKE at COSY
STORI08
Lanzhou, China: 14.09.2008 – 18.09.2008

D Diploma and Ph.D. Theses, Habilitation

1. Bachelor, Master, Diploma

1. S. Bertelli,
   Studio della reazione di deuteron breakup in esperimenti di spin-filtering per la polarizzazione di fasci di antiprotoni,
   University of Ferrara, Italy

2. I. Császár,
   Bau einer Ionisationskammer zur Untersuchung von laserbeschleunigten Ionen,
   Hochschule Merseburg (FH).

3. P. Goslawski,
   Hochpräzise Impulsbestimmung des COSY-Beschleunigerstrahls im Rahmen der Messung zur Bestimmung der η-Masse am Experimentaufbau ANKE,
   Universität Münster

4. Martin Hausner,
   On the charge dependence of ρ meson properties,
   Universität Bonn

5. S. Kölling,
   The two-pion exchange contribution to the nuclear current operator in chiral effective field theory,
   Universität Bonn

6. David Minossi,
   Modified effective range expansion for nucleon-nucleon scattering in chiral effective field theory,
   Universität Bonn

7. G. Oswald,
   Bau, Test und Inbetriebnahme einer Ionisations- und Proportionalkammer zum Nachweis laserbeschleunigter Ionen,
   Hochschule Merseburg (FH).

8. M. Westig,
   Preparation of a precision spectroscopy measurement of metastable Hydrogen and deuterium with a modified Lamb-shift polarimeter,
   Universität zu Köln

9. M. Zielinski,
   Feasibility study of the $\eta' \to \pi^+\pi^-\pi^0$ decay using WASA-at-COSY apparatus,
   Jagiellonian University Cracow, Poland

2. Ph.D.

10. D. Chiladze,
Polarised Charge-Exchange Reaction $dp \to (pp)n$ Studies at the ANKE-COSY Spectrometer,
Tbilisi State University, Georgia

11. M. A. Leonova,
Achieving high spin-flip efficiency with an rf magnet and discovery of spin-resonance strength formulae problem,
Michigan University, U.S.A.

12. M. Lesiak-Bzdak,
Production of the eta meson in the $d+d \to {}^4He+\eta$ reaction using the polarised deuteron beam,
Jagiellonian University Cracow, Poland

13. V. S. Morozov,
Using spin resonances to manipulate the polarization of spin-1/2 and spin-1 particle beams,
Michigan University, U.S.A.

14. P. Vlasov,
Analysis of the $\eta \to 3\pi^0$ decay in the pp interaction,
Ruhr-Universität Bochum

15. X. Yuan,
Measurement of the $dd \to \alpha K^+K^-$ production cross section with the ANKE spectrometer at COSY-JÃ$\frac{1}{4}$lich" ,
IMP Lanzhou, China

3. Habilitation

16. A. Lehrach,
Strahl- und Spindynamik von Hadronenstrahlen in Mittelenergie-Ringbeschleunigern,
Rheinische-Friedrich-Wilhelms-Universität Bonn
Schriften des Forschungszentrums Jülich; Reihe Schlüsseltechnologien / Key Technologies 08 II, 2008, ISBN 978-3-89336-548-7

E Awards & Offers for Professorships

I. Császár: *Best Bachelor Thesis 2008* Hochschule Merseburg

S. Krewald: *Outstanding Referee Award* by American Physical Society

H. Machner: *Merentibus Award* by Jagellionian University, Cracow (May 2008)

U.-G. Meißner: *Outstanding Referee Award* by American Physical Society

C. Hanhart: Received call as Associate Professor/Senior Lecturer at the Department of Physics and Astronomy, Uppsala University, Sweden

Yu. Senichev: Received Professorship with Specialization "Physcis of Charged-Particle Beams and Accelerator Physics" from Ministry of Education and Science, Russia

M. Wolke: Accepted position as Associate Professor/Senior Lecturer in Experimental Hadron Physics at the Department of Physics and Astronomy, Uppsala University, Sweden

F Funded Projects

Project	Responsible	Partner Institute	Funded by
Virtual Institute Spin and Strong QCD	U.-G. Meißner	GSI, Univ.'s Bern, Bonn, Ferrara, Cracow, Torino	HGF
Few Nucleon Systems in χEFT	E. Epelbaum	Univ. Bonn	HGF
CARE	R. Tölle		EU/FP6
TA-COSY	D. Grzonka		EU/FP6
Hadron Physics Theory Netzwerk	U.-G. Meißner	Network	EU/FP6
Pellet Target	M. Büscher	ITEP, MPEI Moscow (Russia)	EU/FP6
EURONS/EXL	D. Grzonka		EU/FP6
EUROTRANS/NUDATRA	F. Goldenbaum		EU/FP6
DIRAC Secondary Beams	R. Tölle		EU/FP6
DIRAC Phase 1	R. Tölle		EU/FP6
DIRAC Secondary Beams PANDA-2	J. Ritman		EU/FP6
DIRAC Secondary Beams PANDA-4	J. Ritman		EU/FP6
Advanced Residual Gas Profile Monitor	J. Dietrich	GSI	EU/FP6
Design Study for Pick-up Electronic Development	J. Dietrich	GSI	EU/FP6
Project FAIR	R. Toelle	GSI	EU/FP7
Scalar Mesons	M. Büscher	ITEP, INR Moscow (Russia)	DFG
Pellet Target	M. Büscher	ITEP, MPEI Moscow (Russia)	DFG
Laser applications of a pellet target	M. Büscher	ITEP, MPEI Moscow (Russia), Univ. Düsseldorf	DFG
K^- Production in Nuclei	M. Hartmann	ITEP Moscow (Russia)	DFG
Isospin Violation	M. Büscher	IMP Lanzhou (China)	DFG
Jets in Hard Processes	N.N. Nikolaev	Landau Inst., ITEP Moscow (Russia)	DFG
Properties of Unstable Nuclei	S. Krewald	Petersburg State Univ., IPPE Obninsk (Russia)	DFG
Pion Reactions on Few Nucleon Systems	C. Hanhart	ITEP Moscow (Russia)	DFG
ATRAP	W. Oelert	Univ. Mainz	DFG
Fundamental Research with Hadrons	W. Oelert	Jagiellonian Univ. Cracow (Poland)	DFG
Neutron Properties from light nuclei	E. Epelbaum	Univ.'s Bochum, Bonn, Gießen	SFB/TR 16
Broken Symmetries	H. Machner	Univ. Helsinki (Finland)	DAAD
PPP Kanada	D. Grzonka	York Univ., Toronto (Canada)	DAAD
PANDA luminosity monitor	J. Ritman	Madagascar	HGF-DAAD
Rare Decays of η and η' Mesons	S. Schadmand	Indian Inst. of Technology Bombay	DAAD/DST India
Polarization observables in $\bar{p}d$ elastic scattering	J. Haidenbauer	JINR Dubna (Russia)	Heisenberg-Landau Program
Eta-Meson Physics	H. Machner	BARC Mumbai (India)	Int. Büro BMBF
Target Development for nuclear physics experiments at COSY and AEA cyclotron	J. Ritman	AEA Cairo (Egypt)	Int. Büro BMBF
Medical Applications of Accelerators	J. Dietrich	iThemba LABS (South Africa)	Int. Büro BMBF
A Pellet Target for PANDA	M. Büscher	ITEP, MPEI Moscow (Russia) Uppsala Univ. (Sweden), GSI	INTAS
Advanced Beam Dynamic for Storage Rings	A. Lehrach		INTAS
Projectile Electron Losses in the Collisions of Fast and Relativistic Low Charged Ions	G. Baur	GSI, Stockholm, Tashkent, Moscow, Arkhangelsk	GSI-INTAS
Polarized Target	F. Rathmann	PNPI Gatchina (Russia)	ISTC
Baryon Resonance Analysis	U.-G. Meißner	JLAB (U.S.A.)	JLAB
Development of a high energy electron cooler	J. Dietrich	TU Dortmund; BINP Novosibirsk, JINR Dubna (Russia)	HGF
Calculations of the Radiation Load to the PANDA MVD	J. Ritman	Israel	NRW-Israel

G COSY-FFE Projects

Project	Responsible	Institute
Frozen Spin Target	Prof. W. Meyer	Univ. Bochum
Entwicklung von Software zur Teilchenidentifikation und Erkennung von split-offs im el.-magn. Kalorimeter des WASA-Experiments	Prof. U. Wiedner	Univ. Bochum
Zusammenarbeit von HISKP-Bonn an internen Experimenten an COSY	Prof. J. Bisplinghoff	Univ. Bonn
Theorectical studies of strangeness and charm production at COSY and PANDA/FAIR	Prof. H.-W. Hammer	Univ. Bonn
Entwicklung eines Partialwellenprogrammes für die Analyse von Daten von WASA	Prof. E. Klempt	Univ. Bonn
Inelastic baryon resonances from lattice QCD	Prof. A. Rusetsky	Univ. Bonn
Zusammenarbeit an COSY H-Strahl Laserdiagnose	Prof. T. Weis	Univ. Dortmund
COSY-TOF detector	Prof. H. Freiesleben	TU Dresden
Bau von Detektoren für ANKE und K^--Nachweis	Prof. B. Kämpfer	FZ Dresden
Measurement of the degree of polarisation of laser accelerated protons	Prof. O. Willi	Univ. Düsseldorf
Bau eines Cherenkovdetektors für WASA at COSY	Prof. W. Eyrich	Univ. Erlangen-Nürnberg
Experimente mit COSY-TOF	Prof. W. Eyrich	Univ. Erlangen-Nürnberg
Polarization experiments with ANKE at COSY	Prof. E. Steffens	Univ. Erlangen-Nürnberg
FPGA-based trigger system for WASA	Prof. W. Kühn	Univ. Gießen
Schwellenexperimente an COSY-11 und ANKE	Dr. A. Khoukaz	Univ. Münster
Baryon resonance, g_A und die effektive Restrukturierung der chiralen Symmetrie	Prof. A. Schäfer	Univ. Regensburg
Installation und Inbetriebnahme des WASA-Detektors am COSY-Ring und Durchführung von Experimenten an WASA at COSY	Prof. H. Clement	Univ. Tübingen
Experimente an COSY-TOF	Prof. H. Clement	Univ. Tübingen

Project	Responsible	Institute
Lattice calculations of axial charges for baryons	Prof. C. Gattringer	Univ. Graz (Austria)
Polarized internal target for ANKE at COSY	Prof. M. Nioradze	Tbilisi State Univ. (Georgia)
Spin dependence in *pd* interactions	Prof. P. Dalpiaz	Univ. Ferrara (Italy)
Photonendetektor an ANKE	Prof. A. Magiera	Jagellionian Univ. Cracow (Poland)
Investigation of CP symmetry with WASA	Prof. P. Moskal	Jagellionian Univ. Cracow (Poland)
Strangeness production with WASA	Prof. B. Kamys	Jagellionian Univ. Cracow (Poland)
Study of the decay $\eta' \to \eta\pi\pi$ with WASA	Prof. Z. Rudy	Jagellionian Univ. Cracow (Poland)
WASA at COSY	Prof. M. Jezabek	INP Crakow (Poland)
Strange Baryon Produktion at ANKE	Prof. Z. Sujkowski	IPJ Otwock-Swierk (Poland)
Study of the nature of the $\Lambda(1405)$ with WASA	Prof. W. Zipper	Univ. Silesia (Poland)
Neutron tagging and strangeness production at ANKE	Dr. V. Koptev	PNPI Gatchina (Russia)
Set-up and research with the spectator/vertex detection system at ANKE-COSY	Prof. V. Kulikov	JINR Dubna (Russia)
Reanalysis of the measurement of the η mass	Dr. D. Kirillov	JINR Dubna (Russia)
ω-meson production with WASA	Prof. E. Strokovsky	JINR Dubna (Russia)
Development of a frozen-pellet target	Dr. A. Gerasimov	ITEP Moscow (Russia)
ϕ-meson production in *pn* and *pA* reactions	Prof. V. Kiselev	ITEP Moscow (Russia)
Development, commissioning and operation of components for the COSY experiments WASA and ANKE and spin-filtering studies at COSY as preparation of the PAX experiment in the framework of the FAIR project at GSI	Dr. A. Vasilyev	PNPI Gatchina (Russia)
Development of online software tools for COSY-TOF	Prof. V.N. Afanasiev	MIEM Moscow (Russia)
Cooperation COSY-WASA for $pp \to pp\eta$ and $pp \to pp\eta\pi^0$	Prof. T. Johansson	Uppsala Univ. (Sweden)
Trigger based on digitized QDC information for WASA	Prof. B. Höistad	Uppsala Univ. (Sweden)
Search for mixing between light mesons	Prof. A. Rudchik	INR Kiev (Ukraine)
Physics of antihydrogen	Prof. E. Hessels	Univ. of York (Canada)
Unified analysis of meson production in hadronic reactions	Prof. K. Nakayama	Univ. of Georgia (U.S.A.)
SPIN@COSY: Spin-Manipulating Polarized Deuterons and Protons	Prof. A. Krisch	Univ. of Michigan (U.S.A.)

H Conferences (co-)organized by the IKP

H.1 Hadron Physics Summer School 2008

More than 80 graduate and advanced undergraduate students from 14 countries and 4 continents participated in the Hadron Physics Summer School HPSS2008 held at Physikzentrum Bad Honnef, Germany, August 11 – 15, 2008. Similar to the preceding COSY Summer School (CSS) 2002, 2004, and 2006, this school consisted of lectures and working groups on theoretical, experimental, and accelerator aspects. The focus was on current issues in hadron physics with emphasis on the latest programs at the accelerators COSY and ELSA (Bonn), also featuring future FAIR projects like HESR/PANDA and PAX. During the very successful school, the students were given a guided tour to COSY.

The HPSS2008 was jointly organized by scientists working at the IKP and by the DFG Transregio TR 16 (Subnuclear Structure of Matter) of the Universities Bonn, Bochum, and Giessen. In addition, the HPSS2008 was sponsored by DAAD (German Academic Exchange Service) and DPG (Deutsche Physikalische Gesellschaft), making the participation of young motivated students into this challenging enterprise possible.

It is intended to conduct the HPSS every second year. The series will be supplemented by lecture weeks in the alternate years, which will consist of invited lectures and student contributions. The lecture weeks are self-contained and will also be an excellent opportunity for graduate students and early post-graduates to deepen the knowledge gained at HPSS.

For more detailed information, see www.fz-juelich.de/ikp/hpss2008/.

Fig. 59: Participants of HPSS2008 in front of Physikzentrum Bad Honnef.

H.2 The 7th International Conference on Nuclear Physics at Storage Rings, STORI'08

STORI'08, the 7th International Conference on Nuclear Physics at Storage Rings, took place on September 14 – 18, 2008 in Lanzhou (China). It was organized by the Institute of Modern Physics (IMP) of the Chinese Academy of Sciences (CAS) with Guoqing Xiao (HIRFL, Heavy Ion Research Facility in Lanzhou) as Chairman. Approximately 90 scientists from all over the world attended the meeting (see enclosed photograph).
During STORI'08, a wealth of new scientific results from the operating hadron and electron rings as well as new plans were presented in 25 invited talks and 20 contributions — in particular first nuclear mass measurements from the newly commissioned pair of storage rings for ions at Lanzhou, CSRm and CSRe. The attendants not only discussed physics issues but also technological challenges around the rings, like electron and stochastic cooling and polarized beams (of antiprotons), the targets (liquid and cluster jets, pellets and polarized) and the internal and external detectors. A number of talks was devoted to the transition from existing detectors/rings to planned future facilities, *e.g.* from COSY/WASA to HESR/PANDA and from ESR to NESR (at FAIR). A visit to HIRFL-CSR was provided during the meeting, where the impressive progress in setting up and commissioning their storage rings could be observed.
The next STORI conference will be held in 2011 in Frascati (Italy). The chairman will be Stefano Bianco (LNF, INFN): by that time we should be able to witness the start of the construction of new facilities, in particular FAIR at Darmstadt (Germany).

Fig. 60: Some of the STORI'08 participants in front of the IMP main building

H.3 MESON 2008

The bi-annual conference MESON 2008 took place in the Jagiellonian University Kraków, Poland in the time 6 – 10 June. It was jointly organised by Forschungszentrum Jülich, Germany, INFN Frascati, Italy, Jagiellonian University, Kraków, Poland, and Inst. Nuclear Physics, PAN, Kraków, Poland. Again as since 1991 physicists from all over the world met to discuss meson physics. Since mesons and baryons are hadrons, they interact mainly

Fig. 61: Participants of the MSON 2008 in front of the Lecture Hall of the Jagiellonian University, Kraków, Poland.

via the strong interaction. Studies of the production, interactions with mesons and baryons as well as their decays shed light on their structure. Interest in bound states of mesons with nucleons and light nuclei has renewed interest by recent new findings. Probes to produce mesons are by now mainly baryons as well as electromagnetic probes. The detectors are now commensurate in complexity to the problems to be attacked. Just to name a few being represented at the present meeting: ANKE, BABAR, BES, CLAS, CLEO, Compass, COSY-GEM, COSY TOF, Crystal Ball, Crystal Barrel, HADES, SPRING8, WASA. The rich harvest of experimental results was accompanied by theory ranging from π-π interaction to medium modification of mesons in nuclei.
The conference saw presentations from delegates being quite senior and eminent scientists indeed. However, a great number of young researchers from both the experimental and theoretical fraternity complemented the programme. The conference benefitted from suggestions contributed by the international advisory committee. It was supported by

- Forschungszentrum Jülich, Germany
- INFN Frascati, Italy
- Jagiellonian University, Kraków, Poland
- Inst. Nuclear Physics, PAN, Kraków, Poland
- Jefferson Lab, Newport News, Virginia, USA
- Hadron Physics I3 project within FP6

The next conference will take place June 2010 again in Kraków, Poland.

H.4 409$^{\text{th}}$ WE-Heraeus-Seminar; Polarized Antiprotons

The suggestion of the PAX collaboration to utilize polarized antiprotons at the new FAIR facility at Darmstadt has been well received within the hadronic physics community. A polarized antiproton beam would allow unprecedented measurements of many fundamental physics observables. Among them, transversity; this describes the distribution of transversely polarized quarks in a transversely polarized nucleon. Polarized antiprotons would provide in particular a direct determination of transversity by measurement of a double-spin asymmetry in the production of Drell-Yan events. Other aspects address the determination of the phases of time-like electromagnetic form factors, and other scattering observables in hard proton antiproton reactions.
At present, the most promising method fort he production of a polarized antiproton beam is spin filtering, where one employs the spin-dependence of the strong interaction of an initially unpolarized antiproton beam impinging on a polarized hydrogen gas target. Although the proof of principle experiment (FILTEX) has already been successfully carried out in 1993 with a proton beam at the TSR in Heidelberg, the underlying mechanisms are not completely understood yet. In order to accomplish that, a series of judiciously chosen experiments using protons at COSY is necessary. During the past year, the effect of electrons on the polarization of a stored beam was studied. Since little is known about the spin-dependence of the antiproton-proton interaction, subsequently, experiments at the AD have to be carried out. The results of these investigation will provide a data basis which can be used to design an optimized, dedicated storage ring fort he proton of polarized antiprotons, a so-called Antiproton-Polarized Ring, which shall later be employed at the FAIR facility.
With this in mind, the goal of the 409$^{\text{th}}$ WE-Heraeus seminar, which took place during June 23–25, 2008, was to evaluate the physics potential polarized antiprotons would bear for hadron physics. In addition, the status of the experimental and theoretical efforts towards these goals has been emphasized during the meeting. The exciting search for the optimum approach brought together experts in the field with young student — in total 60 participants. This successful combination produced exciting debates.
The organizers and participant would like to thank the Wilhelm und Else Heraeus-foundation for their generous support. We also would like to thank in particular Dr. E. Dreisigacker and Frau H. Uebel of the Heraeus foundation, and the members of the Physikzentrum Bad Honnef for their assistance.

I Teaching Positions

Institute	Name	University
IKP-1	PD Dr. A. Gillitzer	Bonn
	PD Dr. F. Goldenbaum	Wuppertal
	Prof. Dr. H. Machner	Duisburg-Essen
	Prof. Dr. J. Ritman	Bochum
	PD Dr. S. Schadmand	Gießen
	Dr. T. Stockmanns	Bochum
IKP-2	PD Dr. M. Büscher	Köln
	PD Dr. D. Gotta	Köln
	PD Dr. F. Rathmann	Erlangen-Nürnberg
	Prof. Dr. H. Ströher	Köln
	Dr. M. Wolke	Bochum
IKP-3	Prof. Dr. G. Baur	Basel
	Prof. Dr. E. Epelbaum	Bonn
	Univ. Doz. Dr. J. Haidenbauer	Graz
	PD Dr. C. Hanhart	Bonn
	Prof. Dr. S. Krewald	Bonn
	Prof. Dr. U.-G. Meißner	Bonn
	Prof. Dr. N.N. Nikolaev	Moscow
	Dr. A. Nogga	Bonn
	PD Dr. A. Wirzba	Bonn
IKP-4	Prof. Dr. Dr. h.c. J. Dietrich	Dortmund
	PD Dr. A. Lehrach	Aachen, Bonn
	Prof. Dr. R. Maier	Bonn

J Beam Time at COSY

The scheduled beam time for COSY in the year 2008 was 7224 hours. With an down time of 375 hours the COSY complex features a reliability of 95%. Two main causes for downtime are the aged cyclotron and the magnetic septum of COSY needed for external experiments. The distribution of user hours is listed in Table 4 and depicted in Fig. 62.

Table 4: Overview over COSY user beam time in 2008.

Date	Experiment	Duration	Reaction, experiment #
19.01.08–27.01.08	WASA	1 week	$pn \to d\pi\pi$, 183
09.02.–24.02.	PAX	2 weeks	$\vec{p}$-depolarization, 181
08.03.–30.03.	ANKE	3 weeks	$\vec{d}p \to {}^3\mathrm{He}\,\eta$, 187
26.04.–04.05.	WASA	1 week	$pp \to pp\eta$, 182
05.05.–11.05.	WASA	1 week	$pp \to pp\eta'$, 184
17.05.–25.05.	SPIN@COSY	1 week	$\vec{d}$ beam, 180
31.05.–08.06.	WASA	1 week	$\vec{d}d \to {}^4\mathrm{He}\,\eta$, 186
09.06.–15.06.	dEDM	1 week	$\vec{d}$ beam, 176.1
21.06.–06.07.	WASA	2 weeks	$dd \to {}^4\mathrm{He}\,\pi^0$, 173.1
12.07.–27.07.	ANKE	2 weeks	$pn \to d\omega$, 175.1
02.08.–10.08.	TOF	1 week	commissioning, 179
30.08.–07.09.	PAX	1 week	accept.studies, 190
13.09.–21.09.	dEDM	1 week	$\vec{d}$ beam, 176.2
27.09.–26.10.	WASA	4 weeks	$pd \to {}^3\mathrm{He}\,\eta$, 188
01.11.–16.11.	WASA	2 weeks	$pp \to pp\eta$, 182
22.11.–30.11.	SPIN@COSY	1 week	$\vec{d}$ beam, 180.1
06.12.–21.12.	TOF	2 weeks	Hyperon prod., 141.4
Total '08		27 weeks	

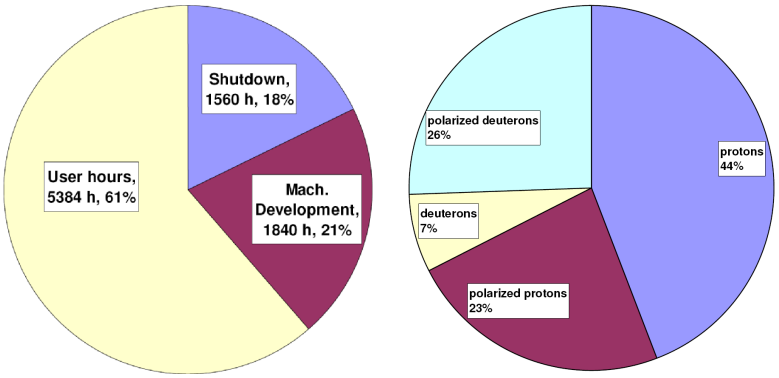

Fig. 62: COSY beam-time statistics. The scheduled beam time sums up to 7224 hours with a reliability of 95%.

K Personnel

K.1 Scientific Staff

Prof. Dr. G. Baur (IKP-3)

Dr. U. Bechstedt (IKP-4)

Dr. K. Bongardt (IKP-4)

DI N. Bongers (IKP-4)

DI R. Brings (IKP-4)

PD Dr. M. Büscher (IKP-2)

DP A. Chechenin (IKP-4) (until 15 Februar, 2008)

DP E. Czerwinski (IKP-1)

Prof. Dr.Dr.h.c. J. Dietrich (IKP-4)

DI N. Dolfus (IKP-TA)

Dr. M. Döring (IKP-3)

Dr. R. Engels (IKP-2)

Prof. Dr. E. Epelbaum (IKP-3)

DI F.-J. Etzkorn (IKP-4)

Dr. P. Fedorets (IKP-2)

Dr. O. Felden (IKP-TA)

Dr. W. Gast (IKP-1)

Dr. R. Gebel (IKP-4)

Dr. M. George (IKP-1) (until 30 September, 2008)

PD Dr. A. Gillitzer (IKP-1)

PD Dr. F. Goldenbaum (IKP-1)

PD Dr. D. Gotta (IKP-2)

Dr. F. Grümmer (IKP-3)

Dr. D. Grzonka (IKP-1)

DI W. Günther (IKP-4)

Dr. F.-K. Guo (IKP-3)

Univ. Doz. Dr. J. Haidenbauer (IKP-3)

PD Dr. C. Hanhart (IKP-3)

Dr. M. Hartmann (IKP-2)

M. Hausner (IKP-3) (until 30 July 2008)

Dr. V. Hejny (IKP-2)

DI K. Henn (IKP-4)

DP M. Hodana (IKP-1)

Dr. F. Hügging (IKP-1) (until 30 April 2008)

Dr. V. Kamerdjiev (IKP-4)

Dr. A. Kacharava (IKP-2)

D. Khaneft (IKP-2)

DP P. Klaja (IKP-1)

St. Kölling (IKP-3)

DP A. Kowalczyk (IKP-1)

Prof. Dr. S. Krewald (IKP-3)

DI K. Kruck (IKP-4)

Dr. A. Lehrach (IKP-4)

Dr. B. Lorentz (IKP-4)

Prof. Dr. H. Machner (IKP-1)

Prof. Dr. R. Maier (IKP-4)

Prof. Dr. U.-G. Meißner (IKP-3)

DP M. Mertens (IKP-1)

DP S. Mikirtychiants (IKP-2)

D. Minossi (IKP-3)

DI I. Mohos (IKP-4) (until August 2008)

Dr. M. Nekipelov (IKP-2)

Prof. Dr. N.N. Nikolaev (IKP-3)

Dr. A. Nogga (IKP-3)

Prof. Dr. W. Oelert (IKP-1)

DP D. Oellers (IKP-2)

Dr. H. Ohm (IKP-2)

DI N. Paul (IKP-1)

Dr. C. Pauly (IKP-1)

Dr. M. Pavon-Valderrama (IKP-3)

Dr. D. Prasuhn (IKP-4)

Dr. A. Raccanelli (IKP-4)

PD Dr. F. Rathmann (IKP-2)

DP Ch.F. Redmer (IKP-1)

DP M. Retzlaff (IKP-4)

DI A. Richert (IKP-4)

Prof. Dr. J. Ritman (IKP-1)

Dr. E. Roderburg (IKP-1)

DI J. Sarkadi (IKP-TA)

DP P. Saviankou (IKP-3)

Dr. H. Schaal (IKP-1)

PD Dr. S. Schadmand (IKP-1)

Dr. R. Schleichert (IKP-2)

DI G. Schug (IKP-4)

Dr. Th. Sefzick (IKP-TA)
DI E. Senicheva (IKP-4) (until 31 March 2008)
Dr. Y. Senichev (IKP-4)
DI M. Simon (IKP-4)
Dr. A. Sokolov (IKP-1)
Dr. R. Stassen (IKP-4)
Dr. H. Stockhorst (IKP-4)
Dr. T. Stockmanns (IKP-1)
DP Th. Strauch (IKP-2)
Prof. Dr. H. Ströher (IKP-2)
T. Tolba (IKP-1)
Dr. R. Tölle (IKP-4)
DI T. Vashegyi (IKP-4)
Dr. N. Vasiukhin (IKP-4) (until 31 May 2008)
DP P. Vlasov (IKP-1)
Chr. Weidemann (IKP-2)
DP D. Welsch (IKP-4)
Dr. P. Wintz (IKP-1)
PD Dr. A. Wirzba (IKP-3)
DI J.-D. Witt (IKP-4)
Dr. M. Wolke (IKP-2)
Dr. E. Zaplatin (IKP-4)
F. Zarife (IKP-4) (until 14 March 2008)

K.2 Technical and Administrative Staff

J. Ahlschläger (IKP-4)

J. Artz (IKP-TA)

C. Berchem (IKP-TA)

P. Birx (IKP-4) (until 31 January 2008)

M. Böhnke (IKP-4)

J. Borsch (IKP-TA)

P. Brittner (IKP-4)

J. But (IKP-TA)

W. Classen (IKP-4)

M. Comuth-Werner (IKP-TA)

B. Dahmen (IKP-4)

C. Deliege (IKP-4)

W. Derissen (IKP-TA)

G. D'Orsaneo (IKP-2)

R. Dosdall (IKP-1)

R. Enge (IKP-4)

P. Erben (IKP-2)

B. Erkes (IKP-4)

W. Ernst (IKP-TA) (until 31 May 2008)

K. Esser (IKP-TA)

H.-P. Faber (IKP-4) (until 30 November 2008)

H.-W. Firmenich (IKP-TA)

J. Göbbels (IKP-TA)

H. Hadamek (IKP-TA)

R. Hecker (IKP-4)

E. Heßler (IKP-TA)

M. Holona (IKP-TA)

H.-M. Jäger (IKP-1)

H. J. Jansen (IKP-TA)

A. Kieven (IKP-4)

Ch. Krahe (IKP-TA) (until 31 March 2008)

M. Kremer (IKP-TA)

G. Krol (IKP-4)

M. Küven (IKP-TA)

K.-G. Langenberg (IKP-4)

H. Metz-Nellen (IKP-TA)

S. Müller (IKP-TA)

M. Nau (IKP-TA) (until 31 March 2008)

R. Nellen (IKP-TA)

St. Nießen (IKP-TA) (until 31 March 2008)

H. Pütz (IKP-4)

G. Roes (IKP-TA)

N. Rotert (IKP-4)

D. Ruhrig (IKP-4)

T. Sagefka (IKP-4)

F. Scheiba (IKP-4)

H. Schiffer (IKP-TA)

J. Schmitz (IKP-4)

F. Schultheiß (IKP-TA)

H. Singer (IKP-4)

D. Spölgen (IKP-2)

G. Sterzenbach (IKP-1)

J. Strehl (IKP-TA)

J. Uehlemann (IKP-1)

P. Wieder (IKP-2)

J. Wimmer (IKP-1)

H. Zens (IKP-4)

IKP-1 = Experimental Hadron Structure
IKP-2 = Experimental Hadron Dynamics
IKP-3 = Theoretical Nuclear Physics
IKP-4 = Large-Scale Nuclear Physics Equipment
IKP-TA = Technical Services and Administration